An Observational and Numerical Study of Mountain Boundary – Layer Flow

by
Robert Mason Banta

Department of Atmospheric Science
Colorado State University
Fort Collins, Colorado

Colorado State University

Department of Atmospheric Science

Paper No. 350

AN OBSERVATIONAL AND NUMERICAL STUDY OF MOUNTAIN BOUNDARY-LAYER FLOW

by

Robert Mason Banta

Research Supported by the

National Science Foundation
Under Grant ATM-8113082

and

the South Park field project
was also sponsored in part by
U.S. Department of the Interior,
Bureau of Reclamation
Under Contract 7-07-83-V0006

Department of Atmospheric Science

Colorado State University

Fort Collins, Colorado

June, 1982

Atmospheric Science Paper No. 350

ABSTRACT OF THESIS

AN OBSERVATIONAL AND NUMERICAL STUDY
OF MOUNTAIN BOUNDARY-LAYER FLOW

The following dissertation is a combined observational and numerical study of the dissolution of the nocturnal cold air layer, which forms in the lower regions of a mountain basin, and of the effect that this has on the development of local wind systems in the basin. The observational part of the study is based on data taken during the South Park Area Cumulus Experiment in 1977 (SPACE-77). The numerical modeling results were obtained from a dry, two-dimensional, fine resolution (Δ_x=200m., $\Delta_z \simeq$100m.) version of the cloud model developed by Tripoli and Cotton (1982).

In the observational portion of this study surface mesonet charts and time plots of meteorological data reveal three types of local winds: downslope winds, upslope winds and afternoon winds which correspond in direction with the winds above the ridgetops. Vertical profiles of potential temperature, moisture, and winds accompanying these wind systems were determined from rawinsonde and tethered balloon sounding, and vertical potential temperature cross sections were both inferred and determined from aircraft data. The structure which arises from these considerations indicates that a zone of convergence exists to the lee of the main ridge at the western edge of South Park. This region is called a "leeside convergence zone" in this study, and it is believed

to be important in the initiation of mountain-generated, deep convective clouds and cloud systems.

In a second aspect of the observational study, it is shown that the observed increase in gustiness of the afternoon surface winds at a site is due to the rapid increase in the height of the convective boundary layer over that site.

The numerical modeling experiments reproduced the observed features of boundary-layer and local-wind development quite well. Data generated by the model were then used to eveluate the forces important in driving the local wind systems. The horizontal pressure-gradient force proved to be important in producing upslope, as expected. The afternoon winds shift occurred mostly through the effect of the turbulent diffusion of upper-level momentum downwards, and through the horizontal advection of the afternoon winds.

Robert Mason Banta
Department of Atmospheric Science
Colorado State University
Fort Collins, Colorado 80523
Summer, 1982

ACKNOWLEDGEMENTS

I would like to express my appreciation to Prof. William R. Cotton, my thesis advisor, for his support, encouragement, and many helpful suggestions throughout the course of this research. I also thank him and the other members of my graduate committee, Dr. Donald H. Lenschow, Dr. Wayne H. Schubert, and Dr. Robert N. Meroney, for their constructive comments which have helped in formulating the final version of this manuscript.

I especially appreciate the laborious hours spent by Brenda Thompson, who typed the final version of the manuscript, and Lucy McCall, who drafted the figures which appear in this paper. Polly Cletcher and Julie Svoboda also typed portions of this paper or the rough draft, and Duayne Barnhart made the photographic reductions of the figures, so to them I am also indebted.

Individuals who have contributed substantially to various aspects of this study, both through helpful discussions and through more concrete contributions, were Dave Hahn, Kelvin Danielson, and Ray George. The many discussions with Dave Bader and Fred Toepfer have also been very beneficial.

In a study that involves acquisition, reduction, and analysis of field data, a large number of individuals make important contributions at various stages of the work. Some of those individuals who made important contributions to this study were: Dudley Friday, Stacy Ming, Abdelmalek Kiroane, Jerry Albright, Steve Semmer, Dave Whiteman, Dave

ACKNOWLEDGEMENTS

I would like to express my appreciation to Prof. William R. Cotton, my thesis advisor, for his support, encouragement, and many helpful suggestions throughout the course of this research. I also thank him and the other members of my graduate committee, Dr. Donald H. Lenschow, Dr. Wayne H. Schubert, and Dr. Robert N. Meroney, for their constructive comments which have helped in formulating the final version of this manuscript.

I especially appreciate the laborious hours spent by Brenda Thompson, who typed the final version of the manuscript, and Lucy McCall, who drafted the figures which appear in this paper. Polly Cletcher and Julie Svoboda also typed portions of this paper or the rough draft, and Duayne Barnhart made the photographic reductions of the figures, so to them I am also indebted.

Individuals who have contributed substantially to various aspects of this study, both through helpful discussions and through more concrete contributions, were Dave Hahn, Kelvin Danielson, and Ray George. The many discussions with Dave Bader and Fred Toepfer have also been very beneficial.

In a study that involves acquisition, reduction, and analysis of field data, a large number of individuals make important contributions at various stages of the work. Some of those individuals who made important contributions to this study were: Dudley Friday, Stacy Ming, Abdelmalek Kiroane, Jerry Albright, Steve Semmer, Dave Whiteman, Dave

ACKNOWLEDGEMENTS

I would like to express my appreciation to Prof. William R. Cotton, my thesis advisor, for his support, encouragement, and many helpful suggestions throughout the course of this research. I also thank him and the other members of my graduate committee, Dr. Donald H. Lenschow, Dr. Wayne H. Schubert, and Dr. Robert N. Meroney, for their constructive comments which have helped in formulating the final version of this manuscript.

I especially appreciate the laborious hours spent by Brenda Thompson, who typed the final version of the manuscript, and Lucy McCall, who drafted the figures which appear in this paper. Polly Cletcher and Julie Svoboda also typed portions of this paper or the rough draft, and Duayne Barnhart made the photographic reductions of the figures, so to them I am also indebted.

Individuals who have contributed substantially to various aspects of this study, both through helpful discussions and through more concrete contributions, were Dave Hahn, Kelvin Danielson, and Ray George. The many discussions with Dave Bader and Fred Toepfer have also been very beneficial.

In a study that involves acquisition, reduction, and analysis of field data, a large number of individuals make important contributions at various stages of the work. Some of those individuals who made important contributions to this study were: Dudley Friday, Stacy Ming, Abdelmalek Kiroane, Jerry Albright, Steve Semmer, Dave Whiteman, Dave

Stevens, Bill Strayer, Lyle Lilie, Randy Horn, Gary Peterson and Connie Banta.

Finally, I would like to express my appreciation and gratitude to my colleague, Greg Tripoli. Wide-ranging discussions with him have contributed to ideas appearing in all parts of this study, and his expertise and willingness to help with problems contributed greatly to the modeling portions of this study.

The micrometeorological towers and equipment used in South Park, which had previously been assembled and used by Paul Katen, were loaned to us by Professor Elmar R. Reiter. Some of the data analysis was performed at the Colorado State University Computer Facility, and the rest of the data analysis and all of the modeling were done at the Computer Facility of the National Center for Atmospheric Research (NCAR) in Boulder, Colo. Also, the Portable Automated Mesonet and a Boundary Layer Profiler (tethered balloon) were provided by the Field Observing Facility at NCAR.

This research was sponsored by the National Science Foundation under Grant ATM-8113082, and the South Park field project was also sponsored in part by the Bureau of Reclamation of the U.S. Department of the Interior, under Contract 7-07-83-V0006.

TABLE OF CONTENTS

LIST OF FIGURES

I. INTRODUCTION

Local wind systems in mountainous terrain have been extensively studied over the past several decades, including exhaustive efforts by the Germans and Austrians in the 1920's and 1930's. A resurgence of interest in complex-terrain meteorology has arisen in recent years. Two reasons for this are: (1) Activities in more remote or rugged areas have required a knowledge of air flow patterns there. These activities include energy development (and associated population growth which causes air pollution problems), fighting forest fires, weather modification, and weather forecasting studies. (2) Advances in technology have allowed much more sophisticated observations to be made and have made available the means to perform sophisticated numerical simulations of atmospheric processes. These allow investigators to describe meteorological phenomena which were previously unmeasurable and/or unknown.

In the following dissertation examples of both of the kinds of advances in technology described in (2) will be applied to the problem of air flow in a broad valley in the Colorado Rocky Mountains. First, data from an intensive field measurement project have been analyzed to determine the extent and structure of the local wind systems. Instrumentation for this project included a surface mesonet, meteorological radars, rawinsonde, tethered balloon systems, micrometeorological towers, an instrumented aircraft, and others. Second, a version of the Colorado

State University Cloud/Mesoscale Numerical Model was applied to case studies obtained from field data. These numerical modeling studies are used to further investigate the causes of the local wind systems observed in the field.

One important and immediate conclusion from the observational study was that the progress of the daytime wind systems was closely tied to changes in the structure of the atmospheric boundary layer. Thus, this dissertation is a study not only of the winds in the mountains, but also of the evolution of the daytime boundary layer over the mountains. The study, therefore, has applicability to transport and diffusion of atmospheric contaminants over mountainous terrain. This is because transport is accomplished by the local winds, which change with diurnal changes in boundary-layer structure, while diffusion is controlled by turbulence, which is modulated in a diurnal cycle by changes in boundary-layer structure.

A second aspect of this study is a discussion of some mechanisms for producing updrafts in the mountains. These mechanisms are likely to be important in the initiation of mountain cumulus clouds and cloud systems. This aspect of the study thus applies to studies of mountain-generated clouds and cloud systems, whether for modification or for forecasting purposes.

II. BACKGROUND STUDIES

This dissertation is an investigation of the daytime boundary layer over mountainous terrain. Since boundary-layer growth is of necessity tied to the evolution of the local wind systems in the mountains, this is also an investigation of the thermally-forced ridge-valley wind systems which occur in mountain valleys.

The dry daytime boundary layer over flat land, which has been extensively studied, is in general a well-mixed layer in which strong mixing is driven by heating from the ground; this subject will be reviewed in a later section of this chapter. The mixed layer is a layer in which mean potential temperature (θ), water-vapor mixing ratio (q), and the mean wind components tend to be nearly constant with height, as shown in Fig. 2.1. The well-mixed boundary layer will be referred to in this study as the "convective boundary layer" or CBL.

The thermally-driven, local wind systems in the mountains have been studied extensively over the past several decades. In the next section previous studies of mountain-valley wind systems which form a background to the present study will be discussed. Then studies of the structure of the convective boundary layer will be reviewed briefly in Section B.

A. Mountain-Valley Wind Systems

According to the classic theory of local winds in the mountains, winds in a mountain valley tend to blow up the valley towards the mountains during the day ("valley wind") and down the valley away from

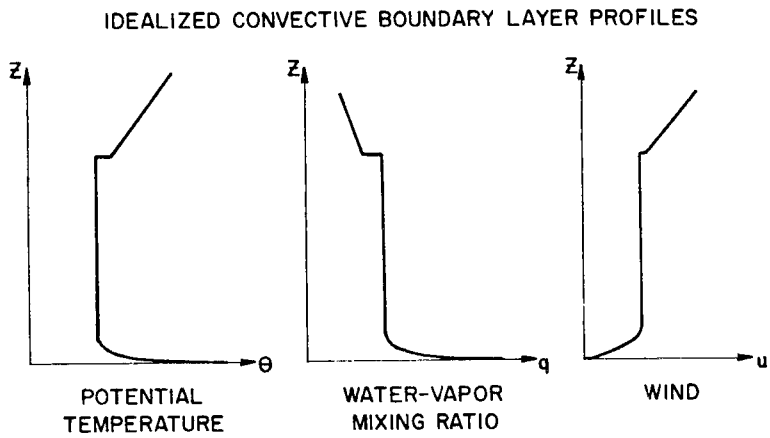

Figure 2.1: Idealized profiles of potential temperature, water vapor mixing ratio, and winds in the horizontally-homogeneous convective boundary layer (after Tennekes and Driedonks, 1981).

the mountains at night ("mountain wind"). Comprehensive reviews of the theory have been presented in a large number of publications, such as Wagner (1938), Defant (1951), Geiger (1965) and Yoshino (1975), to name just a few. In the following sections, the important aspects of that theory as they apply to this study will be discussed, including slope winds, the mountain-valley winds, and the interaction between these two types that occurs as part of the daily cycle. Following that discussion, some other observational studies, which do not necessarily conform to the theoretical model, will be presented. Then follows a discussion of studies describing the thermal structure which accompanies these winds. Finally, other studies which have described convective boundary layers (CBL's) over mountainous terrain will be discussed.

1. Slope winds

Slope winds are winds which blow parallel (or antiparallel) to the local fall line of the terrain. Downslope winds are produced by cooling at the surface; upslope winds, by heating.

Downslope winds are also called drainage winds, since they result from the heavier cold air draining off the slopes and into the lower areas of the valley. Geiger (1965, p. 412 and pp. 393 f.) describes the downhill flow of cold air as being like the flow of a viscous liquid, but, more like thick syrup (or "porridge") than like water.

Because of this resemblance between downslope winds and the drainage of a viscous liquid, it is relatively easy to have an intuitive feeling for downslope winds. Unfortunately, this is not the case for upslope. Fluid parcels heated at the surface have a tendency to rise vertically (i.e., antiparallel to the gravity vector), but the rising parcels never encounter a solid surface as do the cold, sinking parcels in downslope. One could argue that the stable nocturnal inversion "lid" acts as a solid surface, inhibiting the further rise of warmer parcels and deflecting them up the slope. If this were the case, however, one would expect to see the maximum in the profile of horizontal upslope windspeeds to occur near the top of the upslope layer (at least in the upper half). But, when such a maximum is observed, it is almost always just above the surface, i.e., very low in the upslope layer. Thus, explanations of upslope which employ only the vertical balance of forces are insufficient, since they do not describe how vertical momentum is turned into horizontal momentum. An example of this kind of explanation, though somewhat disguised through the use of a co-ordinate transform, is that of Prandtl (1942), which is described by Defant (1949, 1951).

Most plausibly, upslope is a baroclinic phenomenon. Wenger (1923) successfully applied Bjerknes' circulation theorem to a triangular region near a heated slope to determine upslope accelerations [this was briefly reviewed by Thyer (1966)]. In even simpler terms, the situation can be described as follows: During the transition from nighttime downslope to morning upslope, there is a pressure surface which is nearly level, called p_o on Fig. 2.2, which is coincident with the level surface

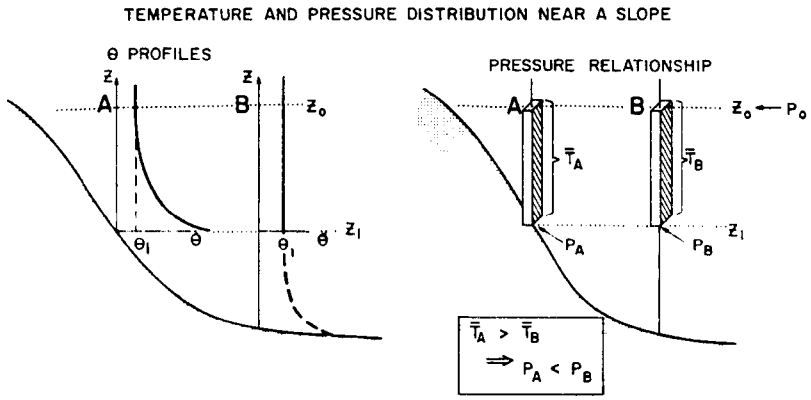

Figure 2.2: Potential temperature profiles, and corresponding pressure values, in two columns of atmosphere near a slope. Assuming normal unstable boundary layer structure (i.e. CBL structure) over the slope, and assuming that the mean CBL potential temperature is θ_1, the θ profiles below point A and point B, and between level z_o and level z_1, will be as shown in the left-hand diagram. The column below A, containing warm air from the surface layer next to the slope, has a higher mean potential temperature, and thus a higher mean temperature, than the column below B. The hydrostatic pressure at the base of the A column is therefore less than that at the base of the B column, as shown in the right-hand diagram. This indicates a pressure force directed toward the slope.

z_o. We choose a point A on p_o which is nearer to the heated slope, and a point B, which is farther away. From each point, we integrate downward hypsometrically (hydrostatically) to obtain the pressure at level z_1, which is at the earth's surface for column A. The mean temperature in

column A, being closer to the slope, is warmer than in column B, so p_A (the pressure below A) is less than p_B (the pressure below B). Thus, the horizontal temperature gradient gives rise to a horizontal pressure gradient. The pressure gradient, in turn, produces an acceleration toward the slope, i.e. in the slope direction. Since the vertical temperature lapse rate is largest next to the surface, the largest horizontal temperature differences - and thus the largest horizontal pressure gradients - will occur closest to the surface. However, surface-based friction is also greatest at the ground, so any maxima in the upslope wind profile should be just off the ground, low in the upslope wind layer, as observed.

Incidentally, the same argument applies in reverse for downslope flow. Although the intuitive argument presented above seemed to indicate a gravitational or "buoyancy" explanation, a major contribution to the downslope acceleration of the drainage winds must be the establishment of a baroclinic pressure gradient force directed away from the slope.

2. Mountain-valley winds

The slope winds described in the previous section can occur over relatively large mesoscale areas - several tens of kilometers to several hundreds of kilometers - in situations where there are long, linear ridges of mountains. More often in mountain meteorology, however, slope winds have been discussed in the context of a mountain valley, where they are comparatively small-scale phenomena; upslope winds are a relatively thin (100-300 m depth) layer of air moving up the sidewalls of a valley, while downslope is a still thinner layer of air draining down the sidewalls. Thus, slope winds in a valley operate on a scale considerably smaller than the valley itself. The wind systems which occur on scales

comparable with the size of the valley are the mountain-valley wind systems. The daytime valley ("upvalley") wind blows into the valley from the adjacent plains, while the nighttime mountain (or "downvalley") wind blows down the valley toward the plains.

The theory for mountain-valley winds was described by Wagner (1932, 1938). He hypothesized that there was a certain level, which he called the "effective ridge height", at which the constant pressure surface is horizontal. This height is generally about the height of the nearby ridges. Below this height, the amplitude of the diurnal temperature variation - at any level - is greater over the mountains than over the plains, i.e., the air over the mountains is warmer during the day and colder at night than the air at the same level over the plains. This effect is due in part to the fact that the total mass of air to be warmed or cooled is less over the mountains than over the adjacent plain, when one considers volumes of equivalent cross-sectional area below "effective ridge height." As was the case for the slope winds, the valley-to-plain horizontal temperature gradient implies a hydrostatic horizontal pressure gradient, which produces a relative low over the valley (compared with the plain) during the day and a relative high at night; these pressure gradients in turn produce upvalley acclerations of the winds during the day and downvalley accelerations at night. Moreover, because of the nature of this explanation, up- and down-valley winds would be produced even if the floor of the valley were level, i.e. did not slope up towards the mountains.

A number of studies, some of them summarized by Wagner (1938), have validated this theory. They found that an "effective ridge height" as defined does in fact exist, and that the magnitude of the diurnal temperature variation is often more than twice as great over the mountains as over the plains. The valley-plain temperature (and pressure) difference increases from zero at effective ridge height to a maximum at the ground.

3. The Wagner-Defant model

Since both the slope wind systems and the mountain-valley wind systems occur in the same valley, it remains to describe how they interact. The theory describing these processes was presented by Wagner (1932, 1938), later to be summarized in a now-famous illustration by Defant (1949, 1951). According to this theory, the slope winds precede the mountain-valley winds in the diurnal cycle, and they also rearrange mass in the valley. In this way, they help to set up the valley-scale pressure gradients which lead to the establishment of mountain or valley winds.

More specifically, after sunrise the sunlit slopes of the valley begin to heat. The bulk of the air over the valley is still cold, so that the pressure continues to be relatively high there and the valley-scale winds continue downvalley. Despite this, upslope flow develops along the warming valley sidewalls. The evacuation of mass from the air over the valley by this upslope flow (and its replacement by warmer air from above), combined with increasingly intense heating of the air, produces a decrease in pressure over the valley. As this pressure drop continues, the pressure difference between valley and plain equalizes, and the downvalley wind ceases. As these processes, including the upslope winds along the sidewalls, continue through the morning, the valley pressure continues to drop relative to the plain, and the

winds begin to blow up-valley. The entire process culminates when the intense heating of the slopes desists in the afternoon, shutting off the upslope flow up the sidewalls, leaving only upvalley flow in the valley.

At night, of course, the opposite occurs. Cooling along the slopes and at the valley bottom produces drainage and down-valley winds in a manner analogous to the process just described for upslope. For further details on these processes, the reader is referred to the review article by Defant (1951), or just about any of the other papers referenced in this section.

4. Other processes observed in the mountains

The theory described in the previous sections gives a good general framework in which to envision the organized wind systems in the mountains. However, the interaction of winds with mountains is a very complex phenomenon, and things do not always work the way the theory predicts. There are many important processes which the theory does not consider. Among them, the theory does not take into account the thermal structure (stability) of the atmosphere in and above the valley. Another important consideration is the topographical geometry of each valley in which observations are made. Additionally, the theory essentially considers only a "valley in a box", i.e., a valley isolated from gradient winds or larger-scale weather systems. Any of these effects can have a major impact on how the mountain wind systems develop. In developing theories of how the valley atmosphere interacts with the large-scale atmosphere, it is of interest to consider other flow phenomena in the mountains which have been reported in the literature. Therefore, in the following section, a variety of features and effects that have been observed in flow over the mountains will be mentioned.

One of the most important effects on the development of local wind systems in mountain valleys is the topographical geometry of the valley itself. For example, in his validation of his model, Wagner (1938) points out that the mountain-valley breezes are less well-developed in shorter, shallower valleys. In long, deep valleys, however (such as the Inn valley in Austria), the mountain-valley wind systems are always well developed — in the absence of overriding synoptic weather systems. Apparently the longer and deeper the valley, the better developed are the valley wind systems.

Other variations of topography in and around a valley can produce interesting results. For example, rugged terrain features in the mountains can produce localized eddies of various kinds which affect the mean flow in the valley. Using oil fog for flow visualization in a mountain canyon, Start el al. (1975) found three mechanisms by which "enhanced mechanical turbulence" is produced: interaction of gradient-level flow with the ridge tops, flows originating in side (or "feeder") canyons interacting with flow in the main canyon, and wake effects of flow around obstacles and around other topographic variations within the valleys. Ridgetop effects have been observed as an enhancement of turbulence downstream from a ridge (Davidson, 1963; Raymond and Wilkening, 1980) and as the formation of an organized, counter-rotating eddy [Start et al. (op. cit.), Ficker (1913)]. Side canyon effects have been observed by MacHattie (1968) and start et al. (op. cit.). Finally, Geiger (1965) has noted the effects of valley constrictions on drainage winds, while Start et al. found unexpected transport patterns of their tracer substances in the wake of rugged topographical features. Based on their diffusion and flow

visualization studies, Start et al. conclude the following about classic ridge-valley flow models:

> ...canyon winds seldom behave in as uncomplicated a way as air flows described by simple models of density flows. Instead, the air is in a highly disrupted or turbulent state — a state in which air flows may have really been on the average as described by simple mountain-valley circulations, but with an enhanced turbulent state.

Places where different wind systems oppose each other produce interesting flow situations. Defant (1951) reviews the Maloja effect, in which more intense wind systems from a larger valley reach over a pass to produce apparently anomalous winds in a second, smaller valley. Wagner (1938) discusses a similar case, but in this case the wind system coming over the pass does not reach the ground in the second, smaller valley. Wilkens (1955) describes a case where there is a mountain range at the head of a valley, running perpendicular to the axis of the valley. Because of the diurnal phase difference between the slope wind systems and the mountain-valley wind systems, the downslope winds start down the slopes of the mountain range in the evening before the up-valley winds cease, and the upslope winds start in the mountains in the morning before the down-valley winds cease in the valley. These result in regions of convergence and divergence, respectively, and since the slope winds override the valley winds, a very strong vertical wind shear zone occurs at the boundary between the two air masses. Wilkens presents an interesting series of pictures showing how this shear zone affects the dispersion of smoke from a smoke bomb.

Departures from the Wagner-Defant model also occur when one of the slopes in a valley remains shaded after sunrise, while the other is insolated. Gleeson (1951) showed that this should lead to a cross-valley

circulation, while Hewson and Gill (1944) showed that downslope flow continues on the shaded slope while upslope and upvalley winds develop in other regions of the valley.

Variations of the Wagner-Defant model have been described by a number of studies which have found "afternoon wind" systems. Two types of afternoon winds were noted by Schroeder (1961) in a study in which mountain-valley wind systems seemed to interact with seabreeze effects in Southern California. Using averaged wind data, MacHattie (1968) found evidence of an afternoon wind system in a valley in southwestern Alberta. He attributed the appearance of these winds to the downward mixing of gradient-level winds. Banta and Cotton (1979, 1981) presented case studies which similarly showed an afternoon wind system; these results will be discussed later in this dissertation.

The influence of larger-scale processes — strong gradient-level winds and large-mesoscale to synoptic-scale pressure gradients — is another important (even if obvious) effect. Geiger (1965, p. 401) shows that strong foehn winds and frontal passages can interrupt the cold air drainage into a sinkhole. Cramer and Lynott (1970) show an instance where a large-scale pressure gradient prevents local-scale winds from forming. They present mesoscale analyses of the development of a heat trough in southwestern Oregon. Their surface potential temperature analysis for the afternoon of 5 July 1960 shows a valley east of Corvallis, Oregon where strong pressure-gradient winds overwhelm the local-scale forcing. The actual winds are easterly, downvalley winds aligned with the pressure force, instead of westerly, upvalley flow which would be expected at that hour of the day in a west-facing canyon. (Farther south, the exact location of the trough is in doubt, so the surface winds do not show this behavior). This

paper and others [e.g., Schroeder (1961), Schroeder and Fosberg (1966)] describe interactions between ridge-valley wind systems and another mesoscale flow phenomenon, the west coast seabreeze.

Many features of heated flow in and among mountains have been investigated using aircraft data. Some of these studies have involved flow over an isolated range of mountains surrounded by plains [Braham and Draginis (1960), Raymond and Wilkening (1980)], while others have described flow over a ridge [Fosberg (1969), Hahn (1980)]. The studies of isolated mountains were conducted during morning hours and revealed a "convective core" just downwind of the highest peaks. This core had a nearly-neutral (dry adiabatic) temperature lapse rate and consisted of air which was rising in the mean. Although the horizontal dimension of the core was about the width of the mountain ranges concerned, i.e., 15-20 km or more, individual updrafts and downdrafts were only 3-4 km across. These smaller, more intense updrafts were what led to the formation of cumulus clouds. Braham and Draginis (1960) hypothesized that valley breezes were important in forcing these updrafts, while both they and Raymond and Wilkening (1980) discussed the importance of the mountains as a "high-level heat source" in forcing low-level convergence about the mountain range.

The aircraft observations of airflow over a ridge presented by Fosberg (1969) reinforce earlier observations based on pibal and rawinsonde observations (Fosberg, 1967). These observations, taken in the presence of large-scale subsidence, weak gradient-level winds, and the California seabreeze, showed the development of a "hot cap" and a "convective chimney" over the ridge. Fosberg also interpolated his data to a rectangular grid, diagnostically analyzed the vorticity and stream function fields in the vertical (x-z) plane, and evaluated some of the terms in the vorticity

equation, including half of the solenoid term (the part with the horizontal temperature gradient)*. His analysis of this part of the solenoid field revealed a solenoid "cell" (i.e., maximum) which started out below the walls of the canyon which ran up to the ridge, later to move toward the ridge and upward in agreement with the movement of the main organized updraft. This agreement suggests that the upslope and updrafts result from a thermally-driven direct cell.

Aircraft cross sections of flow over the Mosquito Range west of South Park and the associated boundary-layer structure were presented by Hahn (1980). Hahn's study, which was also based on data from SPACE-77, included analyses of two moist days and two dry days. These analyses included cross sections of potential temperature, water-va;or mixing ratio, turbulent kinetic energy (TKE), and certain terms in the TKE equation which could be evaluated from aircraft data. Some of Hahn's results from the dry days, which are also the subject of this dissertation, will be described later where appropriate.

The purpose of the preceding section has been to give some appreciation for the diversity of flow-related phenomena which have been observed in the mountains. Some of these phenomena have included effects of topography, effects of gradient winds and large-scale pressure gradients, and the presence of localized updrafts over mountains. In the next section, some effects of thermal stratification and the pooling of cold air will be considered.

---

* This term is the entire solenoid term if the x-z vorticity equation is derived from a Boussinesq set of equations, but it is only half of the solenoid term if one strats with primitive equations.

5. Nocturnal cold pool dissolution

Cold air which drains off the slopes at night accumulates in the low areas of a valley. Geiger (1965, pp 396 ff) and Yoshino (1975, pp 425 ff) discuss studies which characterize these accumulations as pools or "lakes" of cold air. Vertical temperature profiles through this cold air pool reveal that strong nocturnal inversion. Thus, the existence of a cold air pool implies a certain thermal structure which occurs while drainage winds are taking place.

The establishment of a daytime boundary layer over the mountains involves the erosion of this nocturnal inversion layer, i.e. the dissolution of the cold pool. Several mechanisms have been proposed by which this could occur. Davidson and Rao (1958) and Ayer (1961) argued that, as the ground heats during the morning, enhanced thermal and mechanical turbulence is produced at the mountain tops and advects over the valley. They hypothesized that mixing, caused by this enhanced turbulence at the top of the cold pool, eats away at the cold pool from above. This explained the observed behavior of the inversion layer, which was that the top of the inversion layer descends with time as heating progresses. Whiteman and McKee (1977) and Whiteman (1980) proposed another mechanism for the inversion descent. According to their theory, upslope air escaping up the sidewalls of the valley leads to a divergence of mass in the center of the valley just above the valley floor. To maintain mass continuity, this low-level mass divergence must produce a subsidence of the cold air over the center of the valley. This process continues until all the cold air sinks, is heated and is evacuated up the sidewalls -- or, as sometimes happens, until the heating stops in late afternoon. Using a version of the

CSU Cloud/Mesoscale model somewhat simular to the one described in Chapter VI of this thesis, Bader (1981) gave further support to many of Whiteman's ideas. However, while Whiteman seemed to envision this process as more or less continuous, recent numerical simulations by Bader (1981) indicate that the process occurs in pulses, because of the turbulent structure of the flow and the presence of gravity waves in the stable inversion layer.

A different mechanism was proposed by Lenschow et al. (1979), who studied the dissolution of cool pockets which formed at night in topographical depressions in the relatively flat terrain of the high plains of eastern Colorado. They found that when a certain "slope Richardson number" exceeds its critical value, the turbulent drag force (Reynolds' stress) at the top of the cold air layer is sufficient to pull the cold air out of the depression. Once the cold air is out of the depression, it mixes with the turbulent air above, and thus the cold-pool air is dissolved. The air replacing the cool air in the depression is warm air. In addition to their studies over relatively flat terrain, Lenschow et al. used some of our South Park data to show that a similar phenomenon occurs over the mountains.

6. Observations of convective boundary layer structure over mountainous terrain

The occurrence of a well-mixed, dry adiabatic, convective boundary layer over the mountains has been documented in a number of studies. Holzworth (1964, 1979) noted the frequent presence of a very deep afternoon mixed layer (greater than 3 km AGL) over the western U.S. Raymond and Wilkening (1980) also report that the depth of the afternoon boundary layer over New Mexico frequently exceeds 2 km. above the mountain tops and 3 km. above the adjacent plain. Cramer and Lynott

(1961) analyzed cross sections which showed the presence of a deep, dry adiabatic convective layer, which resembled a CBL over horizontally-homogeneous terrain. Subsequent studies of theirs [Cramer and Lynott (1970), Cramer (1972)] showed that CBL structure is a common feature in the daytime boundary layer over the mountains. In the valleys which they studied, Whiteman and McKee (1977, 1978) and Whiteman (1980) found CBL structure beneath the stable nocturnal inversion layer after morning heating had started.

7. Summary of mountain-valley wind systems

The purpose of Section A has been to provide an overview of flow phenomena which have been observed to occur in mountainous terrain. The most straightforward phenomena discussed were the traditional slope and mountain-valley wind systems. Other processes which affect flow include geometrical terrain effects, such as obstacles, side canyons, and shaded slopes, and the effects of the larger-scale weather systems, including upper-level winds and pressure gradients. The presence of updrafts produced by solar heating of elevated mountainous terrain is another important observation of flow in the mountains, since these updrafts lead to cumulus cloud formation. Finally, observed aspects of the vertical thermal structure over the mountains were discussed, including observations of the nocturnal inversion layer or cold pool and observations of CBL's over the mountains.

The overall purpose of this study is to further investigate the relationships between the thermal structure and the flow processes which occur in the mountains. Since the thermal structure involves the structure of the boundary layer over the mountains, we must first consider

the observed structure of the boundary layer over flat terrain, as there already exists a considerable literature on that subject.

B. The Convective Boundary Layer Over Flat Terrain

The convective boundary layer (CBL) as discussed in this paper refers to a turbulent, well-mixed layer adjacent to the earth's surface, in which the turbulent processes are driven by heating at the surface. As shown in the profiles presented in Fig. 2.1, the strong vertical mixing in a CBL tends to produce values of horizontally-averaged potential temperature, mixing ratio, and momentum that are constant with height [Tennekes and Driedonks (1981), Betts (1973, 1974) and Deardorff (1974a, 1978) among other have presented such proviles based on observations]. A review of boundary-layer structure and processes which are relevant to the current study is presented in Appendix A. The purpose of this section is to briefly summarize the important points that are discussed in greater detail in Appendix A.

Studies of the CBL can be divided into two general approaches: those describing the large-eddy structure of the CBL and those describing the vertical structure of the CBL, which is assumed to be horizontally homogeneous. For most convective situations over land, the large eddies are called "thermals" or "plumes". The following properties of plumes have been described by Priestly (1959), Warner and Telford (1963, 1967), Kaiwal and Businger (1970), Wilczak and Tillman (1980), and Lenschow and Stephens (1980). Thermals have been identified on high-resolution Eulerian temperature traces as "ramps" or regions of elevated but highly variable temperature, interspersed among quiescent regions of relatively uniform temperature. Inside the thermals, fluctuations in vertical velocity are highly correlated with the temperature fluctuations, so

that the thermals are a mechanism by which the atmosphere transports heat upwards. The lapse rate within the thermals is superadiabatic, but outside, it is dry adiabatic down to very close to the ground. The structure of thermals varies with height. Very close to the ground the temperature fluctuations are highly random and disorganized, with little tendency to form "disturbed" and "quiescent" regions. A little higher, the fluctuations organize into disturbed regions which are tens of meters across, while still higher these disturbed regions or thermals merge and coalesce into structures which ultimately become hundreds of meters in diameter in the central portions of the CBL. Since a highly disorganized layer exists between the earth's surface and the level where thermals have a distinct structure, Warner and Telford (1967) concluded that thermals do not necessarily originate at identifiable terrain irregularities.

The second approach to studying the unstable boundary layer was to describe the vertical structure of the horizontally-homogeneous CBL. If one assumes that the properties of the field of thermals are homogeneous in the horizontal, then one can form stable horizontal averages of meteorological quantities at many vertical levels. As discussed above, the vertical profiles in the main part of the CBL for θ, q, and u tend to be constant with height. The top of the CBL is marked by a temperature inversion, with the inversion height denoted z_i, and above this convective inversion is the "free atmosphere" with a stable θ-profile and gradient winds. The lowest approximately 10% of the CBL (i.e., from the surface up to around 0.1 z_i) is the "constant-flux" or "surface" layer. The mean-θ profile in the surface layer is superadia-

batic (unstable), moisture generally decreases with height there, and u increases with height from a value of zero very close to the ground.

The diurnal cycle of the θ-profile results from heating at the ground during the day and cooling at night. These processes have been described, e.g., by Deardorff (1974a, 1978), Coulman (1975a, 1980) and Kaimal et al. (1976) Figure 2.3 shows the cycle, starting with late

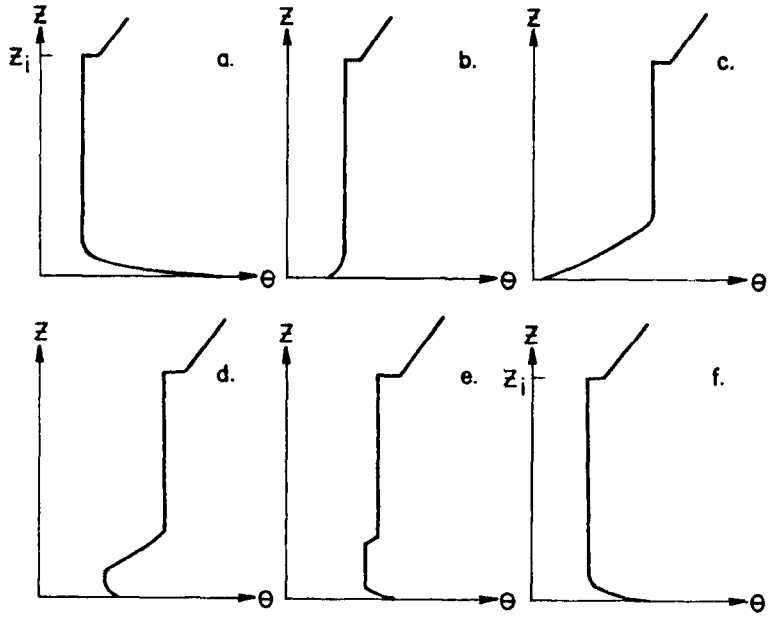

Figure 2.3: Diurnal cycle of the potential temperature profile. See text for discussion.

afternoon on one day and ending with the afternoon of the next day. In late afternoon (profile a) the nearly-neutral CBL extends to z_i, the height of the capping inversion at the top of the CBL, which is usually 1-2 km over land in midlatitudes. As the surface cools in the evening, a shallow inversion forms at the base of the neutral layer (profile b). Cooling continues during the night, and the nocturnal inversion layer deepens (profile c). After sunrise the next morning,

the surface heats and a shallow CBL forms at the base of the nocturnal inversion layer (profile d). As surface-based heating persists, the shallow CBL deepens (profile e), until finally the nocturnal inversion is completely eroded, and the turbulent CBL rapidly grows to the top of the neutral layer (profile f).

III. THE SOUTH PARK EXPERIMENT: TERRAIN AND INSTRUMENTATION

Scientists from Colorado State University and several other institutions conducted a field project in the Colorado mountains in July and August of 1977. The location of the project was South Park, a broad basin between the Mosquito Range and the Front Range of the Rocky Mountains centered about 100 km southwest of Denver. The Base Site for this project was located about 9 km south of the town of Fairplay, Colorado. The project was called the South Park Area Cumulus Experiment of 1977, or SPACE-77.

The purpose of SPACE-77 was to investigate the initiation, development, and propagation of cumulus congestus and cumulonimbus clouds in the mountains and the subsequent organization of these clouds into mesoscale systems. Another objective of this overall endeavor was to study aspects of the mountain boundary layer (which becomes the sub-cloud layer when clouds form) and the dry-convective mesoscale circulations which contribute to the initiation, grwoth and movement of cumulus clouds. A third objective was to provide data for developing and testing numerical models of the boundary layer, cumulus clouds, and mesoscale systems over mountainous terrain. The current study is aimed at achieving the last two objectives.

The instrumentation used in this study includes rawinsonde, a Tethersonde* tethered-balloon sounding system, the Portable Automated

* Tethersonde is a registered trademark of the Atmospheric Instrumentation Research Co. of Boulder, Colorado.

Mesonet (PAM) system [developed by the Field Observing Facility (FOF) of the National Center for Atmospheric Research (NCAR), Boulder, Colorado], the NCAR Queenair aircraft, and micrometeorological towers equipped with UVW anemometers and thermistors. Later in this chapter several of these instrumentation systems will be discussed in greater detail. First, however, the topography of South Park and some of its implications for the behavior of local wind systems in the Park will be discussed.

A. Terrain of South Park

The dictionary defines a mountain "park" as a "level valley between mountain ranges", but a more precise definition would be "a broad, flat-bottomed basin surrounded by mountains"*. Thus, South Park is a relatively wide park - approximately 50 km west to east - in the Colorado Rockies. Figure 3.1 is a topographical map of South Park with the mesonet (PAM) stations indicated by the numbered dark circles (and a star for the Base Site). The higher terrain surrounding the Park is shaded, while the low-lying river valleys which drain to the east are cross-hatched. Our areas of interest are the valleys of the South Platte River and its tributaries, several of which flow through the region indicated by the dashed rectangle on Fig. 3.1. This rectangle encloses six PAM stations, and this region will be referred to as "central South Park". The streams flowing through central South Park flow from the north-northwest (NNW) toward the south-southeast (SSE). Thus, upslope or upvalley winds in this rectangle are generally from a southerly through easterly direction, while downslope or downvalley winds blow from the north or from the west.

---

* The former definition is from Webster's Third New International Dictionary - Unabridged (B.C. Merriam Co., Springfield, Mass., 1966). the latter definition came from an anonymous reviewer of a paper which we submitted for publication.

III. THE SOUTH PARK EXPERIMENT: TERRAIN AND INSTRUMENTATION

Scientists from Colorado State University and several other institutions conducted a field project in the Colorado mountains in July and August of 1977. The location of the project was South Park, a broad basin between the Mosquito Range and the Front Range of the Rocky Mountains centered about 100 km southwest of Denver. The Base Site for this project was located about 9 km south of the town of Fairplay, Colorado. The project was called the South Park Area Cumulus Experiment of 1977, or SPACE-77.

The purpose of SPACE-77 was to investigate the initiation, development, and propagation of cumulus congestus and cumulonimbus clouds in the mountains and the subsequent organization of these clouds into mesoscale systems. Another objective of this overall endeavor was to study aspects of the mountain boundary layer (which becomes the sub-cloud layer when clouds form) and the dry-convective mesoscale circulations which contribute to the initiation, grwoth and movement of cumulus clouds. A third objective was to provide data for developing and testing numerical models of the boundary layer, cumulus clouds, and mesoscale systems over mountainous terrain. The current study is aimed at achieving the last two objectives.

The instrumentation used in this study includes rawinsonde, a Tethersonde* tethered-balloon sounding system, the Portable Automated

* Tethersonde is a registered trademark of the Atmospheric Instrumentation Research Co. of Boulder, Colorado.

Mesonet (PAM) system [developed by the Field Observing Facility (FOF) of the National Center for Atmospheric Research (NCAR), Boulder, Colorado], the NCAR Queenair aircraft, and micrometeorological towers equipped with UVW anemometers and thermistors. Later in this chapter several of these instrumentation systems will be discussed in greater detail. First, however, the topography of South Park and some of its implications for the behavior of local wind systems in the Park will be discussed.

A. Terrain of South Park

The dictionary defines a mountain "park" as a "level valley between mountain ranges", but a more precise definition would be "a broad, flat-bottomed basin surrounded by mountains"*. Thus, South Park is a relatively wide park - approximately 50 km west to east - in the Colorado Rockies. Figure 3.1 is a topographical map of South Park with the mesonet (PAM) stations indicated by the numbered dark circles (and a star for the Base Site). The higher terrain surrounding the Park is shaded, while the low-lying river valleys which drain to the east are cross-hatched. Our areas of interest are the valleys of the South Platte River and its tributaries, several of which flow through the region indicated by the dashed rectangle on Fig. 3.1. This rectangle encloses six PAM stations, and this region will be referred to as "central South Park". The streams flowing through central South Park flow from the north-northwest (NNW) toward the south-southeast (SSE). Thus, upslope or upvalley winds in this rectangle are generally from a southerly through easterly direction, while downslope or downvalley winds blow from the north or from the west.

---

* The former definition is from Webster's Third New International Dictionary - Unabridged (B.C. Merriam Co., Springfield, Mass., 1966). the latter definition came from an anonymous reviewer of a paper which we submitted for publication.

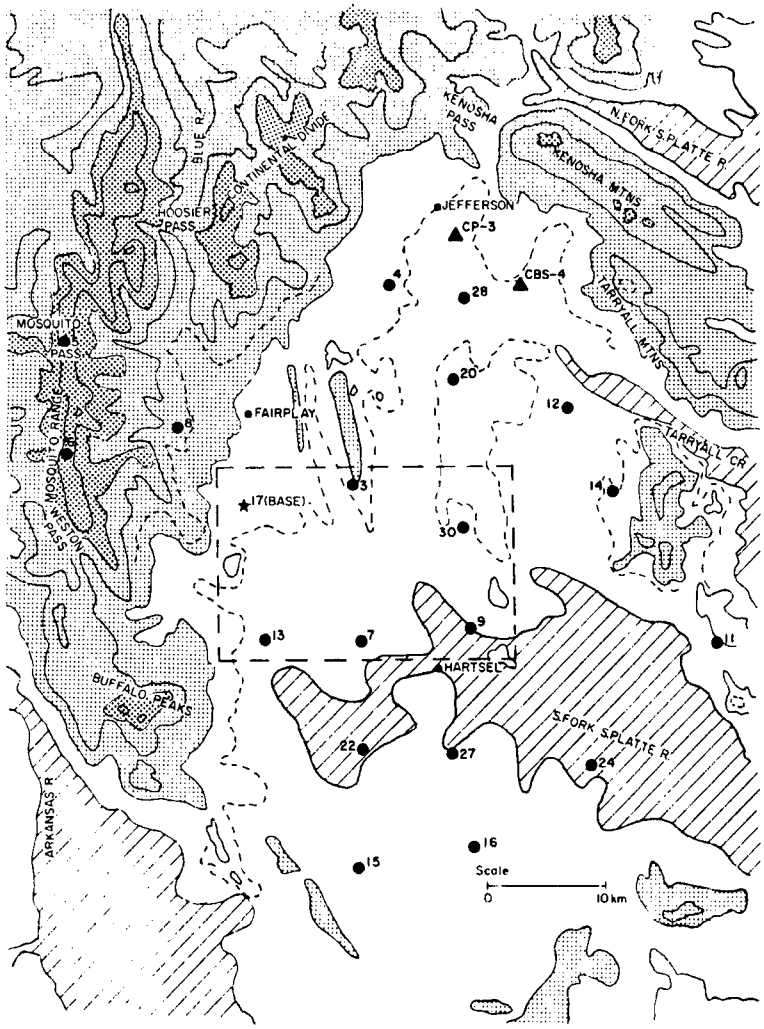

Figure 3.1: Topography map of South Park, Colorado. Regions below 9000 ft. (2744 m) are cross hatched; regions above 10,000 ft. (3049 m) are lightly shaded; and regions above 12,000 ft. (3659 m) are heavily shaded. The base site is indicated by a star, and two of the microwave radar sites, by triangles. The dark numbered circles represent the locations of the 20 PAM stations used in SPACE-77.

The Base Site was established on the east-facing slope leading up to the Mosquito Range. Several instrumentation systems were located at this Base Site, including the rawinsonde and tethersonde launching sites, the communications trailer for the PAM (Portable Automated Mesonet), the micrometeorological towers, ground communication for

the aircraft, and other systems which participated in SPACE-77, such as a lidar from NOAA (see Danielson and Derr, 1978). The ridges of this range reach over 4000 m elevation, so the drop in elevation from the ridgetops to the floor of South Park exceeds 1 km. A small stream, Four Mile Creek, flows southward less than 2 km east of the base site. The creek then turns southwestward and flows just east of PAM Station 7 before joining the South Fork of the South Platte River near the town of Hartsel. The significance of these terrain characteristics in determining the wind flow fields will be discussed in later chapters of this paper.

B. Instrumentation Used in This Study

The instrumentation described in this section includes the PAM system, the Tethersonde, the NCAR Queenair, and the micrometeorological tower systems.

1. Portable automated mesonet (PAM)

NCAR's PAM, or Portable Automated Mesonet, is a system of surface meteorological observing stations which are linked to a main base station by radio. The remote observing stations are each equipped with dry- and wet-bulb thermistors, an aneroid pressure sensor, a wind vane and a cup anemometer mounted at 4 m, a tipping bucket rain gauge, and a transmitter with a directional antenna mounted at a height of 15 m. Output from each sensor was sampled once per second, and then every minute a 60-sec average was computed. These 1-min averages from each sensor were then relayed to the base site every minute. Thus, meteorological data from the PAM are available at intervals of 1 minute. Further discussion of the technical aspects of the PAM is given by Brock and Govind (1977).

A very useful feature of the PAM is the ability to obtain mesoscale data and analyses in the field. Many of the PAM illustrations in this paper are based on hard copies which were made in the field. Some aspects of the usefulness of the PAM in South Park are described by Cotton and George (1978).

2. Tethersonde system

Tethersonde is a trademark for a tethered balloon atmospheric sounding system manufactured by Atmospheric Instrument Research Co. of Boulder, Colorado. The principal components of the system are an airborne instrument package with a radio transmitter, a blimp-shaped, helium-filled balloon, a ground station with a radio receiver and a data recorder, and an electric winch to let out or pull in the tether line. The airborne package measures pressure, dry- and wet-bulb temperature, and wind direction and speed. The data are sampled in succession as instantaneous values over a data cycle of 20-30 sec. A discussion of the technical aspects of this system was given by Morris et al. (1975). Additionally, Whiteman (1980) performed several tests on the operational characteristics of the system as a whole.

Pressure is measured by a small aneroid transducer located inside the plastic instrument package. Atop the package is a tube-shaped radiation shield ventilated by a fan. Two matched bead thermistors, one for dry-bulb and one for wet-bulb temperature measurement, are located inside the tubular shield. Although the time constant for the thermistors themselves was 10 s according to manufacturer's specifications, Whiteman (1980) found the time constant of the entire system to be somewhat longer - 13 s with nearly fully-charged batteries in the airborne package, to 18 s when the batteries became weak. The accuracy of these thermistors was reported

to be $\pm 0.5^{\circ}C$, although Whiteman found somewhat higher discrepancies ($0.8^{\circ}C$) above $20^{\circ}C$.

The winds are measured by a cup anemometer and a magnetic compass needle. The anemometer is rather sensitive, with a reported accuracy of ± 0.25 m/s. Determination of wind direction depends on the fact that the blimp-shaped balloon orients itself so that it faces into the wind. The instrument package, which is prevented from twisting by a relatively rigid rigging configuration, contains a movable magnetic compass needle in conjunction with a potentiometer that remains fixed relative to the instrument package. As noted in both references cited above, we also found the balloon to be a good indicator of wind direction except when a wind direction shift of large magnitude (i.e., near 180°) occurred. In this case the balloon would drift overhead maintaining its original orientation until the tether line became tight - only then would it swing around to the new wind direction.

The height of the balloon was determined hydrostatically from pressure and temperature data. Since the boundary layer was heating up during the soundings, this can produce an error in the computed height values. To keep these errors small, the soundings presented in this paper are of relatively short duration, and in both the up soundings and the down soundings, heights were integrated upward from the ground.

3. NCAR Queenair aircraft

The NCAR Queenair 304-D was flown on selected days in July during SPACE-77 to obtain mean and fluctuating values of wind velocities, pressure, temperature, and humidity. The aircraft flights were mostly performed on days when there was significant cloud activity, but there were three dry days when data were taken: 18, 28, and 30 July.

The wind-measuring systems in the Queenair have been described in detail by Lenschow et al. (1978). Aircraft-measured air motion is determined from two instruments: an inertial navigation system (INS) which determines the aircraft's movement relative to the earth, and a gust probe which determines the movement of the air relative to the aircraft. These two systems are used to determine the mean horizontal wind and all three components of the turbulent wind velocities, as described by Lenschow et al. (1978):

> These components are obtained by subtracting the velocity of the airplane with respect to the earth measured by the INS from the velocity of the air with respect to the airplane measured by the gust probe sensors.

Each system contributes to the total wind-measurement error. The error due to the gust probes is less than ± 1 m/s, while the INS has a time-dependent error of less than ± 0.5 m/s per hour of flying time. Thus, as summarized by Hahn (1980), the aircraft-measured horizontal winds have a total error of less than $\pm(1.0 + 0.5\ t)$ m/s, where t is the flight time in hours. Since most flights were less than 2 hr, the largest error expected for any of the winds discussed in this paper is less than ± 2 m/s. The response frequency of the gust probe system was estimated by Lenschow et al. (1978) to be less than 4 Hz.

The aircraft temperature measurements used in this study were made with a 25 μm platinum resistance wire thermometer (Rosemount). Its error in clear air is $\pm 0.5^{\circ}C$ (Lenschow and Pennel, 1974), and the time constant is around 1 s because of heat exchange between the wire and its housing. For the analyses presented here it was not necessary to use the time-filtering function described by Wyngaard et al. (1978). Hahn (1980)

applied this correction to a sample leg of South Park data and found the adjustment to be negligible - the maximum error he found was 0.05°C. If we had been computing fluxes or other quantities that depend upon phase shifts and high-frequency response, however, it would have been necessary to apply the correction.

A major source for error in the temperature measurements are the unavoidable changes in altitude which occur along a flight leg. Unless the aircraft is penetrating a very stable layer (i.e., isothermal or temperature inversion), increases in altitude will produce lower temperatures, while decreases in altitude produce higher temperatures. These effects produce spurious horizontal temperature gradients along flight legs. However, since the aircraft measurements were taken mostly in regions of neutral static stability (i.e., dry adiabatic layers), using potential temperature nearly eliminates this source of error (Wyngaard et al., 1978). Thus, all aircraft cross sections given in this paper are in terms of potential temperature.

The humidity in this study was measured using a cooled-mirror dew-point hygrometer. The accuracy of the dew-point hygrometer is $\pm 1^{\circ}C$ above freezing and $\pm 2^{\circ}C$ below freezing. The response time of the instrument is limited by the fact that the sensor mirror can only be heated or cooled at a rate of $2^{\circ}C/sec$, so that step-changes in moisture are poorly sampled. When the data are averaged over several hundred meters of aircraft path, however, (as we have done in this study), this effect is minimized.

The aircraft altitude determinations were found by Hahn (1980) to be in error. Aircraft heights presented below have all been corrected

using Hahn's method, which involved matching the aircraft pressure with the rawinsonde's pressure, then using the rawinsonde-derived height.

Data were sampled at two different frequencies. Slower-response instruments, like the Rosemount temperature and dew-point hygrometer, were sampled at 1 Hz. Fast response instruments, like the air motion system, were sampled at 8 Hz. Since the Queenair generally flew at about 80 m/s, these translate to sampling distances of about 80 m and 10 m, respectively.

4. Micrometeorological towers

Two towers equipped with micrometeorological wind and temperature sensing instruments were operated at the base site. The larger tower was 23 m tall and had wind and temperature instruments at the top and at a height of 9 m. The smaller tower was about 15 m tall; this tower had wind and temperature instruments at the top, and a temperature sensor mounted on a boom at a height of 1 m above the ground. After 2 August, a bivane anemometer was also mounted on the smaller tower, at a height of approximately 4 m. Data from the taller tower are available from 18-20 July and 23 July to the end of the project (13 August). Data from the smaller tower are available from the evening of 29 July to the end of the project.

The wind-measuring instruments were three Gill UVW anemometers (R.M. Young Co., Model 27002). This instrument consists of three propeller anemometers with their axes mounted at mutual right angles, to measure the three orthogonal components of the total wind vector. McBean (1972), Horst (1973), Gill (1975), and Katen (1977) have discussed sources for error in

UVW-measured winds. The major source of error for winds greater than about 0.5 m/s (the threshold value below which the propeller does not turn is about 0.2 m/s) is the deviation of the response of the propellers from the theoretical cosine angular response function. The data in this paper have been corrected for non-cosine response in accordance with correction factors recommended by Gill (1975). A second source for error, as noted by Horst (1973) and Katen (1977) is propeller inertia, which affects higher frequencies. Since we were interested in mean values and variances (mean-square values), which are mainly affected by the longer wavelength eddies in the unstable surface layer, we did not correct the data for propeller inertia. Horst (1973) presented evidence that this could lead to significant errors in estimates of $\overline{w'^2}$ during stable or neutral conditions (e.g., measured values less than 85% of actual values for a 20 m tower during neutral stability conditions). However, this represents a "worst-case" situation in our study, since (1) the important observations in this paper were taken during unstable conditions, so that the important eddy frequencies were much lower and (2) the response for all the other variables (e.g., $\overline{u'^2}$, $\overline{v'^2}$, $\overline{u'w'}$) was much better than for $\overline{w'^2}$.

The response characteristics of the propeller anemometers used in the UVW are expressed by a distance constant, which was determined by the manufacturer to be 1.0 m. According to Gill (1975), "the instrument measures gust wavelengths of 12 m and greater with good accuracy".

Mean temperature and temperature gradients were measured using thermistors mounted in aspirated radiation shields. The thermistors used were made by Yellow Springs Instrument Co. (Thermilinear Component No. YSI 44212) and were specified by the manufacturer to be accurate and

interchangeable to within $\pm 0.1^{\circ}C$. Each thermistor system was mounted inside a radiation shield which was aspirated by an electric fan. Thus, the time constant for the entire system was relatively long, probably 5 to 10 sec. Since temperatures were averaged over several minutes at least in this paper, the exact value of this time constant is not important to the results.

One bivane anemometer (R.M. Young Co., Model No. 21002) was used during the last half of the experiment for qualitative measurements of the wind vector and for measurements of total wind speed and speed fluctuations. The bivane rotates in both azimuth and elevation so that the propeller always points directly into the wind; thus, it provides a good measurement of statistics related to total wind speed. However, Katen (1977) found that the vane did not respond well to fluctuations in elevation angles, especially at higher frequencies. Therefore, we have not performed any detailed analyses of the bivane data.

Thus, the instrumentation on the two towers consisted of three UVW anemometers, four thermistor systems, and one bivane anemometer. Data from these instruments were digitized in the field and recorded on magnetic tape at intervals of about 0.87 s. The entire data-gathering equipment was housed in a camper which sat on the back of a pick-up truck. Most of the tower wind instrumentation and data-acquisition equipment had been assembled by Dr. Paul C. Katen for his study of lead transport near highways (Katen, 1977).

IV. OBSERVATIONS OF LOCAL WIND SYSTEMS IN SOUTH PARK

In the following chapter analyses of the observations taken during SPACE-77 will be used to describe the mesoscale wind systems and the boundary-layer structure which occurred in South Park. The objective of this part of the study is to determine those flow processes which occur on a "typical dry day" in the summer in South Park. A typical dry day in this paper will refer to a day in which thermal forcing by local terrain features predominates in determing the low-level wind field, i.e. in which this local forcing is not overwhelmed by larger-scale pressure gradients or by circulations accompanying deep cumulus clouds.

A gross indicator ow whether a day was dry or not is the amount of precipitation which fell over South Park on that day. Fig. 4.1 shows the average amount of precipitation per station in millimeters, collected at all twenty PAM sites for each day from 11 July to 12 August. The time series can be divided into four general periods: a generally dry period from 11-18 July, a moist period from 19-27 July, a dry period from 28 July - 3 August, and a moderately moist but variable period from 4 August to the end of the project (12 Aug). During the first dry period, no boundary-layer data were taken, so this period has not been analyzed very intensively. During the next, wet period synoptic conditions were favorable for deep, precipitating systems to form on most days. One such day which has

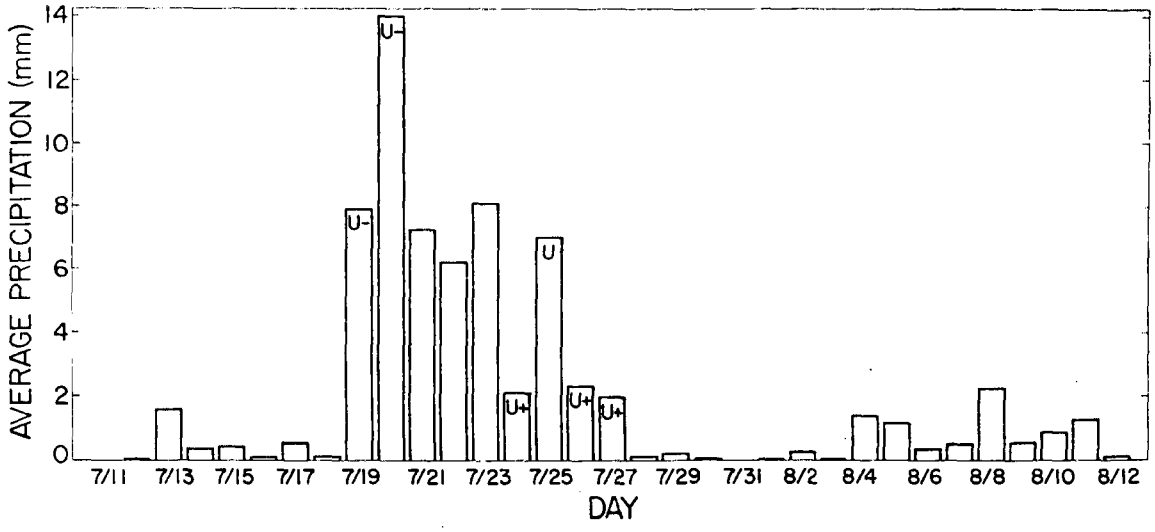

Figure 4.1: Average precipitation per site for each day of SPACE-77 as determined by PAM raingauges. U represents days when precipitation was underestimated because of equipment (power) outages which frequently accompanied thunderstorms. U- indicates a slight underestimate and U+, a large underestimate. Figure courtesy of Kevin Knupp.

been intensively analyzed was 19 July [George (1979), Cotton et al. (1982), Knupp and Cotton (1982a,b)]. The third period, which was very dry, provided several days which were well suited to investigating the dry local wind systems. The small amounts of precipitation which occurred on these days fell mostly in the hills at the eastern rim of South Park, so that the clouds which produced this precipitation had little effect on our area of interest in central South Park and in the South Platte valley (Knupp, personal communication). The final period consisted of many different kinds of days. August 4, e.g., was a severe weather day [George (1979), Cotton et al. (1982)], August 5 was moist and cloudy, while August 6, 7 and 9 were dry days during which the local wind systems were well developed. August 8 was an anomaly; even though storms which formed in South Park produced more rain over the PAM network than on any other day during this period,

the local wind systems which formed in the morning were more characteristic of a dry day. This day will be further discussed in a later section.

The real criterion for determining whether a day was a typical dry day or not is how the local-scale winds develop. The development of the winds at the surface is the subject of the next section. In the second and third sections, the vertical structure of these winds will be described using vertical soundings and vertical cross-sections of potential temperature. Finally, the fourth section focuses on the horizontal extent of the upslope wind layer and how this leads to a zone of convergence in the Park. This convergence zone is likely to be important in the initiation of convective clouds over the mountains.

A. Surface and Mesonet Observations of Local Wind Systems

The Wagner-Defant model for local winds in a mountain valley was discussed in Chapter II. According to this model, nighttime winds are downslope or downvalley, and after sunrise the winds reverse to upslope and then upvalley directions. Around sunset the winds reverse back to a downslope or downvalley direction. According to this theory, these wind systems are forced by cooling or heating at the earth's surface.

Both the downslope-downvalley types of wind systems and the upslope-upvalley types were observed on dry days in South Park. Additionally, a windshift was observed to occur in late morning or early afternoon from upvalley winds to winds which corresponded in direction with the upper level winds above the ridgetops. Because the upper level winds on dry days were generally from a westerly direction, these winds have been called the "afternoon westerlies" (Banta and

Cotton, 1979, 1981). In the following section surface observations of these various wind systems using PAM data will be presented.

Surface mesonet charts for three wind systems on 9 August are shown in Fig. 4.2. Early morning downslope winds can be seen in the

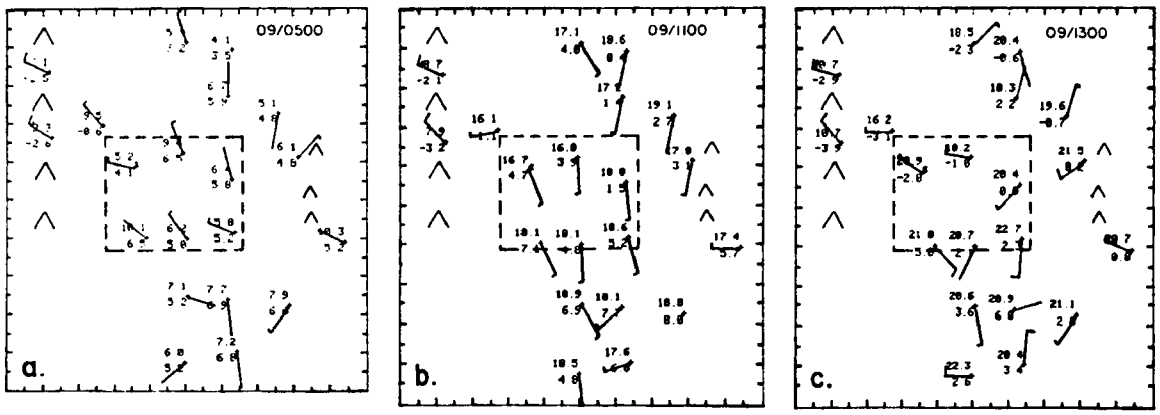

Figure 4.2: PAM surface charts showing three wind regimes on 9 August. (a) Drainage flow in the central South Park rectangle, (b) upslope regime flow, and (c) afternoon westerlies in the northwest sector of the rectangle. Temperatures and dew points are in ^{o}C, and wind speeds are indicated as follows: a half barb indicates 5 kt. (2.5 m/s), and a full barb indicates 10 kt. (5 m/s).

central South Park rectangle in Fig. 4.2a (recalling from Fig. 3.1 that downslope winds are from a northerly through westerly direction, while upslope winds are southerly through easterly). Fig. 4.2b shows southerly upvalley winds at 1100 in the morning. Later, Fig. 4.2c shows strong westerly winds in the northwest corner of the rectangle at 1300 in the afternoon. These winds were drier than the upslope winds elsewhere in the Park, and they represent the afternoon westerlies referred to earlier.

Fig. 4.3 shows time plots of the wind direction and speed, temperature, and mixing ratio at the Base Site for 9 August. The Base Site, located in the northwest corner of the rectangle, is indicated by an

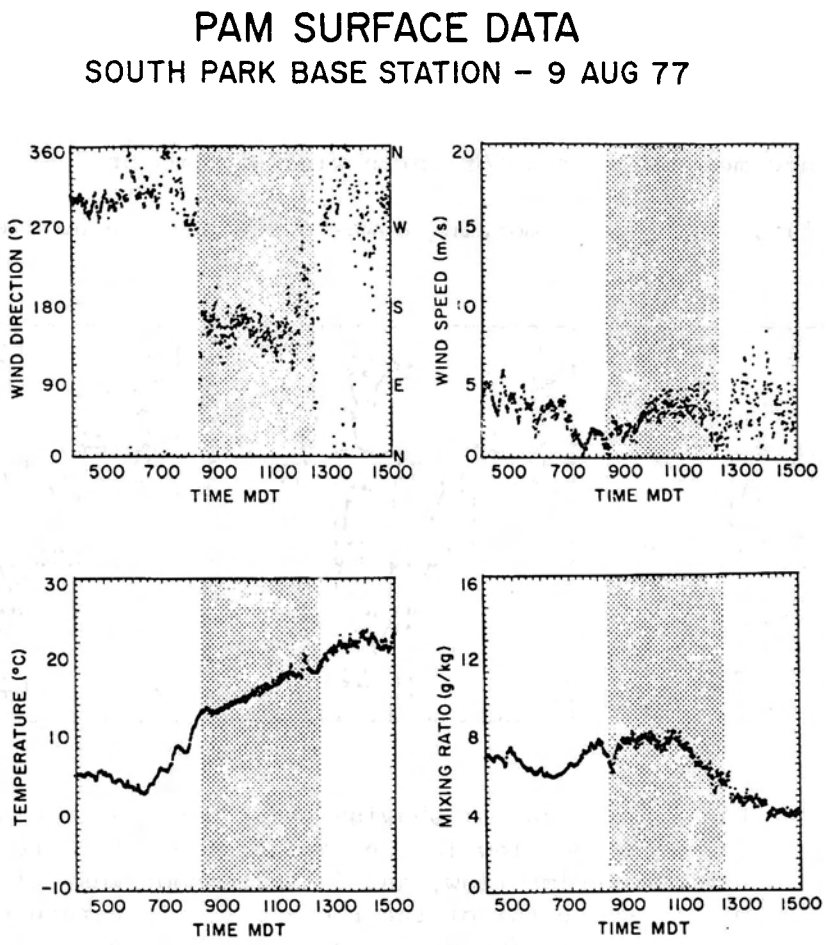

Figure 4.3: Time plots of wind direction, wind speed, temprature, and water-vapor mixing ratio for the PAM station at the Base Site on 9 August. Times of upslope-regime winds are indicated by shading.

asterisk in the PAM charts. Sunrise at the Base Site on this day was about 0630 MDT. The wind direction plot (Fig. 4.3a) shows that the westerly drainage (downslope) flow changed abruptly to southeasterly upslope flow just before 0830. Also, the temperature and mixing ratios rose to values well above their pre-sunrise minima. After 1130 the wind began to change direction again, but it did not actually settle in to a northwesterly direction until after 1230. During this gradual windshift the boundary layer dired out slowly, as shown by the moisture plot (Fig. 4.3d). Also the wind speed plot shows that, although the

winds had about the same mean speed in the afternoon as they did in the morning, they were much more variable in the afternoon. Finally, the temperature plot shows a dip in temperature after the onset of the upslope flow, and a leveling off after about 1300 in the afternoon.

Time plots of data from a different day, 3 August, are presented in Fig. 4.4. Times during which upvalley flow is present at the Base

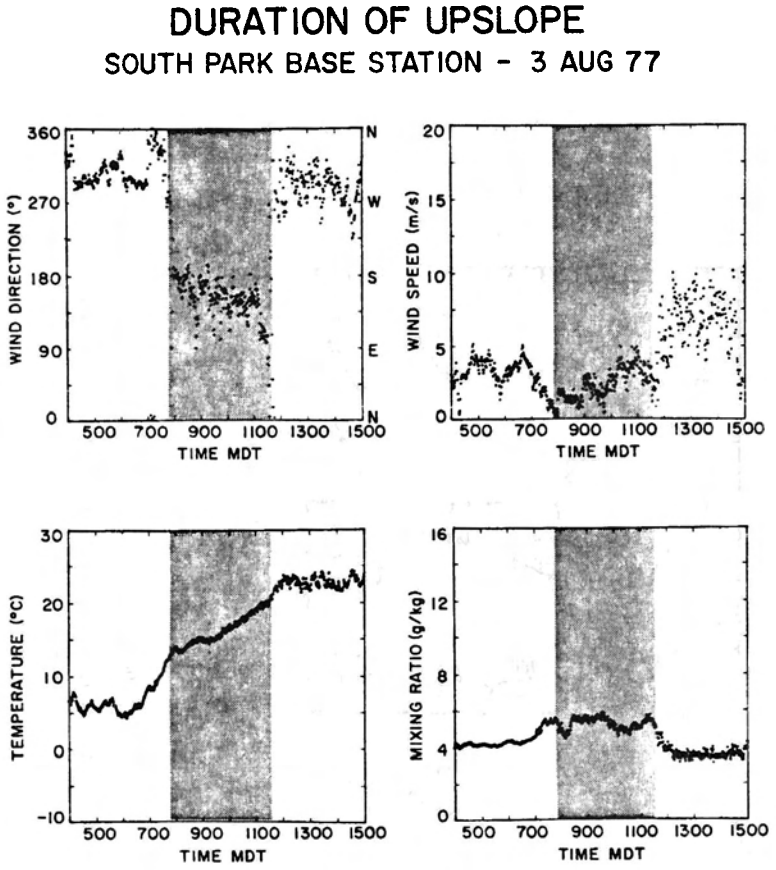

Figure 4.4: Time plots of wind direction, wind speed, temperature, and mixing ratio for the PAM base station on 3 August. Times of upslope-regime winds are indicated by shading.

Site are indicated by shading. On this day, the winds changed direction abruptly both at the shift to upvalley winds and at the shift to the afternoon westerlies. The afternoon winds were both stronger and

gustier than the upslope winds, and again they were drier. Also as in the previous example, there was a dip in temperature just after the shift to upvalley winds, and the temperature leveled off after the onset of the afternoon winds. In contrast to the gradual decrease in moisture in the previous case, on this day a sudden drop in mixing ratio occurred as the afternoon winds took over.

The surface mesonet chart that was given in Fig. 4.2c showed strong westerly winds only in the northwest corner of central South Park. As an example of what frequently occurred on a dry day at a later time in the development of the afternoon wind system, Fig. 4.5

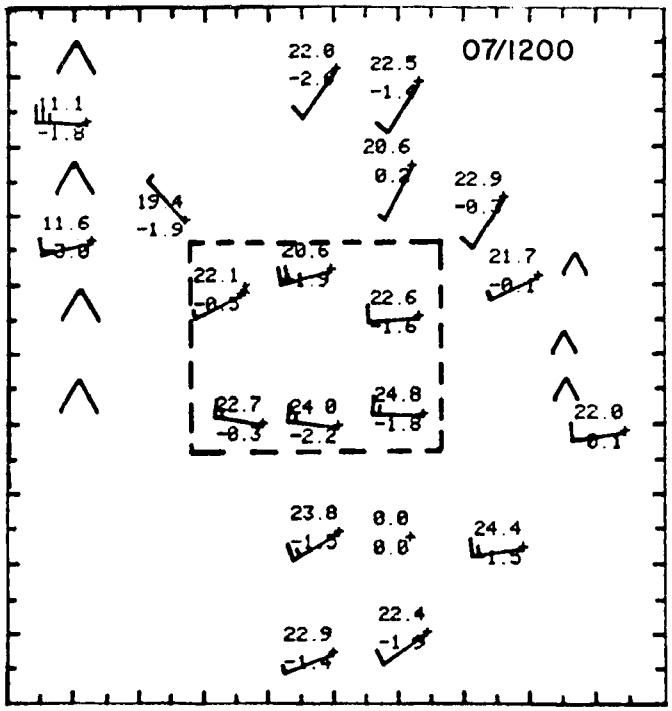

Figure 4.5: PAM surface chart showing the convectively-mixed afternoon wind regime as it occurred at noon on 7 August.

shows a surface chart in which westerlies occupied all of central South Park. In fact, strong winds with a westerly component existed at all stations in the Park. In the central rectangle, the directions

and speeds of the westerly winds were very nearly the same as those of the ridgetop winds. On mnay dry days during SPACE-77, afternoon winds which were similar in direction and speed to the ridgetop winds would invade all of South Park. On such days these winds had a westerly component. Fig. 4.5 shows a good example of this phenomenon.

The morning shift to upvalley winds was not alwyas so abrupt as those which occurred on 3 and 9 August. Also, the winds did not always shift directly to an upvalley direction; sometimes the winds shifted first to an easterly upslope direction before shifting to a south-southeasterly upvalley direction. This latter sequence is in better agreement with the Wagner-Defant model. Fig. 4.6 shows an example of this which occurred on 6 August. The winds shifted through north to an easterly upslope direction after 0800, and the southeasterly upvalley winds were not well established until after 0930.

Because South Park is a basin rather than an obvious mountain valley, there is not always a clear distinction between slope wind systems and along-valley wind systems. For this reason it is convenient to define "regimes" of wind systems, in which upslope and upvalley wind systems are included in one regime, and downslope and downvalley regimes are included in another. Thus, in this paper a wind "regime" will be used as a generic term which includes wind systems that have similar causes, viz. heating, cooling, or mixing. In this paper three regimes will be described. The upslope regime includes both upslope and upvalley winds, whose ultimate cause is the heating of the earth's surface, the downslope regime includes both drainage and downvalley winds, and the regime of the afternoon wind system will be called the

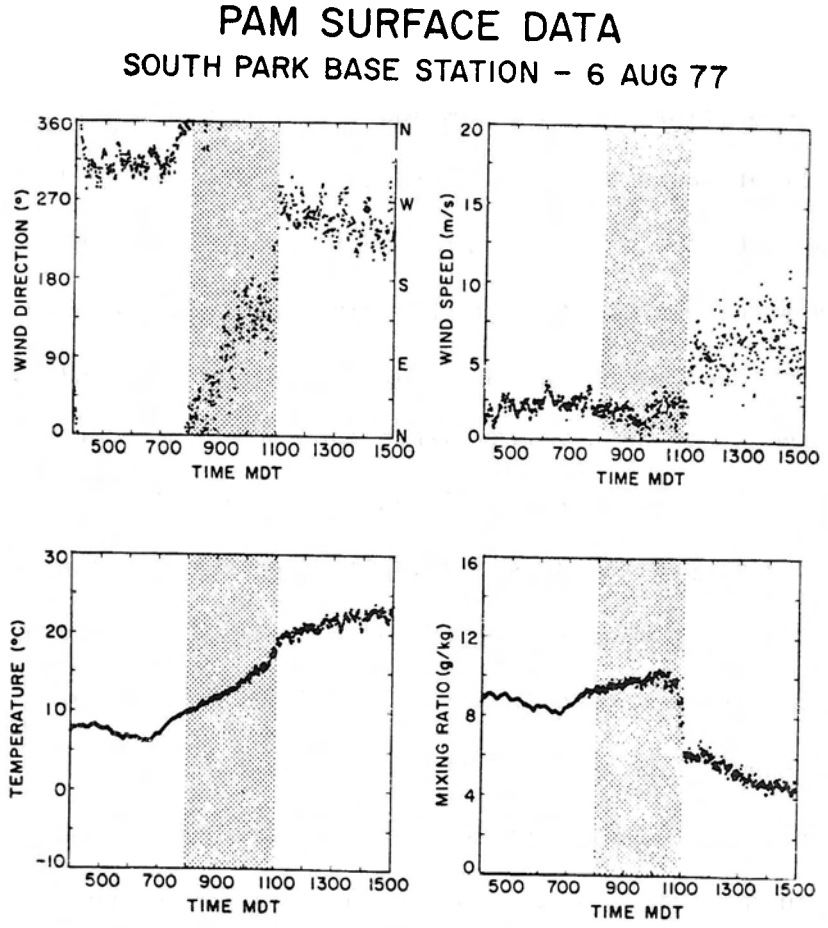

Figure 4.6: Time plots of wind direction, wind speed, temperature, and mixing ratio for the PAM base station on 6 August. Times of upslope-regime winds are indicated by shading.

convective mixing regime for reasons which will become apparent in the next section.

Some uncertainty exists in the nomenclature of the winds aloft when discussing flow in a mountain valley. These winds are often referred to as gradient (or geostrophic) winds. Gradient winds in meterology, however, generally connote winds that are above the frictional influence of the earth's surface. During a sunny afternoon over the mountains, however, a deep convective boundary layer forms

over the mountains, as will be shown in the next section. The winds just above the ridgetops in this case are mixed-layer winds. Since most of the Ekman turning of the winds in a CBL occurs within the convective inversion at the top of the layer, the mixed-layer winds just above the ridgetops are within the frictional influence of the earth's surface. Thus, it is not appropriate to call them "gradient winds". True gradient winds exist only above the afternoon convective inversion, which may be three to five kilometers above the terrain. On the other hand, at night--when the atmospheric boundary layer is stable and shallow--the winds just above the ridges may tend toward gradient balance, so that the term "gradient wind" may be appropriate. To avoid all this confusion, the winds characteristic of levels at or just above the mountain ridges will be called simply "ridgetop winds" in this paper, regardless of whether they are or are not gradient winds.

With the definitions presented in the previous two paragraphs, one can describe the events portrayed in the surface data in this section. On a typical dry day in South Park, three surface wind regimes can be identified. At night drainage or "downslope regime" winds flow from a northwesterly direction in central South Park. An hour or so after sunrise a shift occurs to "upslope regime" winds, which generally blow from a southerly to southeasterly direction and which bring moist air up to the mountain slopes from the lower areas of the South Platte River valley. Finally in late morning or early afternoon, the afternoon westerlies of the convective mixing wind regime take over South Park. These winds are dry and gusty, and they correspond in direction with ridgetop winds.

B. Vertical Temperature Structure of the Wind Regimes

Insight into the causes of the various wind regimes in South Park can be obtained by investigating the vertical thermal structure that accompanies the winds. In this section, vertical profiles of winds and potential temperature based on tethered balloon and rawinsonde soundints will be presented. These profiles are then used to deduce a conceptual model of the potential-temperature cross sections. Finally, aircraft data are presented which support the model cross sections.

1. Vertical profiles of wind and potential temperature at the Base Site

Vertical soundings of winds and potential temperature (θ) were obtained on several days during SPACE-77 using the tethered balloon system. Most of these profiles were obtained from the Base Site, which was located along the east-facing slopes leading up to the high mountains at the western edge of South Park, as depicted in Fig. 4.7 Examples of vertical soundings taken during each of the three wind regimes are given below.

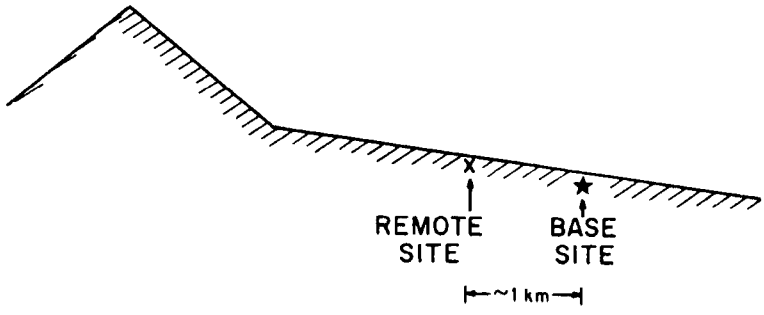

Figure 4.7: Schematic east-west cross section (west is to the left) showing relative location of the base site on the slope leading up to the high mountain range to the west. Also shown is the location of a remote site uphill from the base site from which supplemental tethered balloon soundings were obtained.

In order to understand the evolution of the vertical profiles on a dry day, it is helpful to first describe the state of the boundary layer on the previous afternoon (assuming that the previous day was also dry). The afternoon boundary layer over the mountains is a very deep convective boundary layer (CBL), routinely reaching a depth of over three kilometers--and occasionally reaching five kilometers or more above the ground at the Base Site. The rawinsonde sounding in Figure 4.8, for example, shows the dry-adiabatic CBL which extended to about 3 km on the afternoon of 2 August. Throughout the depth of this

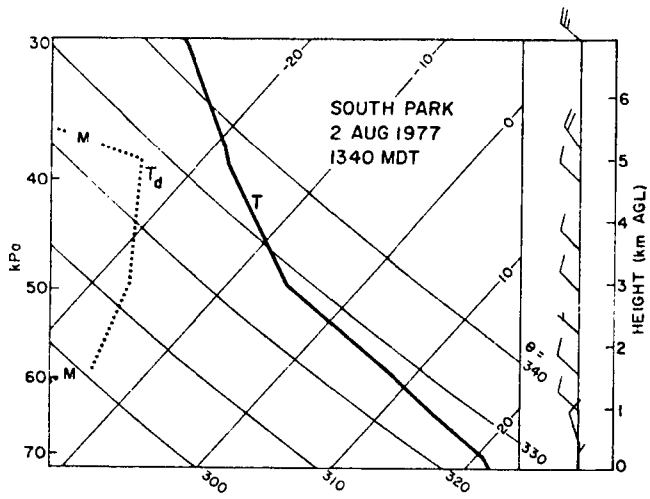

Figure 4.8: Rawinsonde sounding on the afternoon of 2 August showing that the depth of the afternoon CBL reached about 3 km. The slightly stable layer at the base of the sounding probably results from a cloud passing over the sun, and the north-northeasterly winds in the lower part of the sounding illustrate the channeling of northwesterly flow into the valley of Fourmile Creek.

boundary layer over South Park, the θ and winds were well-mixed (although there was some tendency for the winds near the surface to be channeled in the direction of the creek bottom). This kind of sounding is rather typical of the afternoon convective-mixing regime. At night, owing to radiative cooling and the draining of cool air off the slopes

of the mountains, a nocturnal inversion formed in South Park. As shown below, this inversion layer was generally 200-300 m deep at the base site.

a. Results

Tethersonde soundings for 7 August are presented in Fig. 4.9a-4.9f. Most of these soundings reached a height of nearly 500 m.

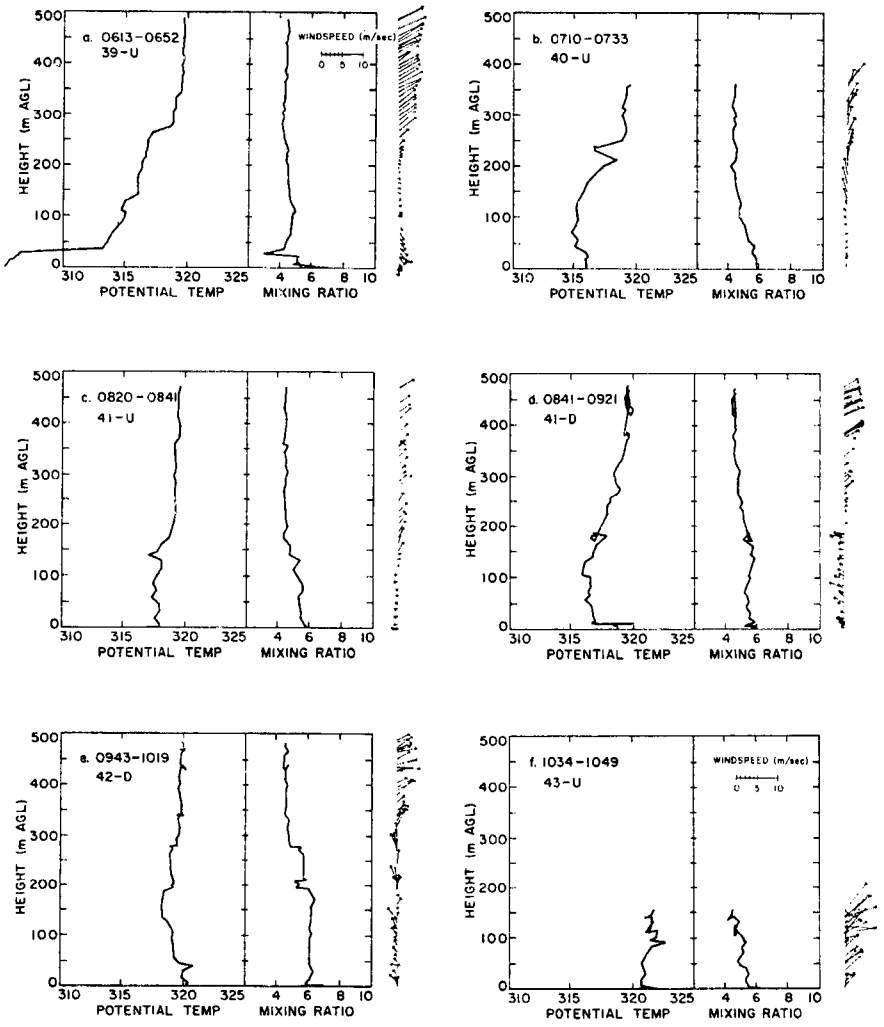

Figure 4.9: Successive Tethersonde soundings taken at the Base Site on 7 August.

A sounding through the drainage flow was taken at about sunrise (Fig. 4.9a). The θ profile shows a strong surface-based radiation inversion below 250 m, with a neutral (constant-

θ) layer aloft. This constant-θ layer is a persistent feature in subsequent soundings, and we shall continue to refer to it as the "neutral layer aloft". The θ value of this neutral layer was about 319 K. The drainage winds in the lower, stable region were strongest just above the surface and were from a northerly through northwesterly direction, while the "ridgetop" winds in the constant-θ layer aloft were from a southwesterly direction. Thus the winds in the two vertical regions did not seem to be coupled.

Figure 4.9b shows incipient upslope flow an hour later. The surface temperature has increased more than 10°C to 14°C, and the light winds in the lowest levels were blowing up the local slope from an easterly direction. At the top of the sounding the winds were still southwesterly, and the neutral layer aloft above 250 m persisted, with a θ value of 319 K. The strange behavior of the θ trace just above 200 m could have been due to a temporary intrusion of warm air at that level, to a discontinuity in the density interface (indicated by the large vertical θ gradient there) moving past the balloon, or perhaps to problems with the instrument system in this situation. The occurrence of rather strong upslope flow at this level - even stronger than at the surface - was a feature absent from most other days, although it did happen on some other occasions.

A feature which was evident on θ profiles taken through incipient upslope on other days (some of which are presented below) was a shallow, surface-based convective boundary layer (CBL) in the lowest 100-200 m. A CBL is not clearly evident on Fig. 4.9b, although one can discern some CBL features. In a later section of this paper we argue that the lack of a clearly definable CBL on individual soundings is

a result of sampling error. Additionally, the CBL which forms beneath the nocturnal inversion is not very deep, especially when compared with the depth of the neutral layer aloft, which may extend to 3 km or more above the ground. For this reason (and for other reasons which we shall discuss later), we call this the "shallow CBL".

The shallow CBL in Fig. 4.9c has grown to a height of 150 m, and in Fig. 4.9d, to a height of 200 m. In these soundings, the top of the shallow CBL is evident from the wind profile: there is easterly, upslope flow below the convective inversion, and southwesterly ridge-top-level flow above. The upper-level winds are still associated with the neutral layer aloft, with $\theta \approx 319$ K, and there is a stable region in the θ profile between this neutral layer and shallow CBL. Loops in the profiles of θ and r_v such as those which appear below 200 m on sounding d often occurred at the top of the CBL's in Tethersonde soundings. They probably result from waves or undulations in the capping convective inversion which advect past the balloon.

Figure 4.9e shows an interesting sounding. The moisture profile and the winds clearly show that the shallow CBL extends vertically to nearly 300 m. The moisture and θ profiles show that the CBL is discontinuous, with an intruding layer of warm, dry air near 200 m. The winds in the CBL are very gusty, and their direction is now from a southerly through southeasterly, up-valley direction, as opposed to the earlier up-slope direction. The neutral layer aloft persists, but the temperature near the surface has warmed so that its potential temperature is greater than the 319 K of the upper neutral region. Moreover, the θ of the shallow CBL has nearly reached 319 K. Thus,

with any further heating the two regions - the shallow CBL and the neutral layer aloft - should become convectively coupled.

The Tethersonde ascent in Fig. 4.9f, started fifteen minutes after the previous sounding had been reeled in, shows that this indeed occurs. The balloon system, which was not designed to be used in winds of over 8 m s^{-1}, could barely be raised to a height of 150 m because of strong, turbulent westerlies. Figure 4.9f shows that these westerlies were dry, and that they extended down to the surface. Figure 4.5 was a PAM surface chart for noon on this day. It shows that dry, westerly winds have taken over all of South Park.

The features revealed by the thethersonde can be summarized as follows: i) at sunrise a nocturnal inversion exists at the surface with drainage winds at the surface and with deep neutral layer aloft above the inversion. ii) Morning heating at the ground produces a shallow CBL just above the surface and below the inversion and the upslope regime winds form in this shallow layer. iii) The shallow CBL grows and warms until it reaches the top of the nocturnal inversion, and during this process the winds in the shallow CBL continue to blow up the slope. iv) Finally the shallow CBL grows into the neutral layer aloft, and westerly winds are mixed downwards to the surface. Further discussion of these processes will be presented later in this section, but first, the following paragraph contains further examples of Tethersonde soundings which illustrate the features mentioned above. These examples illustrate that the phenomena described above occurred frequently in South Park.

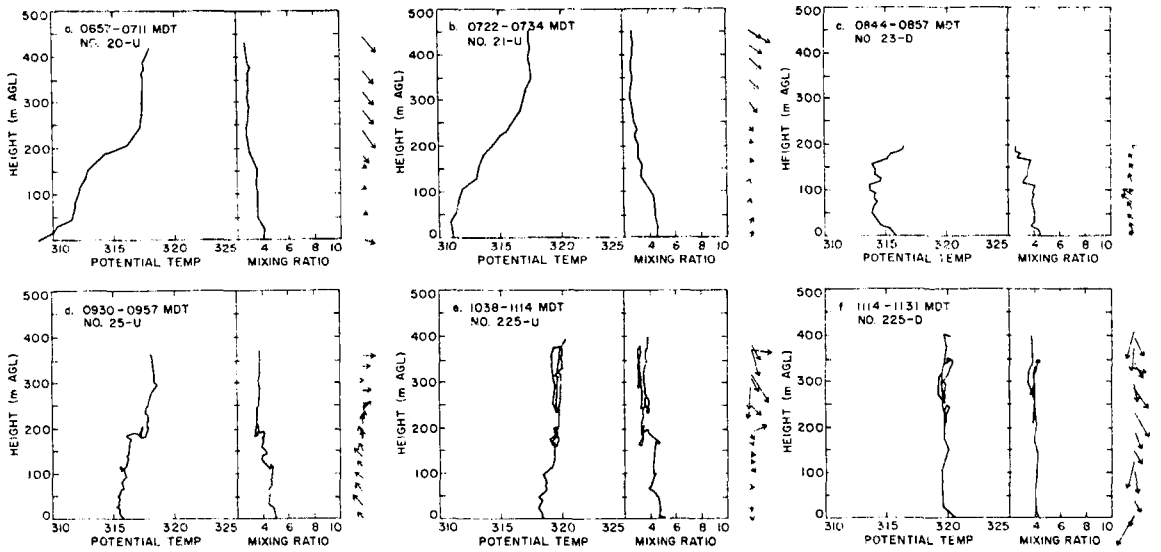

Figure 4.10: Successive Tehtersonde soundings taken at the Base Site on 2 August.

A sequence of Tethersonde soundings for 2 August is given in Fig. 4.10. The nocturnal inversion and downslope regime winds are shown in Fig. 4.10a. The nocturnal inversion is nearly 250 m deep, the neutral layer aloft has a θ of 318 K, and the winds aloft are northwesterly. Fig. 4.10b shows the incipient upslope regime winds forming in the shallow CBL next to the ground. The growth of the upslope layer (i.e., the shallow CBL) is illustrated in Figs. 4.10c and 4.10d. Finally, Fig. 4.10e shows that the shallow CBL and the neutral layer aloft have become convectively coupled, and that strong, gusty northwesterly winds exist down to near the surface. As mentioned in connection with Fig. 4.8, the surface winds themselves seem to be channeled somewhat in the direction of the valley of Four Mile Creek, which runs more northerly past the base site. This channeling effect seems to occur with northwesterly ridge top winds but not with westerly or southwesterly winds aloft.

August 2 was a day on which two tethered balloon systems were operated simulatneously during the morning upslope regime. One was operated at the base site and the other was operated at a site located a little over 1 km west of the base. Thus, this latter site was closer to the mountains than the base, and it was about 100 m higher in elevation than the base. A drawing of the spatial relationship between the base site and the remote site has already been given in Fig. 4.7.

We began soundings at both sites at around 0930, and both soundings reached their peak altitudes at about 1000. Fig. 4.11 shows the profiles from these soundings. The depth of the shallow CBL at the remote site in Fig. 4.11a was around 210 m or so above the ground,

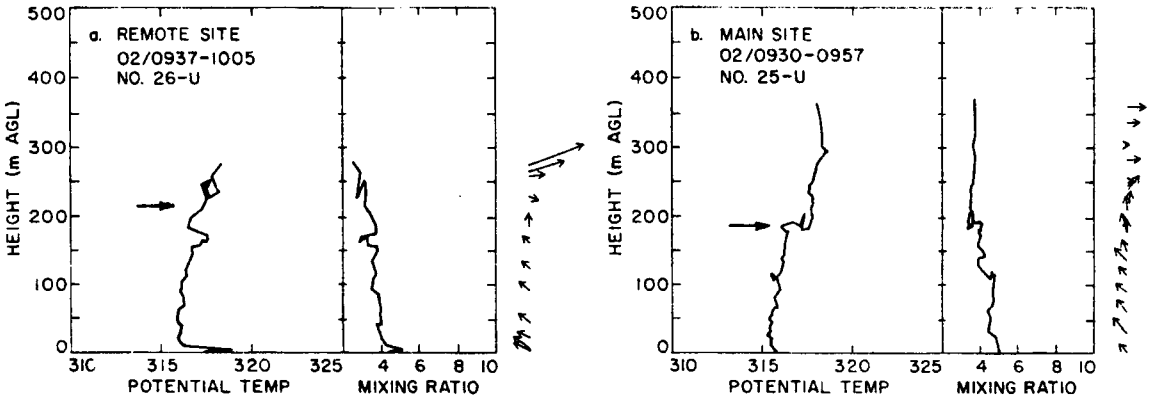

Figure 4.11: Simultaneous Tethersonde soundings through the upslope-regime flow at the Base Site and at a remote site farther up the slope (refer to Fig. 4.7) on 2 August. (a) Remote site: the top of the CBL (arrow) is taken to be above 200 m. despite a discontinuity in θ and mixing ratio (r_v) at ~160 m. This is because values of θ and r_v characteristic of the CBL below are found above the discontinuity. (b) Base Site: the top of the CBL (arrow) is taken to be below 200 m. The upslope winds which appear to extend above this level are a spurious result of the lag in directional response of the balloon system which was described in Chapter III. The slight discontinuity in θ and r_v which occurs just above the 100-m. level may coorespond with the 160-m. discontinuity in the remote-site sounding. The Base-Site sounding in (b) is the same as the sounding in Fig. 4.10d.

while the depth at the base site in Fig. 4.11b (which is the same as Fig. 4.10d) was 190 m. Thus, the upslope layer was deeper at the nigher site. This result is in agreement with the assertions of Defant (1951) and Moll (1935) that the upslope layer should increase in depth as it goes up the slope, because the layer entrains air from above as it moves.

A final example of a sounding through the shallow CBL during the upslope regime is from 6 August (Fig. 4.12). The θ profile is nearly

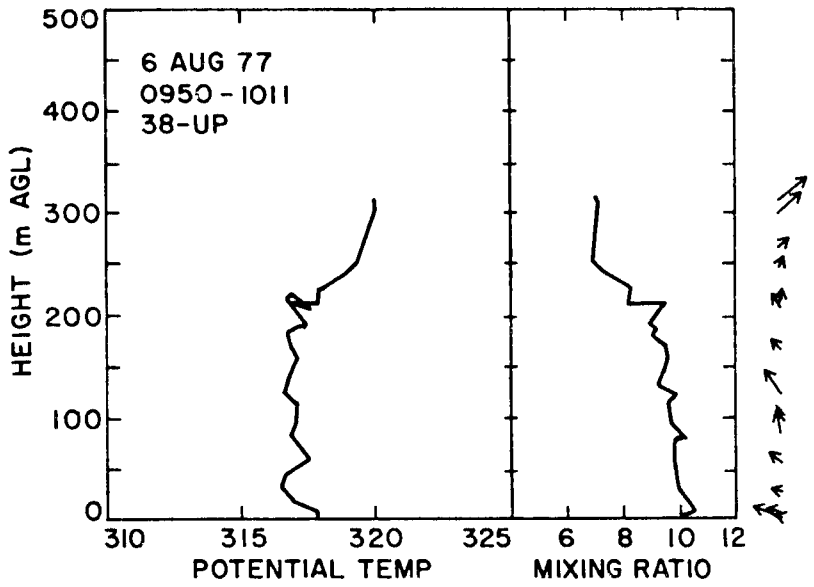

Figure 4.12: Tethersonde soundings of potential temperature, water-vapor mixing ratio, and horizontal wind velocity in the shallow CBL on the morning of 6 August.

constant with height in the shallow CBL below 200 m, although there is considerable turbulent variability. Relatively large moisture values exist in the shallow CBL, but above this mixed layer the mixing ratio drops off rapidly with height. Upslope regime winds in the layer are from a southeasterly direction. As shown in Fig. 4.6, this sounding was taken about an hour before afternoon southwesterly winds reach the surface at the base site.

The view of the evolution of the boundary-layer structure presented above is still somewhat limited, in that it is based on soundings that reach less than 500 m. above the earth's surface. To put these results into better perspective, rawinsonde soundings from 3 August are presented in Fig. 4.13. Earlier, Fig. 4.8 showed a deep CBL on the afternoon of 2 August. Fig. 4.13a shows the sounding at 0600 the next morning. The nocturnal inversion layer is only 300 m deep, while the neutral layer aloft extends to nearly 3 km. The winds near the surface are very light and downslope. Fig. 4.13b shows the sounding four hours later at 1005 in the morning. Although the radiosonde's

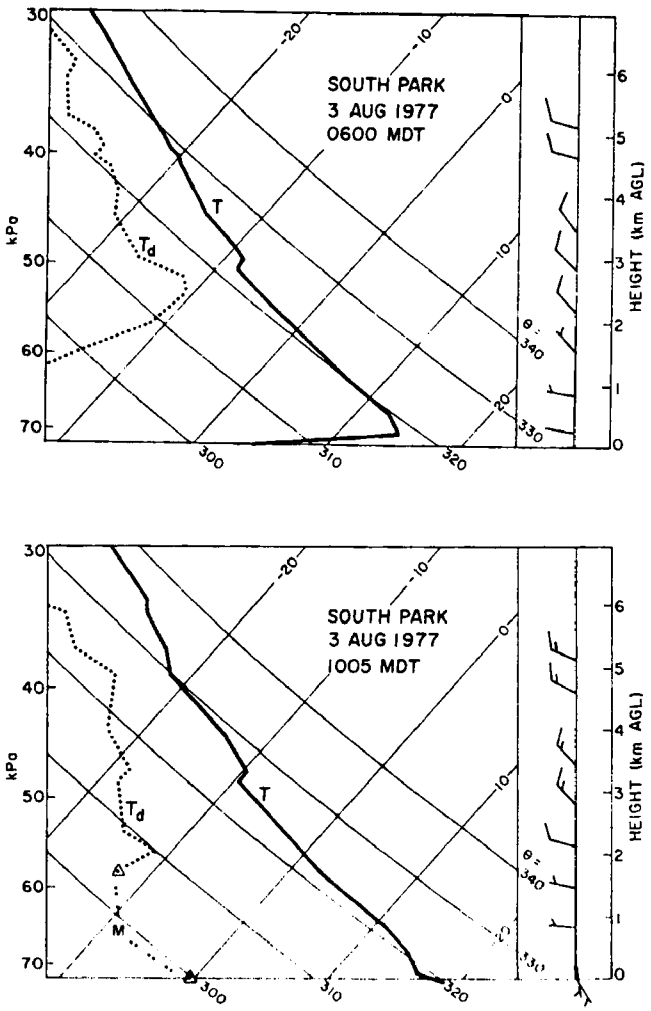

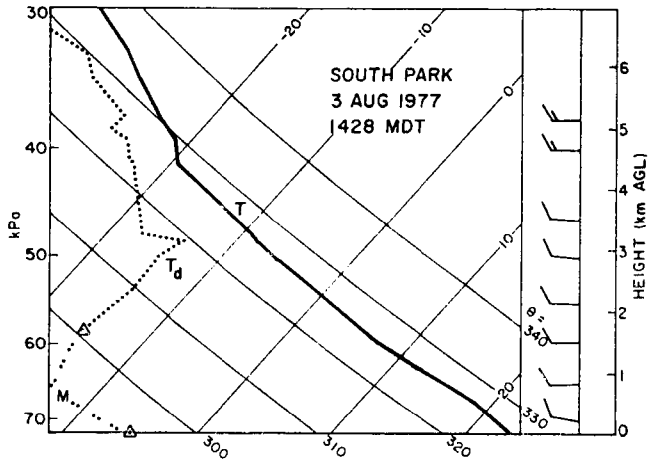

Figure 4.13: Rawinsonde soundings on 3 August showing the three wind regimes. 0600 MDT sounding shows nocturnal inversion and very light surface winds. 1005 MDT sounding shows evidence of the shallow CLB, with upslope flow within. 1428 MDT sounding shows deep afternoon CBL extending to over 4 km, with well-mixed westerlies to this level.

resolution is poor, there is an indication of an unstable boundary layer below 300 m, and the winds in this layer are from an upslope south-easterly direction. In Fig. 4.13c one can see the very deep CBL that has formed by 1428 in the afternoon. The dry adiabatic region extends to nearly 5 km above the ground at the base, and the westerlies are well-mixed all the way down to the surface. Thus, Fig. 4.13 provides a more realistic perspective of the shallow CBL (which contains the upslope winds), namely it is a shallow layer indeed, especially when compared with the depth of the neutral layer aloft or the CLB which forms over the moutains in the afternoon.

b. Discussion

Onset of Afternoon Winds. In the previous results, the appearance of the westerlies at the surface was attributed to convective coupling between the surface-based shallow CBL and neutral layer aloft. In this subsection, the coupling process is further described.

It is convenient to start with the situation as depicted in Figs. 4.9e and 4.10d, where the shallow CBL and the neutral layer aloft are still distinct. They are still distinct because turbulent mixing between the upper neutral layer and the lower region (the shallow CBL) is inhibited by the presence of weak stable layers just below 300 m and 200 m, respectively, which are the last remnants of the nocturnal inversions.

In each case little more heating erases the stable layer. When the stable layer is gone, this allows the turbulence of the CBL, generated by buoyancy in the warm surface layer (i.e., the lowest 10% of the CBL) to grow rapidly upwards into the relatively quiescent neutral layer aloft. Rapid mixing of the shallow CBL and the upper neutral region occurs. The result is a much deeper, well-mixed CBL which extends from the surface to the top of the old neutral layer aloft. In contrast to the shallow CBL, this will be called the "deep CBL" of the "deep afternoon CBL", since it persists all afternoon over South Park on a dry day.

The upper neutral layer was much deeper than the shallow CBL, as mentioned above. Since there was considerably more mass in the region aloft, its properties overwhelmed those of the shallow CBL when the mixing occurred. Thus, one sees dry, westerly flow throughout the new deep CBL; Fig. 4.8f shows the lowest 150 m of this deeper boundary layer.

The picture that one gets of the erosion of the nocturnal boundary layer from the results presented above is not new. Deardorff (1974, 1978), for example, presents θ profiles where "explosive" growth of the CBL occurs into a neutral layer aloft, which was left over from the deep CBL of the previous day. Coulman (1978, 1980) found a similar behavior in the evolving subcloud layer (which <u>is</u> a dry CBL until

clouds form). Additionally, acoustic sounder records have shown the phenomenon of mid- to late-morning explosive CBL growth [McAllister et al. (1969), Russell et al. (1974), Hall et al. (1975)].

Over flat land the nocturnal inversion seems to have little overall effect on the growth of the deep CBL, except to retard its onset [Tennekes (1973) calls it a "morning transient"]. Over South Park, however, we have seen that the presence of a strong stable layer between the shallow CBL below and the strong westerlies above is precisely the feature which decouples the two layers and allows upslope flow to form within the shallow CBL. Otherwise the westerlies would be free to mix down to the surface and no upslope would form at all. This stable layer is the nocturnal inversion.

Comments on Observed CBL Structure. As discussed in Chapter III of this paper, each Tethersonde observation is an instantaneous "snapshot" of conditions at that level. Traditional θ- and q-profiles in the CBL like those discussed by Kaimal et al. (1976) and Deardorff (1978) or modelled by Ball (1960), Tennekes (1973), and Deardorff (1978), are based on values at each level that are averaged over 10 to 20 min or more. The averaging period is selected to be long enough to average over several "thermals" or "plumes" in the CBL. In the lowest part of the boundary layer, the surface layer, these plumes have an unstable, superadiabatic θ profile, but outside the plumes, the lapse rate is neutral down to very close to the ground (Kaimal and Businger, 1970). Thus, a Tethersonde, which does not average its values, may be sampling inside or outside of a plume at any given moment. Profiles from the Tethersonde should reflect this variability, as well as variability from the fact that rising air inside of a plume tends to be warmer (and

often moister) than the sinking air outside of a plume. In other words, Tethersonde observations in the presence of plume convection would be subject to a rather large sampling error. Examples of such effects have been noted in previous discussions.

Whether plumes are actually present in the CBL over South Park is a point which requires further discussion. Acoustic sounders have been used to identify plumes in the atmospheric boundary layer [McAllister et al. (1969), Hall et al. (1975)]. In South Park, two acoustic sounders were operated at various times at the base site, and both verified the presence of plume convection in the CBL. Moreover, data from an aircraft equipped with a gust probe were obtained, which further indicate the plume-like nature of convection over South Park. Some of these results will be discussed in the next chapter. The temperature traces from these data showed characteristic plume "signatures" as described by Kaimal and Businger (1970). Thus, even in the presence of the upslope circulation in South Park, the large eddies in the CBL are plumes.

In view of the variability of the Tethersonde observations it is impractical to establish rigid criteria by which a CBL can be identified on an individual tethered-balloon sounding. Although observation-to-observation variability on a given sounding can aid in locating regions of turbulence - as was evident on many of the soundings presented in this paper - even this is not always a dependable indicator. What makes more sense in interpreting the soundings is to consider the entire sequence of soundings for a given day, as has been done in the results presented above. Individual soundings in the sequence should then be compared with soundings at a similar time in the evolution of the

boundary layer on other days. This interpretation can then be improved by referring to data from other sources, such as rawinsonde, PAM, aircraft, acoustic sounder, and towers equipped with micrometeorological wind and temperature sensors. These data sources were all available during SPACE-77.

Some general characteristics, which are <u>often</u> present on individual Tethersonde soundings of the CBL, can be identified. The bulk or central part of the CBL has a potential temperature and mixing ratio which are nearly constant with height, but which show considerable turbulent variability. The winds at all levels in the CBL blow from similar directions, but show random turbulent fluctuations in both direction and speed. In the lowest few tens of meters (the surface layer), the properties are highly variable - especially θ. If the balloon ascends outside of a thermal, the θ profile may be superadiabatic at some levels. Because the Tethersonde may enter a plume at any level, the warmest temperatures do not necessarily show up at the ground. At the top of the CBL, where an inversion exists, one should find evidence of discontinuities in the θ, mixing ratio, or wind profiles. Since the variability in the Tethersonde soundings of the CBL arises largely through sampling error, we expect to find <u>some</u> soundings which should conform fairly well to the model of CBL structure. Figure 4.14 shows a sounding through the upslope flow on 9 August. This profile reproduces the essential features of the lowest half of the model CBL, although the superadiabatic layer is rather shallow.

The "typical" sequence of soundings which emerges from considering several sequences of observations over South Park (like those presented in Fig. 14.9 and 14.10), as well as information obtained from other

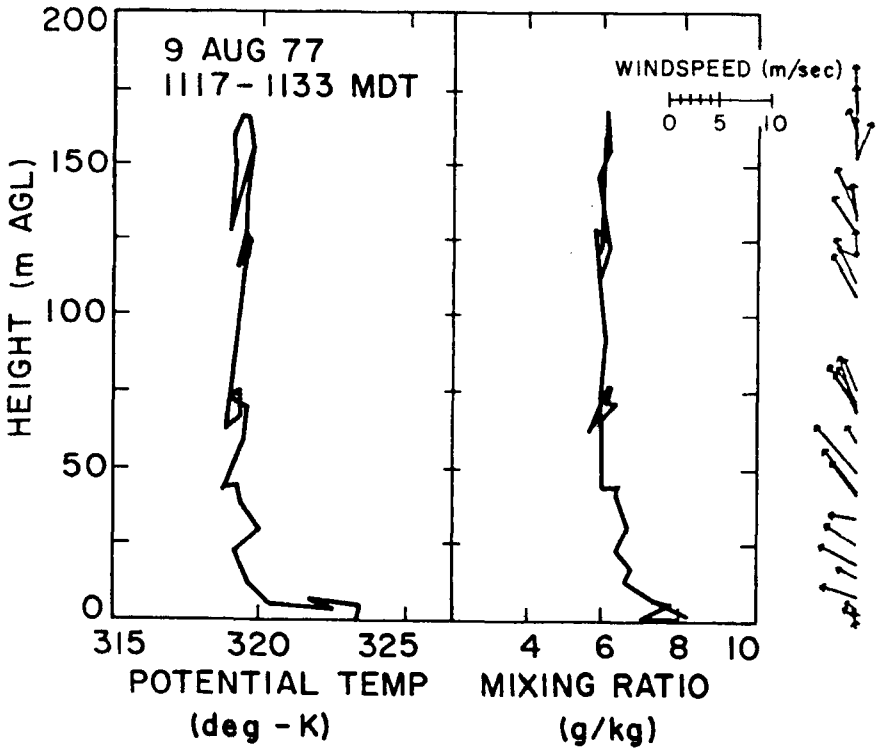

Figure 4.14: Tethersonde sounding to ~160 m. on 9 August, showing lower part of shallow CBL with upslope-regime winds.

data sources, is depicted in Fig. 4.15. Fig. 4.15a represents a sounding taken through the early morning drainage flow (marked D), with the drainage wind shown blowing in a direction somewhat different from the ridgetop-level winds. Fig. 4.15b shows incipient upslope flow (marked U) forming beneath the nocturnal inversion, within a shallow turbulent CBL. Fig. 4.15c shows well-developed upslope flow (marked U), like that which occurs during the mid-morning period, still decoupled from the winds alfot. The direction of the winds in the lower-level could have been shown from a southerly or southwesterly up-valley direction instead of the easterly up-slope direction indicated. Finally, Fig. 4.15d shows the deep CBL and the afternoon wind regime, with winds characteristic of the ridgetop level all the way down to the surface.

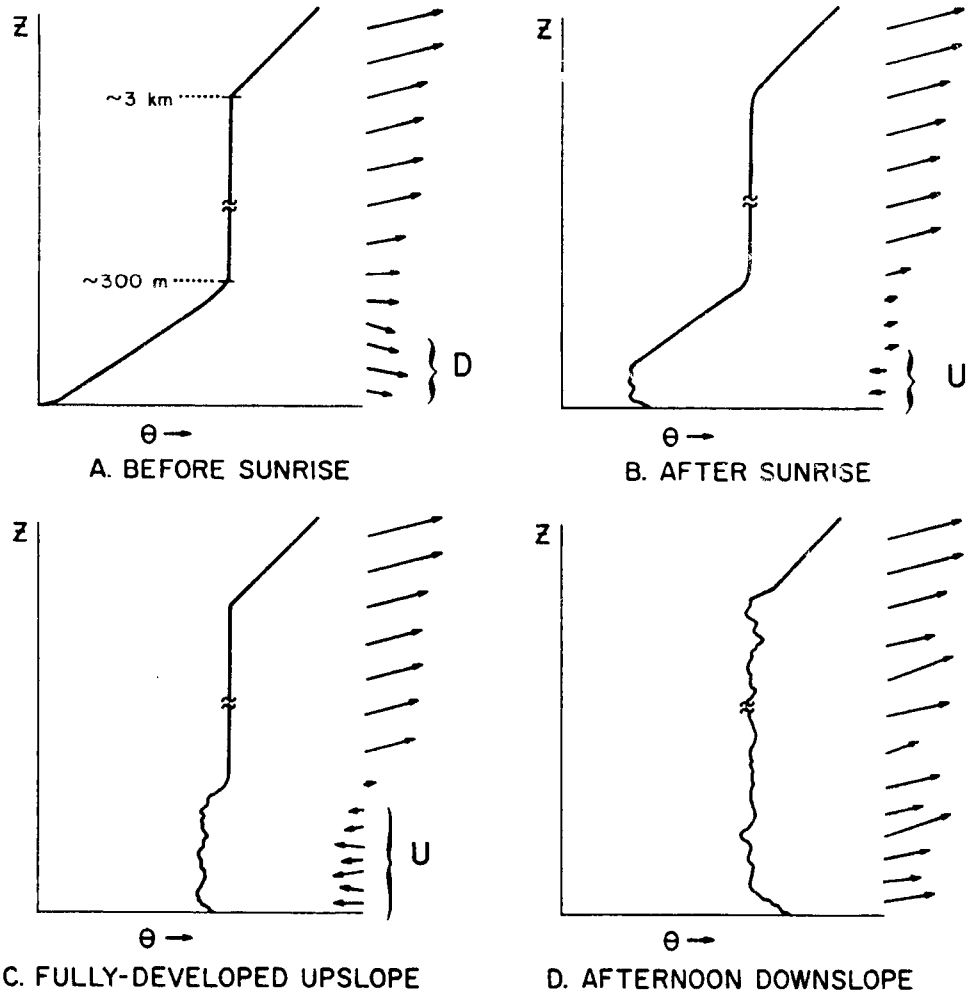

Figure 4.15: Schematic representation of a sequence of potential temperature profiles at the Base Site for a typical dry day.

C. Vertical Cross Sections

1. Potential temperature cross sections inferred from soundings

Using the information present in Fig. 4.15 along with the added knowledge that the earth's surface is either cold (Fig. 4.15a) or warm (Fig. 4.15b-4.15d), Banta (1981) drew hypothetical cross sections of potential temperature. The information which he used in drawing these cross sections are shown in Fig. 4.16.

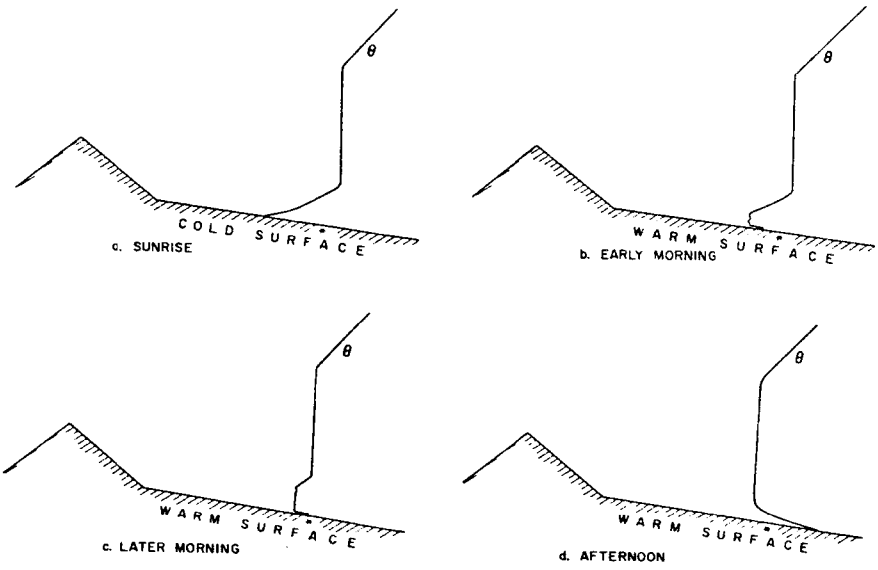

Figure 4.16: Schematic representation of information used to construct potential-temperature cross sections presented in the following figure.

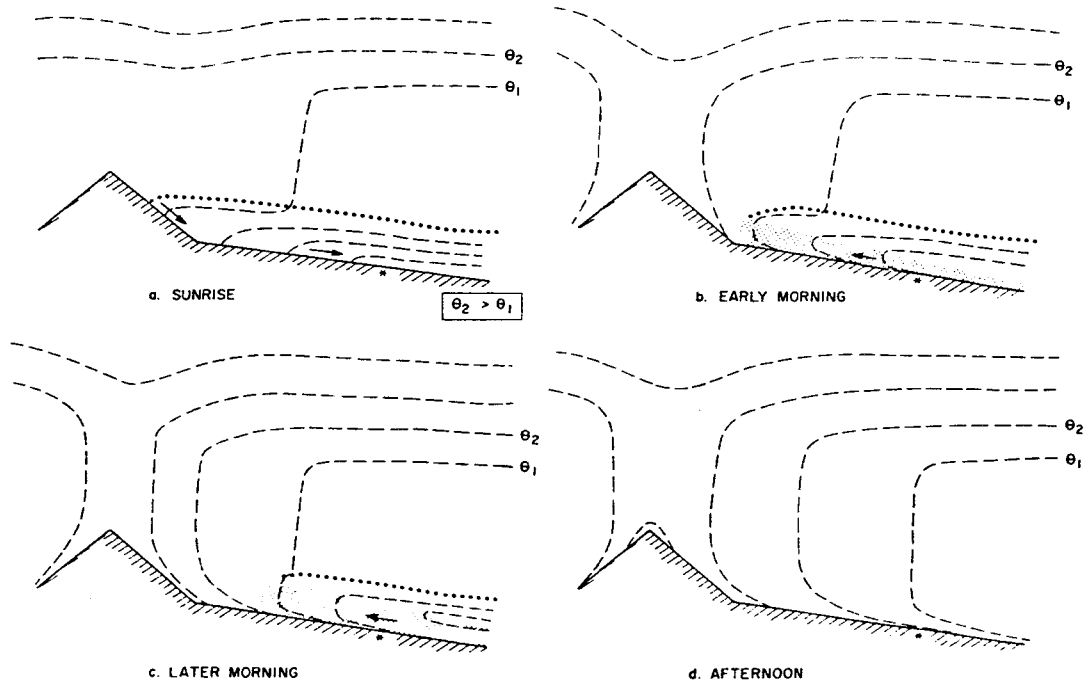

Figure 4.17: Preliminary potential-temperature cross sections as presented by Banta (1981). Dashed lines are isentropes at arbitrary intervals, the heavy dotted line represents the top of the cold-air pool, and the region where upslope-regime winds are present is indicated by shading.

The cross sections which were deduced from this information are presented in Fig. 4.17. One can verify that a vertical profile of θ at the location of the Base Site (asterisk) for each cross section would reproduce the sounding of the corresponding panel in Fig. 4.16. These preliminary cross sections will be refined later in this study by referring to aircraft cross sections and numerical model results. The refined cross sections will be presented in Chapter VII.

2. θ Cross sections determined from aircraft data

Hahn (1980) analyzed aircraft data obtained from NCAR Queenair flights which were flown during SPACE-77. In this section, cross sections based on data provided by Hahn are used to further develop a conceptual model of the mountain CBL.

Because SPACE-77 was a project designed to investigate the formation of cumulus clouds over South Park, most of the flights occurred on moist days, i.e. days in which deep convective clouds formed. The only dry days that were studied were 18, 28, and 30 July. Nevertheless, the early-morning development of the boundary layer on many moist days was the same as it was on dry days, at least until the formation of cumulus congestus clouds, i.e., clouds which have their own dynamics. Therefore some aircraft data from moist days will be presented below, but the cross sections will be from relatively early periods in the development of the boundary layer. The observed structure of the boundary layer is similar to that which would occur on a typical dry day during the same relative time period.

The potential temperature values used in determining the cross sections presented below are values averaged over 200 m of horizontal flight distance. Each 200 m along a flight leg, a simple average is

computed and a point plotted. Potential temperature isentropes were then analyzed at intervals of 1^{o} K, with dashed lines at 0.5^{o} where necessary to improve the clarity of the analysis.

A north-south cross section of potential temperature obtained early on the morning of 30 July is presented in Fig. 4.18. One can see many features proposed in the model cross section presented above.

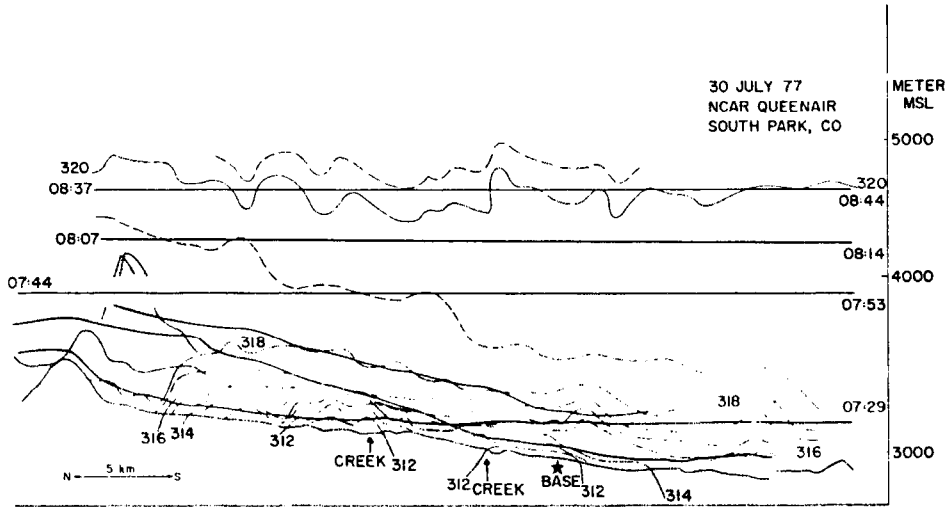

Figure 4.18: Potential-temperature cross section obtained from NCAR Queenair (aircraft) data showing the early-morning downslope regime. The heavy solid lines indicate aircraft flight paths. The light solid lines are isentropes in ^{o}K for even-numbered values of θ, the dashed lines represent odd-valued isentropes. Low-level isentropes were drawn based on four flight legs, although only three are shown (based on an analysis by D.C. Hahn).

A stable nocturnal inversion layer is present next to the ground. The potential-temperature (isentropes) tend to slant downhill. Above the inversion layer, especially to the right of the figure, θ is nearly constant with height until the stable "free atmosphere" is reached. There were also some features which were not suggested in the model cross section. The cold-air layer is very wavy, probably largely owing to the presence of gravity waves in the stable cold air layer.

Also, the coldest "bubbles" at the ground tend to occur at the locations of the creek bottoms (Hahn, personal communication).

The structure of the shallow CBL on the morning of 20 July is shown in Fig. 4.19. This was one of the moist days studied during

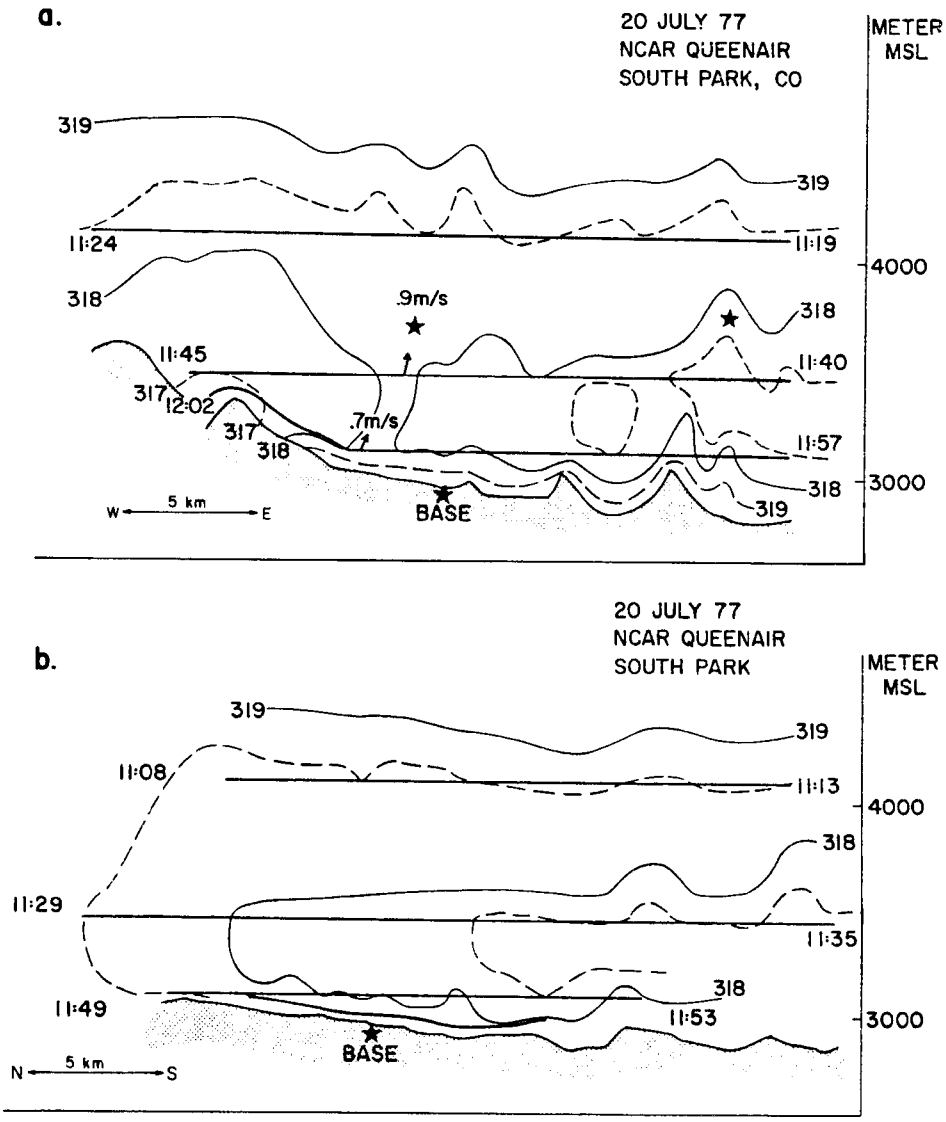

Figure 4.19: Potential-temperature cross sections from aircraft data showing the structure of the shallow CBL on 20 July: (1) east-west cross section; (b) north-south cross section. Both 19 July and 20 July were moist, distrubed days in South Park, so the neutral layer aloft was not well developed. The stars above the second flight leg indicate areas along that leg where well-developed updrafts (~1 m/s) occurred. (Based on an analysis by D.C. Hahn.)

SPACE-77. These cross-sections correspond to the cross sections through the shallow CBL shown in Fig. 4.17b. The overall structure of the shallow CBL in both the observed and the proposed model cross sections are very similar, although the observed isentropes have many undulations which did not appear in the proposed θ cross sections in Fig. 4.17. Many of the undulations in the lower levels of the aircraft cross sections followed terrain features, while in the stable upper levels of the cold air layer, the undulations were due both to terrain features and to gravity waves.

A late stage in the growth of the shallow CBL on 28 July, just before the deep afternoon CBL formed, is shown in Fig. 4.20. The top

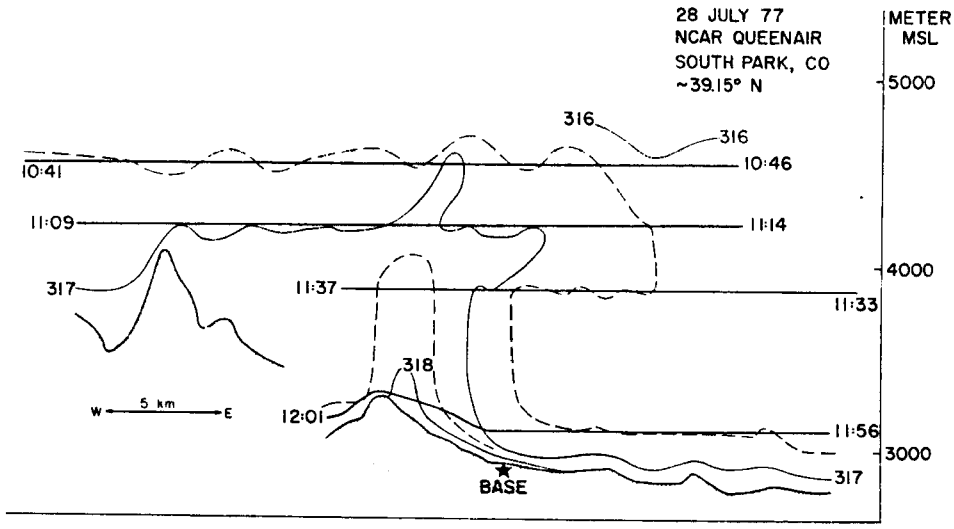

Figure 4.20: Potential-temperature cross sections from aircraft data showing the structure of the late-morning shallow CBL on 28 July. The terrain shown in this east-west cross section includes both the high ridges of the Mosquito Range at the left of the figure, and the lower Sheep Ridge which is just west of the Base Site.

of the shallow CBL, as will be shown below, was almost up to the second flight leg above the surface. Fig. 4.21 shows PAM surface

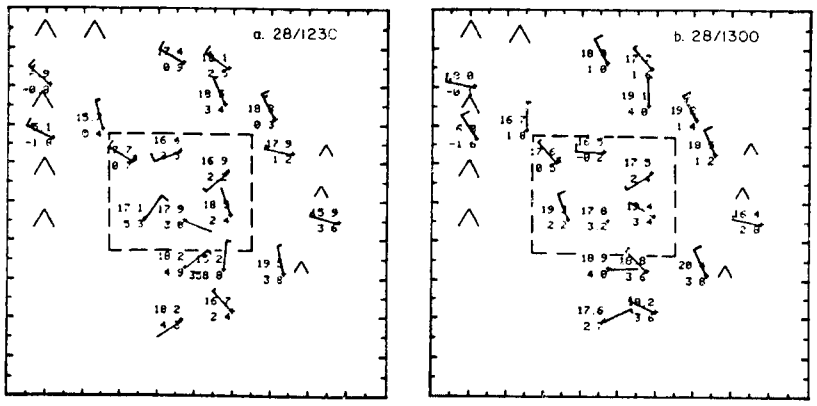

Figure 4.21: PAM surface charts for 28 July, (a) ½-hour and (b) one hour after the cross section in the previous figure. In both (a) and (b), the afternoon westerlies have reached the surface in the vicinity of the Base Site.

charts for 1230 and 1300 on the afternoon of 28 July, a half hour and an hour after the lowest leg in Fig. 4.20 was flown, respectively. These charts show the invasion of westerly surface winds into central South Park, and they show that within an hour or so after the cross section in Fig. 4.20, the deep afternoon CBL has formed over much of central South Park, Thus, the aircraft cross section represents a time in the development of the boundary layer very close to that represented by the soundings of Fig. 4.9e, Fig. 4.10d, and Fig. 4.15c, and by the proposed model cross section in Fig. 4.17c.

Further confidence in these conclusions can be obtained by a more detailed analysis of the aircraft cross sections, including moisture and wind-component analyses performed as the θ analyses were. To supplement the aircraft data, vertical profile data from the 1007 MDT rawinsonde sounding were used to help draw θ and moisture isopleths in the following analyses. The θ analysis, with an exaggerated vertical scale and an isentrope interval of 0.4° K, is given in Fig. 4.22. Regions with θ greater than 317.2 K are cross hatched. Potentially

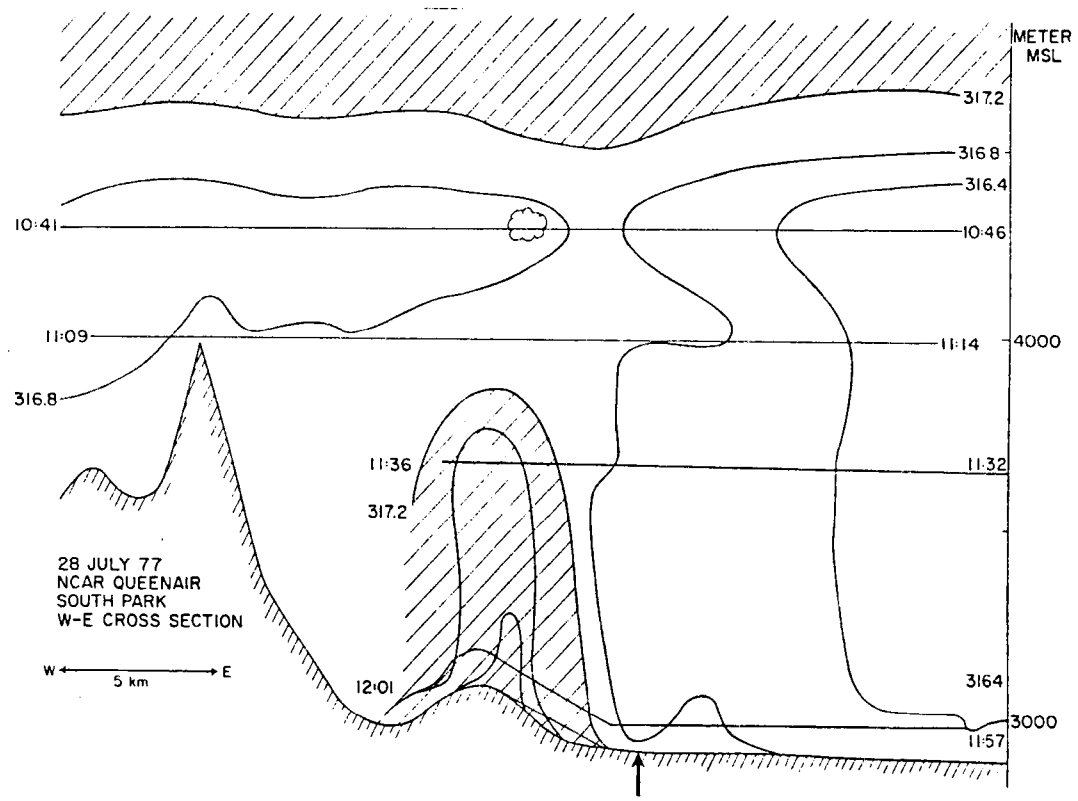

Figure 4.22: Detailed potential-temperature cross section from aircraft data with isentropes drawn at intervals of 0.4 K. Warm areas with $\theta > 317.2$ K indicated by cross-hatching, and a small, nonbuoyant cloud is shown in the upper flight leg.

warmer regions (i.e., regions with larger potential temperature) include the stable free atmosphere above the highest flight leg and a warm tongue extending vertically from Sheep Ridge, the low ridge just east of the main mountain barrier. Above the warm tongue at the middle of the upper flight leg there is a small, dynamically inactive cumulus cloud (Hahn, personal communication). To the right of the warm tongue in the figure, one can see evidence of shallow CBL structure below the second flight leg (from the ground) and evidence of the neutral layer aloft above the second flight leg. The isentrope pattern shown in this figure will be used as a background in the following analyses.

The moisture analysis corresponding to Fig. 4.22 is shown in Fig. 4.23a, superimposed on the θ analysis. The dashed lines are isopleths of water-vapor mixing ratio, drawn at intervals of 0.5 g kg^{-1} The regions where the mixing ratio is greater than 4.0 g kg^{-1} are shaded. One of the major shaded regions is coincident with the shallow CBL. Also indicated on the figure are the mean horizontal winds as measured by the aircraft for segments of each flight leg. The winds were generally westerly except for the lowest flight leg, where the winds were easterly from the lower areas of the Park to just west of the base site (arrow), and a few points along the second flight leg, which are marked by E (easterly) or S (southerly). This figure again indicates that the shallow CBL was just at the second flight leg. The moist region, where mixing ratios were greater than 4.0 g kg^{-1}, extended up to this level. Additionally, the winds at several points along this flight leg had shifted to an upslope direction (E or S) characteristic of the shallow CBL.

Fig. 4.23b shows the vertical velocity analysis for the same cross section. The shading indicates general regions of subsidence. General features shown on this figure are obstacle flow over the main mountain barrier (upward velocities upwind and downward velocities downwind), a general region of ascent near the warm tongue, and a general region of subsidence downwind of the rising air. The lowest flight leg, flown in the unstable surface layer, shows highly variable vertical velocities, but the amplitudes of the departures are smaller than those in the higher legs.

As mentioned above, shortly after this cross section was flown, the deep afternoon CBL became established over the Park. Dry, gusty,

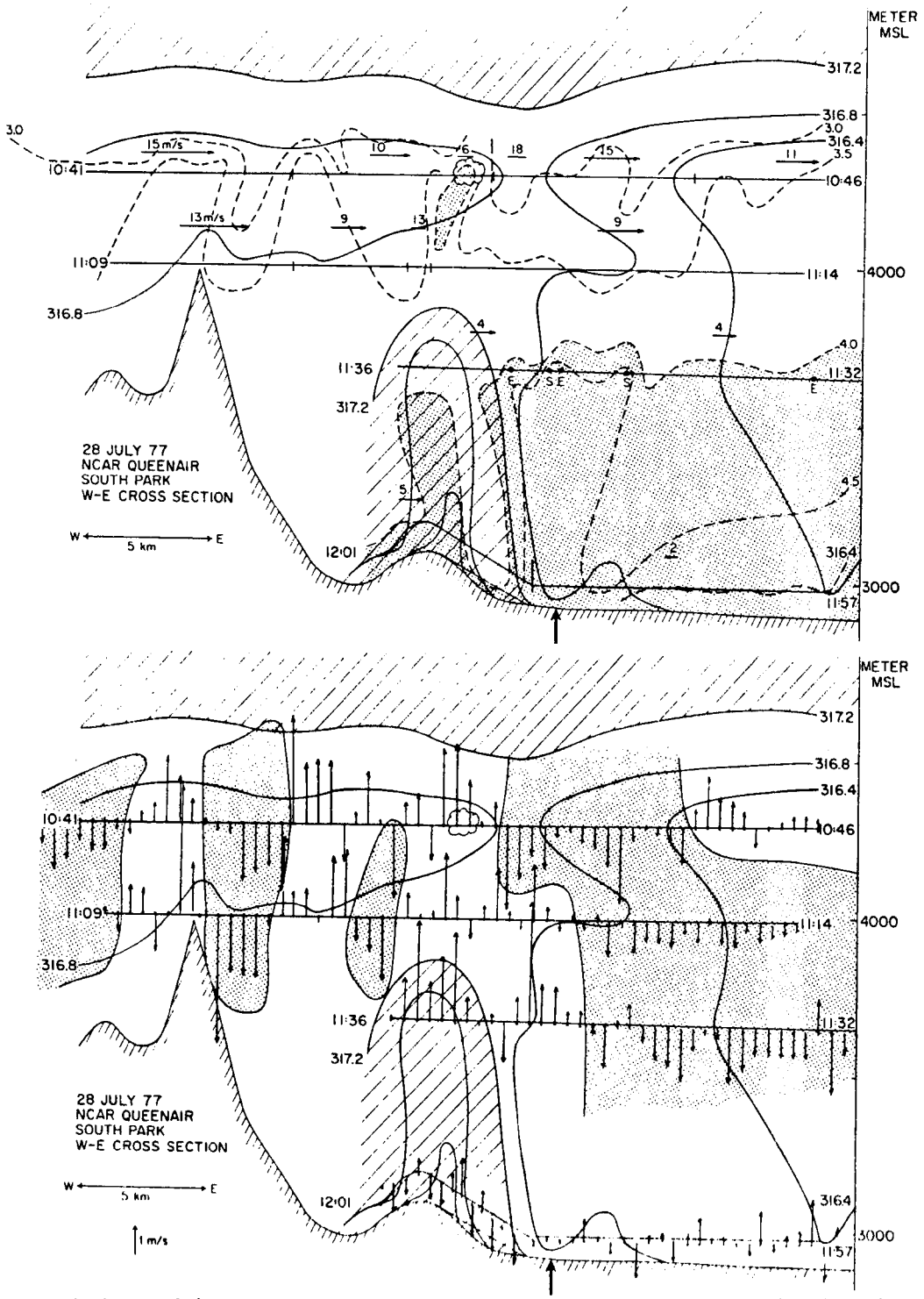

Figure 4.23: (a) Horizontal winds (arrows) with speeds in m/s and humidity mixing-ratio isopleths (dashed, at intervals of 0.5 g/kg) superimposed on θ analysis of Fig. 4.22. Mixing-ratio values of greater than 4 g/kg are indicated by shading, and the lettered dots along the second flight leg from the surface indicate where easterly (E) or southerly (S) winds have penetrated to that level. (b) Vertical velocity values superimposed on θ cross section. Regions where subsidence predominates are shaded.

westerly winds appeared at the surface, and the occurrence of surface westerlies moved from west to east through central South Park. This occurrence was typical of a dry day. A cross section through the deep afternoon CBL was obtained on 18 July. Fig. 4.24a shows the east-west potential temperature cross section for these flights. Over South Park, one sees a warm surface with an unstable surface layer, a deep afternoon CBL extending to nearly 2½ km above the ground, and the edge of the stable atmosphere above. A relatively warm tongue extends vertically from Sheep Ridge, just west of the Base Site. A similar view of the deep afternoon CBL comes from the north-south cross section shown in Fig. 4.24b. The overall structure in both of these observed cross sections supports the proposed model cross section presented in Fig. 4.17d, although there is considerable horizontal variability in the observations which is not intended to be portrayed in the model.

3. Further physical interpretation of cross sections

In the previous two subsections, a conceptual model in the form of potential temperature cross sections was proposed and then verified using aircraft data. These cross sections portrayed the daytime evolution of the convective boundary layer in South Park. The sequence of cross sections, when combined with the surface mesonet observations presented earlier, leads to a physical interpretation of what took place. This physical explanation will be presented in the following subsection.

As before, when we discussed vertical temperature profiles through the wind regimes, it is convenient to consider the state of the boundary layer late in the afternoon of the day prior to the day of interest. A deep, well-mixed, afternoon CBL is present everywhere over South Park, and winds of the convectively-mixed regime are present at

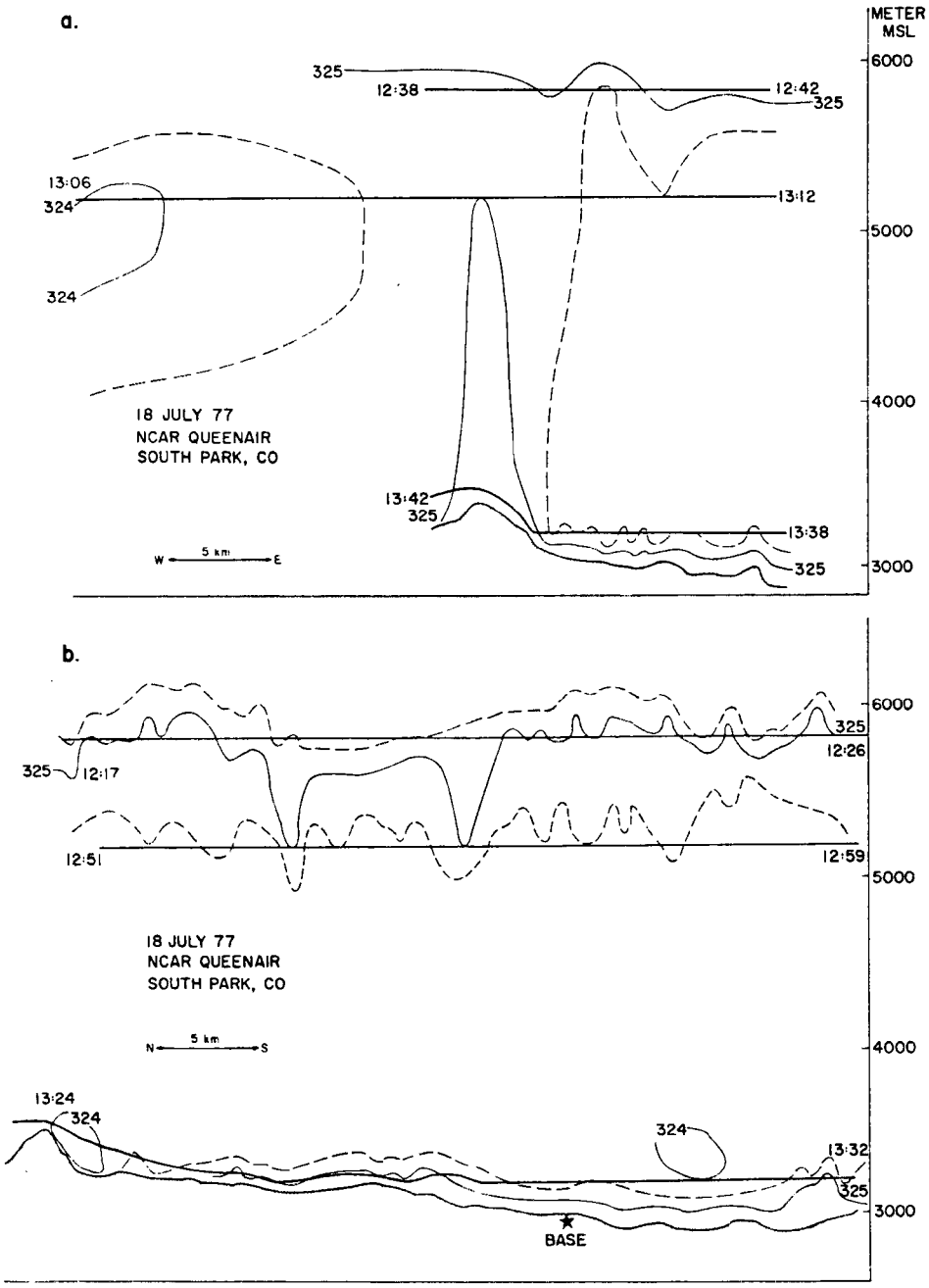

Figure 4.24: Potential-temperature cross sections from aircraft data showing the structure of the deep afternoon CBL on 18 July, which was a dry day: (a) east-west cross section, and (b) north-south cross section. (Based on cross sections provided by D.C. Hahn.)

the surface. After sunset the ground cools. As air near the earth's surface cools at night, two things happen. First, the stable temper-

ature profile of the nocturnal inversion indicates that turbulent mixing is suppressed; thus the winds below the nocturnal inversion become decoupled from the winds aloft. Second, the cool air drains down the slopes forming a pool or "lakes" of cold air in mountain valleys has been described by Geiger (1965, pp. 396ff) and Yoshino (1975, pp. 425ff). Although several river valleys drain South Park to the east, they do not prevent an extensive pool or lake of cold air from forming in the Park at night. Fig. 4.15a represents a sounding through this cold pool, while Fig. 4.17a represents a cross section through it.

After sunrise, heating occurs at the earth's surface. A shallow, ground-based CBL forms at the base of the cold pool. Fig. 4.15b shows a representative sounding taken at this stage. Within the convective layer, upslope winds are generated. The cross section in Fig. 4.17b shows a thin, warming convective layer (shaded) forming at the underside of the cold pool. The winds in this layer are blowing up the slope, with the result that they are producing cold advection along the slope. This cold advection is probably responsible for the dip in temperature observed in the base-station temperature traces in the previous section, and the interplay between the cold advection and turbulent heat flux from the surface can cause the morning temperature to increase in pulses.

As surface-based heating persists, the CBL warms and grows in depth. Fig. 4.15c shows the deeper shallow CBL above the base site, topped by a now-thin stable layer, which is all that remains of the nocturnal inversion. The shaded region in Fig. 4.17c represents the deeper shallow CBL. The thin stable layer at its top (between the shaded region and the dotted line-still representing the top of the cold pool)

continues to decouple the upslope flow in the shallow CBL from the winds aloft.

Finally, the convective layer reaches the top of the cold pool. The pool is heated to the same potential temperature as the air above, and the last vestige of the nocturnal inversion disappears. The deep afternoon CBL establishes itself all the way from the floor of the valley to the top of the former neutral layer aloft (Fig. 4.15d and 4.17d). At this time the boundary layer over South Park is like the deep, well-mixed CBL which had been there the previous afternoon, as mentioned above, and the convectively-mixed wind regime is again established at the surface.

One of the conclusions of this chapter has been that the dissolution of the lake of cold air which forms in the Park at night occurs mostly through the upward growth of the shallow CBL which forms at the underside of the cold-air lake. Other mechanisms have been suggested to account for the dissolution of the cold pool in valleys, as discussed previously in Chapter II.

Some of the previous studies have shown that the top of the inversion layer (cold pool) sinks during morning heating. The observations in these studies, however, were taken in relatively narrow valleys--considerably narrower than South Park.

Using our South Park data, an inspection of rawinsonde and Tethersonde soundings taken on dry days revealed no consistent tendency for the top of the nocturnal inversion layer to lower during the course of the morning. Thus the mechanisms described above seem to have little effect on the eventual dissolution of the inversion layer in South Park.

The second mechanism was that proposed by Lenschow, et al. (1979), namely that turbulent drag forces at the top of the cold pool tend to pull the cold air along, eventually moving it out of the lower areas. While this mechanism presumably operates to aid in cold pool dissolution in South Park, the importance of it compared with the inversion growth mechanism probably varies from day to day, depending for example on the direction and strength of the ridgetop winds, the depth of the cold air pool, etc. It is likely that this mechanism contributes to the eastward propagation of the surface afternoon westerlies across South Park, which has been described earlier in this chapter.

It is important to recognize at this point that the other mechanisms which have been proposed for the destruction of the cold pool in mountain valleys are unquestionably operating in South Park, but because of the broad geometry of the Park these effects are masked by the other processes occurring. Observations in South Park (Hahn, 1980) and modelling results similar to those presented later in this dissertation have shown an enhancement of turbulence in the neutral layer aloft above the cold pool. As postulated by Davidson and Rao (1958) and Ayer (1961), this turbulence is produced by the sunlit ridges and peaks which protrude from the cold air layer. Because of the presence of this turbulence, some erosion of the cold pool must be occurring from above, as proposed in the studies just cited. The effect on the overall dispersal of the cold air pool, however, is negligible. Similarly, because of the morning upslope winds blowing up the slopes ("sidewalls') of the Park, there must be a net horizontal divergence of mass from the lower areas. This must produce some subsidence and inversion descent over the valley, as proposed by Whiteman and McKee (1977) and Whiteman

(1980). South Park is a very wide valley, though, so the total mass of air evacuated by the upslope is small compared with the total amount of mass in the cold air pool. Thus, while some descent of the inversion undoubtedly occurs, the amount is imperceptible in the observations, and the effect is unimportant in the evolution of the inversion layer.

As suggested in the preceding paragraph, the importance of the inversion descent mechanism proposed by Whiteman and McKee (1977) seems to be related in part to the width-to-depth ratio of the valley in question. Inversion destruction in deep, narrow valleys generally involves inversion descent, while destruction through the upward growth of the shallow DBL occurs primarily in wider valleys. This hypothesis is supported by as yet unreported 2-D numerical simulations by Bader (personal communication) in valleys that were 500m. deep. In valley cross sections that were 5 km. from crest to crest, inversion descent occurred, while in valley cross sections that were 7 km. from crest to crest, CBL rise without inversion descent occurred. Also, Whiteman (1980) observed that the only case which he studied in which inversion destruction occurred solely through the growth of the shallow CBL (which he called a "Pattern 1 Inversion Destruction") was in the widest valley he studied. However, it must be pointed out that valley width is not necessarily the whole story, since soundings on other days in the same valley did show evidence of inversion descent. In extremely wide valleys like South Park, on the other hand, inversion descent does not ever seem to paly a role in inversion destruction.

In summary, on most dry days in South Park, the destruction of the nocturnal inversion layer or cold pool occurs chiefly through the upward growth of the shallow CBL which results from surface heating. On some days the drag mechanism proposed by Lenschow et al. (1979) is apparently important, but the other effects and mechanisms which have been proposed from inversion destruction in valleys seem to be unimportant.

D. The Leeside Convergence Zone

In this chapter it has been shown that the daytime progression of the local winds in South Park is best described by considering the processes which affect the extensive pool or lake of cold air which forms at night. The pool is eroded by heating from below, until--on a dry day--it shrinks and disappears. After the disappearance of the cold pool the deep afternoon CBL is established all over South Park, and convectively-mixed winds exist at the surface.

Obviously, there is a transition time between when upslope-regime winds are present beneath the cold pool in most of South Park and when convectively-mixed afternoon winds exist at the surface all over the Park. During this transition time, both upslope-regime winds and westerlies coexist over South Park. The convectively-mixed westerlies exist in the higher areas where the deep CBL has already been established. The areal extent of the cold pool, which can be identified at ground level by the areal extent of upslope-regime winds, steadily shrinks. This shrinking can be attributed to the fact that the cold pool (inversion layer) is shallower at the higher elevations of the Park and to the fact that the drag force at the top of the pool is dragging the cold air downwind.

1. Surface observations at slope and valley sites

To further investigate the behavior of the cold pool, data from two surface mesonet sites were analyzed and compared. The first site was the base site, located on the east-facing slopes of the Mosquito Range and just west of the stream bed of Four-Mile Creek, as discussed in Chapter III; this will also be referred to as the "slope" site. The second site is site 7 on the map in Fig. 3.1. This site is also in the valley of Four-Mile Creek, but it is 170 m lower in elevation than the base site. Thus, it will be referred to as the "valley" site.

Surface data from both stations for 3 August is shown in Fig. 4.25. The upper row reproduces the base station data that were already presented in Fig. 4.4; again, the upslope-regime data are indicated by shading. The lower row in the figure shows the corresponding data for the valley (lower) site. Many features evident in the base-site data can also be seen in the valley site data, such as the early- and late-morning windshifts, the gustiness and dryness of the afternoon winds, etc.

The shaded areas in the lower row of data indicate the duration of the upslope regime, as in the upper row. Two things are evident: the morning shift to upvalley winds was nearly simultaneous at both sites, but the shift to afternoon westerlies occurred nearly an hour earlier at the higher base site than at the valley site. The former observation indicates that, on this day, the upslope winds did not form in the lower areas of the valley and propagate up the slopes in an "upslope front", but rather the tendency towards upslope was felt at all points along the slope at the same time. The latter observation suggests that such a front or discontinuity line could be associated with the afternoon windshift.

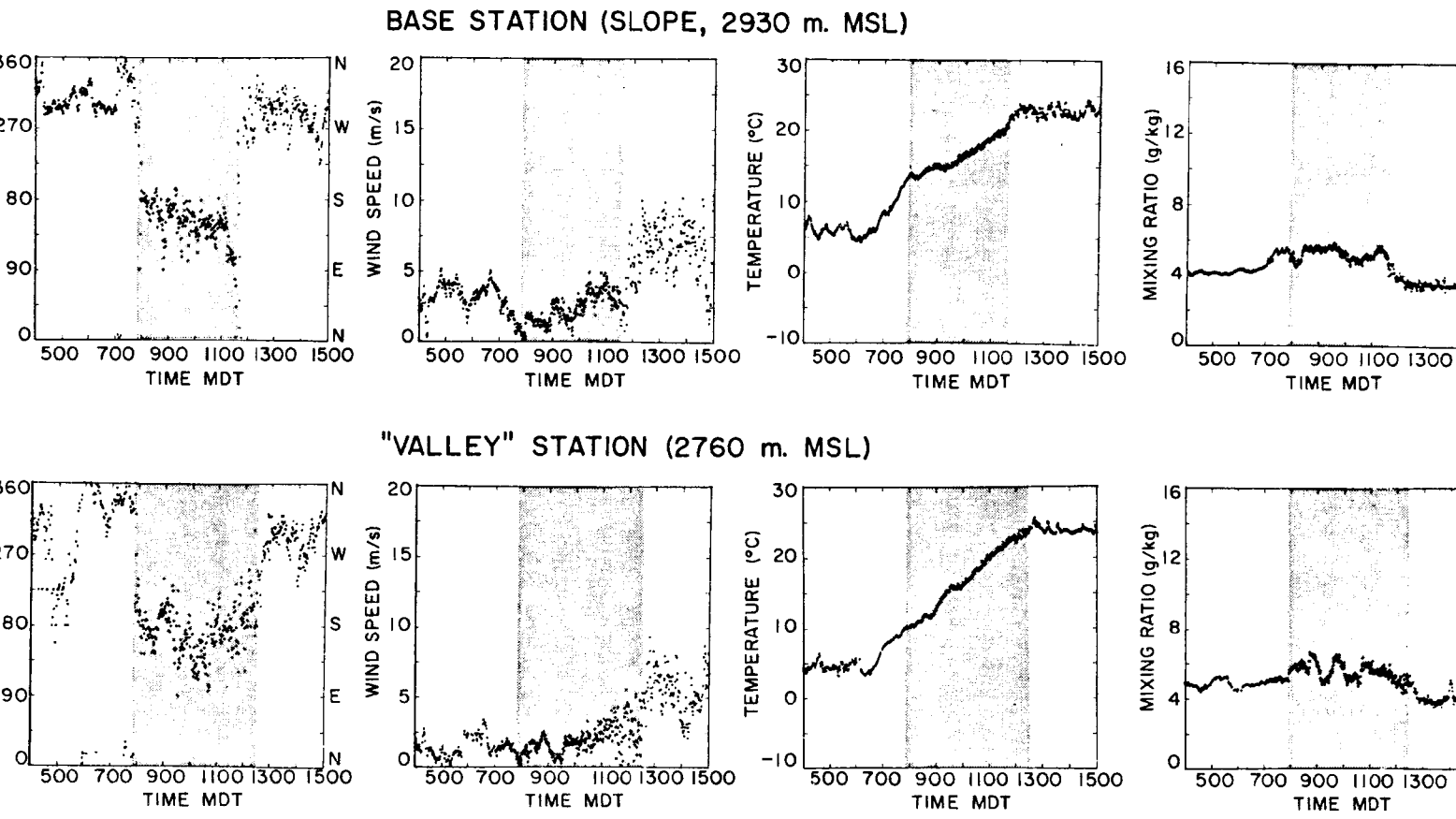

e 4.25: The duration of the upslope-regime wind systems at two stations in South Park on 3 Augu
The upper row represents data for the Base Station and is thus identical to Fig. 4.4.
lower row is data from a station lower down in the valley of Fourmile Creek, Station 7
Fig. 3.1. Times when upslope-regime winds are present at each site are indicated by sh

In order to find out how representative these observations were, the duration of the upslope regime at both stations was determined for eleven dry days during SPACE-77 (including 3 Aug). The results are shown in Fig. 4.26, where the duration of the upslope regime is again

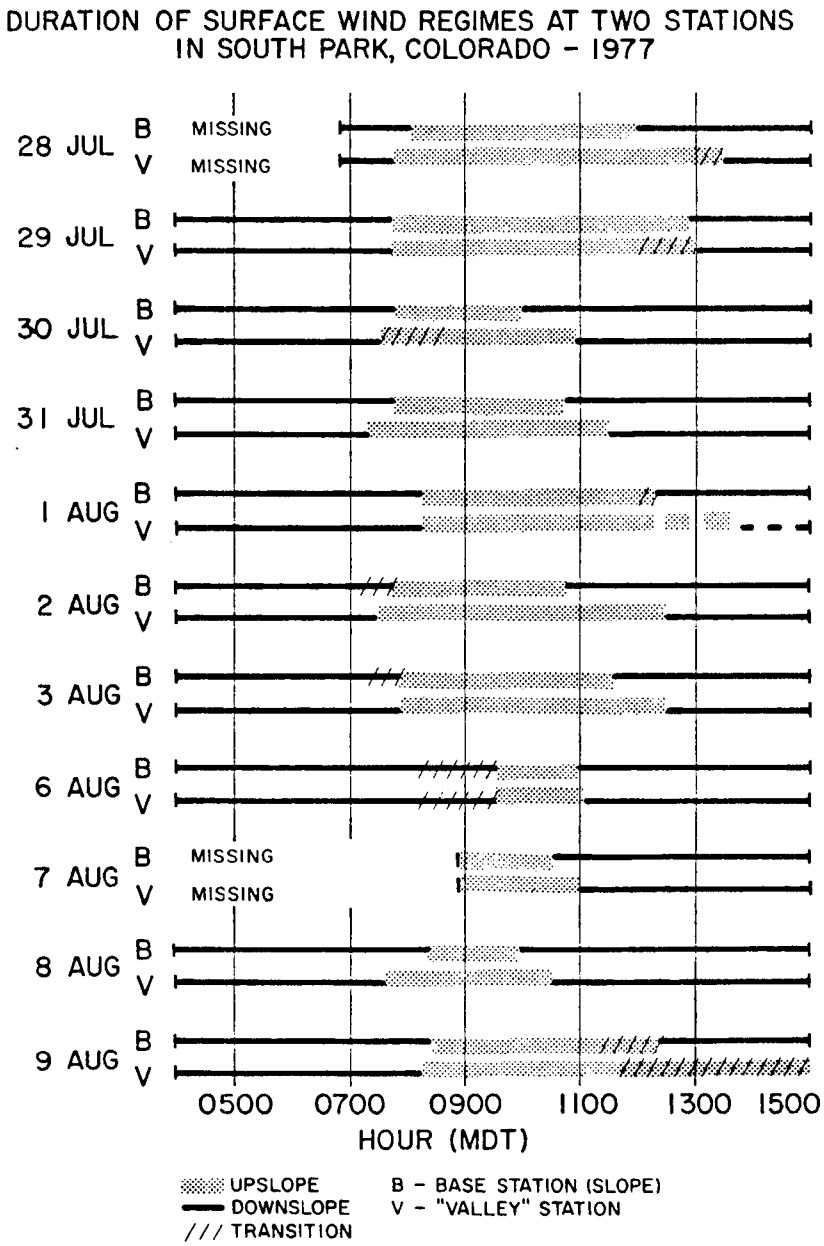

Figure 4.26: Duration of upslope-regime winds (shaded region) at the Base Site and the Valley Site for eleven dry days during SPACE-77. Note that upslope-regime winds always lasted longer at the lower Valley Site than at the uphill Base Site.

indicated by shading. On four of the days, the morning shift to the upslope regime occurred simultaneously, as it had on 3 Aug (above). On one of the days, the morning windshift was not sampled. On all six of the remaining days, the upslope appeared first at the valley station and then at the slope (base) station. Thus on these six days, the upslope winds did propagate up the slope. Moreover, the fact that upslope winds occurred first at the lower site rules out the possibility that the upslope could have been initiated by updrafts that were caused by the heating of the ridgetops and higher elevations.

On all eleven occasions, the afternoon windshift occurred first at the base (higher) site and then at the valley (lower) site, or, in other words, the westerlies propagated down the slope. The reasons why the westerlies should appear first at the upper elevations of the Park have already been discussed. First, the nocturnal inversion is not as deep there as it is lower in the valley. The shallow-upslope CBL may only have to eat vertically through 200 or 300 m of inversion along the slope, whereas lower in the valley it may have to eat through 500 m or so. Second, the drag hypothesis of Lenschow et al. (1979) is consistent with the eastward propagation of the westerlies.

One can generalize the important findings in Fig. 4.26 as follows upslope regime winds tend to occur longer at the lower site. This is true for the afternoon (or late morning) transition, and it also tends to occur at the morning reversal.

When the upslope regime is active during the later morning hours, the east-facing slopes of South Park are a region where upslope or upvalley winds with an easterly component, blowing up from the lower areas of the valley, meet with convectively-mixed winds with a westerly

component, blowing down from the direction of the ridges. The region of confrontation between the two wind regimes is a line of convergence and, as pointed out earlier, the line propagates down the slope.

PAM charts showing the existence of this convergence zone in central South Park are shown in Fig. 4.27. The convergence region is indicated by shading.

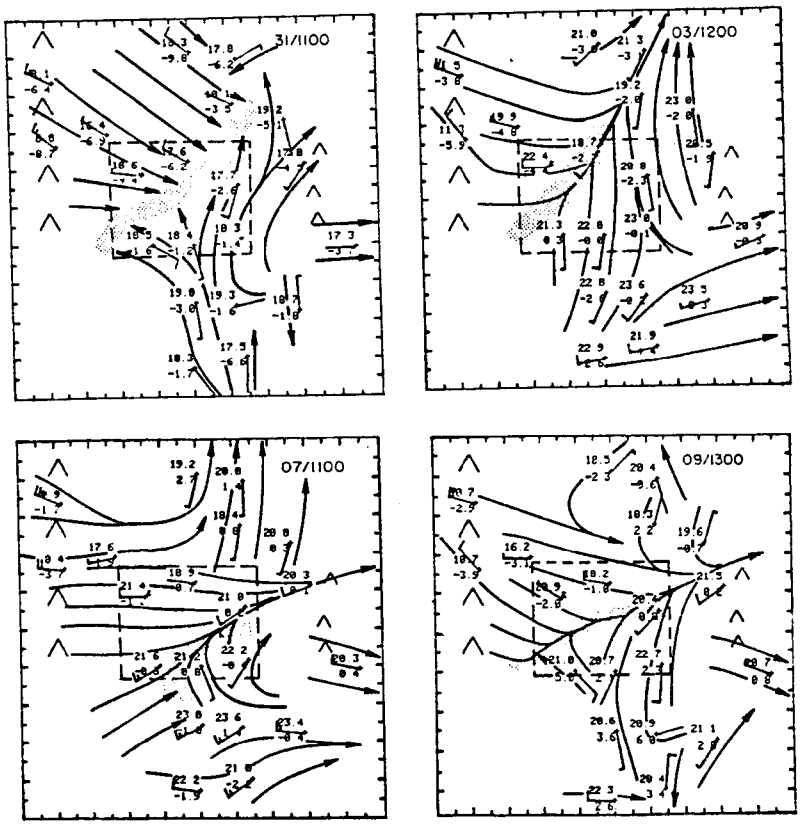

Figure 4.27: PAM surface charts and streamline anlayses showing the existence of a South Park convergence zone on four dry days. The location of the convergence zone is indicated by shading.

The existence of a convergence zone and upward wind velocities to the leeward side of mountains has been observed in other studies. Braham and Draginis (1960), for example, found evidence of convective cores of rising air downwind from the main ridge line of the Santa Catalina Mountains northeast of Tucson, Arizona, using aircraft data.

They attribute these rising currents to the "valley-breeze circulation," although they also mention the importance of the mountain range as a high-level heat source. Orville (1965) studied the initiation of cumulus clouds in the same mountain range using photogrammetric techniques. He found that the initiation of the visual clouds tends to occur downwind (as determined from the Tucson morning rawinsonde) from the ridgetops: on days with northerly ridgetop (3 km MSL) winds, cumuli tend to form south of the main ridge, while on days with southerly ridgetop winds, cumuli tend to form north of the ridge. Thus, the main regions of updraft formation, as indicated by the presence of cumulus clouds, tend to form on the lee side of the main ridge line, consistent with our finding in South Park. In another study, Raymond and Wilkening (1980) analyzed aircraft observations of the dry-convective circulations over the San Mateo Mountains in west-central New Mexico. They found a net convergence of winds at levels below the ridgetops and divergence above, consistent with a view of the mountain range as an elevated heat source, and implying a general region of rising air motion there. This overall region of rising air, which was around 20 km in diameter, is embedded with smaller-scale convective updrafts. The diameter of these smaller-scale eddies, determined by a spectral analysis of the aircraft-measured w component of the wind, was 3-4 km, in agreement with observations reported by Braham and Draginis (1960). Raymond and Wilkening also found that values of the water-vapor mixing ratio were "substantially enhanced downstream of the mountain range, leading to a significant difference between mean and upstream ambient values for upwind-downwind traverses."

2. Initiation of cumulus clouds in the mountains

In addition to providing some evidence for the leeside convergence zone as a feature of the dry circulations over the mountains, these studies also discussed the importance of local-scale features in creating updrafts on at least two different scales. The larger scale pertains to the mountain range as a whole, which acts as an elevated heat source and creates a general region of rising motion. The smaller scale is a scale of localized, more intense updrafts, which could be in the form of random thermals or could be in response to forcing by local features, such as the leeside convergence zone. Either of these types of smaller-scale updrafts could initiate cumulus clouds.

The argument which led to the description of the leeside convergence zone was largely a two-dimensional argument. Conceptually, the height of the ridge was assumed not to vary in the third dimension, and thus the intensity of the convergence also would not vary along the ridge. In reality, however, no such two-dimensional ridge exists, and one expects the intensity of the convergence to vary along the length of a ridge, depending on local terrain geometry, ridgetop winds, depth of cold pool, and a miriad of other causes. For example, a nice instance of such a three-dimensional effect occurred in the numerical model results of Mahrer and Pielke (1977; see Fig. 3 and p. 109 of that paper). Thus, the function of the third dimension is to focus the convergence in some regions and to deintensify it in others. One can view the convergence line, which exists along the edge of the cold pool, as consisting of localized regions of more intense convergence and stronger updrafts, and regions where thes processes are less pronounced.

A region in South Park where the convergence zone was observed to occur during much of the morning on many days was between the base site and site number 8 on Fig. 3.1. Site 8 is located in the valley of Four-Mile Creek just before it comes out of the mountains. Huggins (1975) performed a radar first echo study of a region that included the northern parts of South Park during the summer of 1973. He found that the region around and southwest of Fairplay was a region of above-average first echo formation. Fig. 4.28 is reproduced from Huggins' paper, with the location of Fairplay and our main base site in 1977 indicated. Although this study was from a different year, the results suggest that the preferred region for the convergence zone is also a preferred region for the initiation of cumulus cloud activity.

Although this dissertation is concerned with dry convective circulations in South Park, it is interesting to digress and speculate on the relationship between the leeside convergence zone and cloud formation. One would expect that the zone should be a preferred region for cloud initiation for two reasons: (1) the highest moisture values in the valley most often are advected by the upslope winds from the low areas of the Park into the convergence zone, and (2) a strong and persistent upward movement of air exists in the convergence zone. These conditions not only favor cloud initiation, but they also encourage the continued development of clouds in this region, if the larger-scale environment favored deep convection (e.g. thunderstorm formation). Henz (1973) discussed the importance of "hot spots" along the Front Range (east of South Park) in the formation of thunderstorms and severe weather over the high plains of Colorado. He found that nearly 70% "of all mountain foothill thunderstorms originated in hot spots," and over

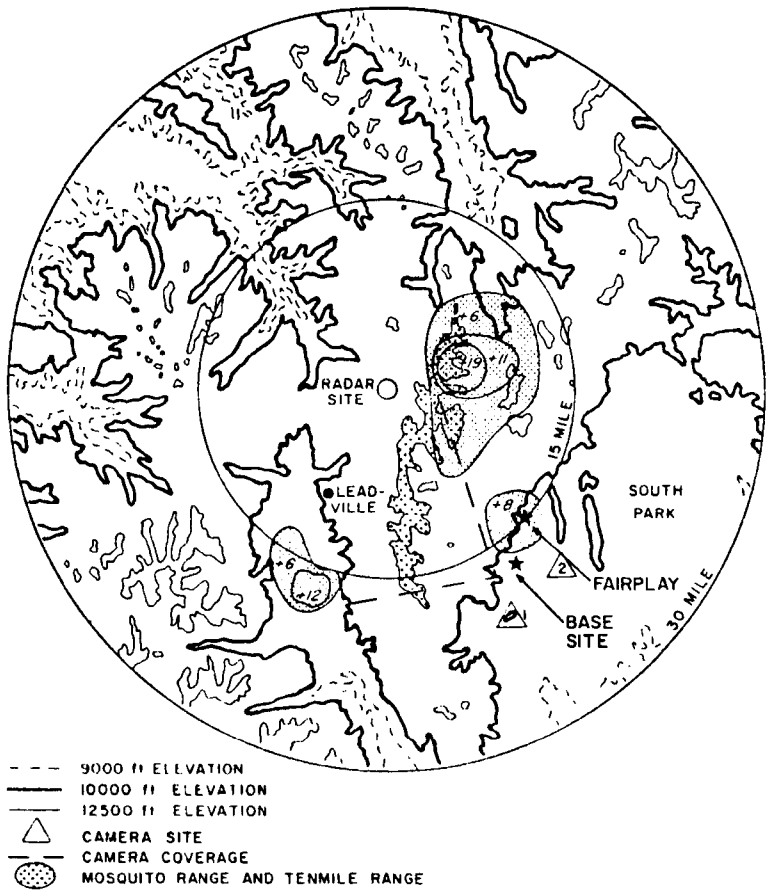

Figure 4.28: Regions of above-average radar first-echo formation (shaded areas) for the summer of 1973 as determined by an M-33 tracking radar located on Chalk Mountain. Although South Park is over a high range of mountains from the radar site, an above-average area of first echo formation was observed northwest of the SPACE-77 Base Site. (Huggins, 1975).

70% of all observed severe weather "was produced by hot-spot-originated convective systems." Unfortunately, Henz's study does not extend as far west as the Mosquito range, but it seems plausible that some (if not many) of the observed "hot spots" are actually regions of enhanced leeside convergence, as discussed in previous paragraphs, or are at least downwind of such regions.

A likely scenario for the development of deep convection is as follows: The potential for deep convection is controlled by the large-

scale environment. On a favorable day, two kinds of shallow clouds form. Some small cumulus form more or less at random, while others form in organized updraft regions, such as the enhanced areas of the leeside convergence zone. The cumuli which form in organized regions would be favored for growth, for the reasons presented above. Thus, these organized regions of updraft and cloud development serve as kindling in preparing the atmosphere for the blaze of deep convection which will occur later in the day.

3. Summary of discussion of leeside convergence zone

In this section evidence has been presented which shows the existence of a dry, mesoscale convergence line at the edge of the cold pool in South Park. On dry days, the cold pool shrinks until dry westerlies take over the Park and the convergence zone disappears. On moist days cumulus cloud development occurs preferentially in regions of organized updrafts, such as the leeside convergence zone. The convergence feeds in water vapor which kindles the moist convection and initiates the development of deep cumulus and cumulonimbus clouds.

E. Recapitulation of Observations Presented in This Chapter

In the preceding chapter observations have been presented in an attempt to describe the interaction between the winds and thermal structure in South Park on a typical dry day. These observations are briefly summarized as follows:

Surface mesonet data showed the existence of three surface wind regimes in South Park: a downslope regime, an upslope regime, and an "afternoon westerly" regime. Vertical θ and wind profiles showed that the upslope winds occupied a shallow CBL which formed beneath

the nocturnal inversion layer, and that the afternoon winds resulted from the downward convective mixing of ridgetop-level winds.

These processes were most easily visualized by considering the pool or lake of cold air which formed in the Park at night. The pool itself was a statically very stable air mass, since θ increased strongly with height in it. Thus, the coupling between the winds aloft and the winds within the cold air layer was very weak. After sunrise, when the earth's surface began to heat, the weakness of this coupling allowed upslope winds to form in a thin layer along the underside of the cold-air lake. If the coupling or mixing were stronger, westerly momentum would be mixed downwards and no upslope would form. The upslope actually formed in a shallow CBL. The shallow CBL grew in depth as morning heating proceeded, so that the upslope layer (which coincided with the shallow CBL) also deepened. Eventually heating from below warmed the cold-air pool to the same potential temperature as the air above, and a deep layer of mixing occurred rather suddenly; this caused the winds in the upper region to mix downwards to the surface.

As heating continued after the cold pool had been dissolved, the afternoon CBL grew in depth. Finally, near sunset, the ground began to cool. Cold air drained off the slopes and into the lower areas of the Park, and formation of another lake of cold air began anew.

V. OBSERVATIONS OF SURFACE-LAYER TURBULENT ENERGY

In the previous chapter observations and interpretations of observations of the mean structure of the evolving daytime boundary layer over South Park have been described. In the following chapter observations of turbulent kinetic energy (TKE) in the atmospheric surface layer over South Park are discussed. The TKE is defined as:

$$TKE \equiv \overline{u'^2} + \overline{v'^2} + \overline{w'^2}$$

where the prime in this case represents an instantaneous deviation from a temporal average, which will be defined below. The measurements discussed in this section were made with the Gill UVW anemometers and with the NCAR Queenaire aircraft, both described in Chapter III.

A. Background

Before presenting any results, it is convenient to describe the observed behavior of velocity variances in the unstable surface layer over flat terrain. The unstable surface layer represents the lowest 10% of a CBL. From the definition given above, it is evident that TKE can be divided into two parts: a vertical part ($\overline{w'^2}$) and a horizontal part ($\overline{u'^2} + \overline{v'^2}$). As discussed in Appendix A, the vertical part has been shown to obey Monin-Obukhov scaling laws in the horizontally-homogeneous surface layer, but the horizontal part does not. Variations of u and v about their temporal mean value in the unstable surface layer are modulated by the passage of large thermal eddies, which occupy the entire depth of the CBL, past the sensor.

We thus have a situation in which variations in the horizontal winds in the lowest levels of the CBL are controlled by circulations (eddies) that are as deep as the CBL itself. The size of these large eddies is thus proportional to the height of the convective inversion, z_i, at the top of the CBL. The maximum values of vertical velocities reached in the middle part of the CBL are proportional to the velocity scale, w_*, which is defined as:

$$w_* = [(g/T_v)\overline{w'T'_{v_o}}\ z_i]^{1/3}. \qquad (5.1)$$

Hence, the magnitude of w in the middle part of the CBL is related to the magnitude of the surface heat flux (which produces the buoyancy force, which in turn drives the vertical acceleration) and to the distance over which the acceleration is allowed to operate (which is proportional to z_i). These accelerations drive the upward branch of circulation cells or thermals, and these cells move with the mean horizontal wind speed in the central part of the CBL (see Appendix A). The lower branch of these cells produces relatively long-period (several minutes) variations in the horizontal velocities near the ground. These long-period variations predominate in the magnitudes of the horizontal velocity variances, $\overline{u'^2}$ and $\overline{v'^2}$. Panofsky et al. (1977) used data from a variety of studies to show that the standard deviation of the horizontal velocity components (which equals the square root of the variance) is an increasing function of w_* in the unstable surface layer, and in fact it is proportional to w_* for large values of the mixed-layer stability parameter $z_i/-L$.

B. Measurements of TKE in the Surface Layer

The time plots of wind speed presented in the previous chapter showed that the afternoon winds were considerably gustier than

the morning upslope-regime winds. To further investigate this increase in gustiness, data from the UVW anemometers were analyzed to determine TKE values as a function of time of the day.

The UVW data were analyzed as follows: Mean values of each velocity component were obtained over time intervals of about 15 min. (representing 1024 observations), and a linear trend was then removed from the data in each 15-min. interval. The mean square of the detrended data was then computed for each averaging interval, e.g.:

$$\overline{u'^2} = \frac{1}{N-1} \sum_{i=1}^{N} \left(u_i - \overline{u(t)}\right)^2,$$

where N is the total number of data points in each averaging interval (1024), and $\overline{u(t)}$ is the linear trend in u. The mean square fluctuation, as defined above, is assumed to represent the variance of u in our horizontally inhomogeneous surface layer. The TKE is then determined from the variances of the three velocity components using the definition of TKE.

The TKE as a function of hour of the day on 3 August is shown in Fig. 5.1 for all three UVW anemometers and the bivane. Sunrise at the base site on this day was around 0615 MDT. Two major features are evident: a maximum in TKE after 0700 during the morning reversal to upslope flow, and a maximum after 1130 owing to the reversal from upslope to afternoon westerly winds (cf. Fig. 4.4). The winds after the 1130 maximum were considerably more turbulent than the winds before.

The behavior of the fluctuating KE based on bivane winds suggests a further interpretation of these maxima. At 0700 there was no increase in the KE of the wind <u>speed</u> fluctuations, as measured by the bivane (which points directly into the wind at all times). Thus, the

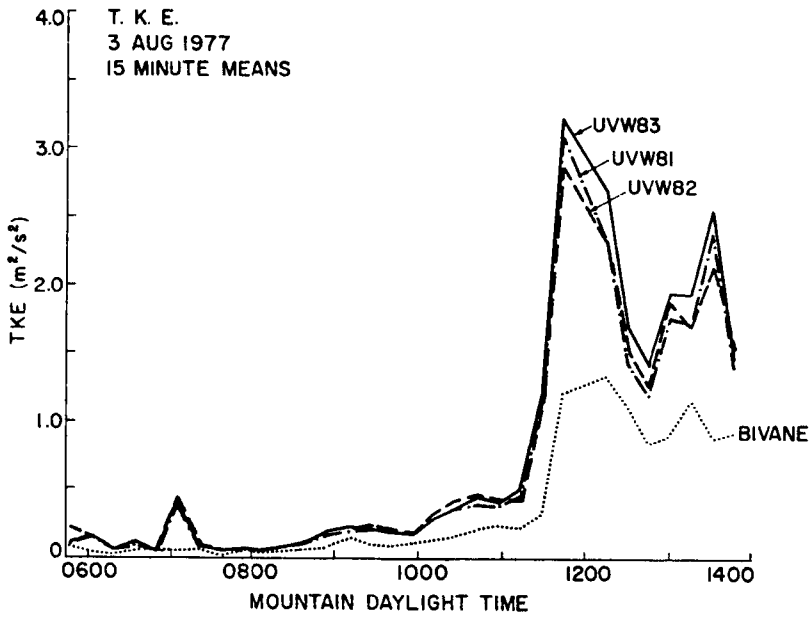

Figure 5.1: Turbulent kinetic energy (TKE) plotted as a function of hour of the day for the three UVW anemometers and the bivane. UVW83 was mounted at a height of 23 m, UVW82 at 9 m, UVW81 at 15 m, and the bivane at about 4 m.

increase in TKE at that time was due to directional fluctuations, i.e., the interplay between the u and v components. Similar behavior occurred after the 1130 wind reversal, when the TKE measured by the UVWs reached a peak while the fluctuating KE measured by the bivane was still on the increase. Thus, the spike in TKE after 1130 was mostly because of fluctuations in wind direction. Stated differently, this meant that the "instantaneous" wind during the averaging interval in question tended to have large deviations in direction from the mean wind, but small deviations in speed. Since these directional deviations arose from diurnal mesoscale flow features, they do not fit the traditional definition of turbulence as given, for example, by Tennekes and Lumley (1972, Ch. 1) or Lumley and Panofsky (1964, Ch. 1). Thus, we must

avoid these time periods when making quantitative extimates of TKE or velocity variances.

The dramatic increase in TKE after the shift to the convectively-mixed surface wind regime was noted in a previous chapter as an increase in gustiness (Fig. 4.4). It is of interest to determine why this increase should occur. Plausible explanations for the increase are related to the sudden increase in the depth of the CBL, as indicated between Figs. 4.15c and d. The jump in z_i should affect the eddy structure of the CBL. For one thing, the deeper boundary layer means that largerterrain features are included with the CBL, and these features can force larger eddies, both thermally and mechanically.

Another effect that an increase in z_i would have was discussed in the previous section of this chapter. An increase in the depth of the CBL causes an increase in the size of the large eddies in the CBL, and this in turn causes an increase in the variances of the horizontal wind components in the surface layer. Thus, if this mechanism were operating, we should expect to see an increase in the horizontal velocity variances, $\overline{u'^2}$ and $\overline{v'^2}$, after the transition. Fig. 5.2 shows the variances of all three wind components for the anemometer at the top of the 15 m tower (UVW-83). As expected, almost all of the jump in TKE is due to a sudden increase in the horizontal variances, with only a small increase in $\overline{w'^2}$ (neglecting the transition observations).

In order to determine whether the jump in horizontal variances could be attributed to the increase in depth of the CBL, calculations are performed below to determine whether the jump is consistent with w_* scaling as presented in the previous section. The consistency will be tested by computing the ratio of the values of $\overline{u'^2}$ and $\overline{v'^2}$ after

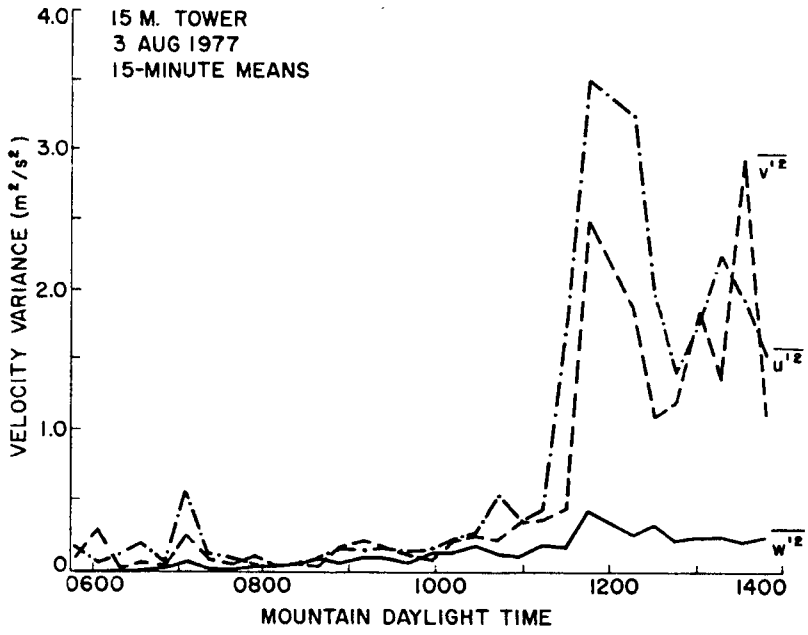

Figure 5.2: Variances of the three velocity components plotted as a function of hour of the day for UVW81, which was at the top of the 15 m tower.

the transition of values before the transition. Those ratios are then compared with the ratios of estimated values of w_* after the transition versus before the transition.

Table 5.1 shows values of both horizontal velocity variances (i.e., $\overline{u'^2}$ and $\overline{v'^2}$) for all three UVW anemometers, for a period before the transition and a period after the transition. Care was taken in selecting the two periods to avoid times of large directional variability owing to windshifts which occur during the transition period. Mean values for the variances of each UVW are computed for both time periods, and the ratios of the mean value after transition to the mean value before are calculated and entered on the line marked "Ratio"; These values range between 4 and 5. The average of all the $\overline{u'^2}$ ratios was 4.5, and of all the $\overline{v'^2}$, 4.7.

TABLE 5.1: HORIZONTAL WIND VARIANCES (m^2s^{-2}) FROM UVW ANEMOMETERS FOR 3 AUG 1977, SOUTH PARK BASE SITE

Time(mid)	$\overline{u'^2}$(81)	$\overline{u'^2}$(82)	$\overline{u'^2}$(83)	$\overline{v'^2}$(81)	$\overline{v'^2}$(82)	$\overline{v'^2}$(83)
Before Transition						
1012	.22	.30	.24	.20	.27	.21
1027	.34	.50	.28	.21	.24	.25
1042	.42	.61	.54	.23	.25	.22
1058	.29	.41	.35	.28	.33	.35
1113	.37	.39	.45	.35	.34	.36
mean	.33	.44	.37	.25	.29	.28
After Transition						
1230	1.6	1.9	2.0	0.9	0.9	1.1
1245	1.0	1.3	1.4	1.1	1.1	1.2
1301	1.6	1.9	1.8	1.6	1.6	1.8
1316	1.7	1.9	2.2	1.4	1.3	1.3
mean	1.5	1.8	1.8	1.2	1.2	1.4
Ratio	4.5	4.1	4.9	4.8	4.2	5.0
Mean Ratio		4.5			4.7	

If the hypothesized scaling laws are appropriate, $\overline{u'^2}$ and $\overline{v'^2}$ should be proportional to w_*^2, the square root of which was defined in (5.1). Thus, we are interested in determining the ratio of w_*^2 [after] to w_*^2 [before]:

$$\frac{w_*^2[\text{after}]}{w_*^2[\text{before}]} \sim \frac{\left(\frac{g}{T}\overline{w'T'}\right)^{2/3}\left(z_i\right)^{2/3}[\text{after}]}{\left(\frac{g}{T}\overline{w'T'}\right)^{2/3}\left(z_i\right)^{2/3}[\text{before}]}.$$

From crude plots of $\overline{w'T'}$ vs. hour of the day (obtained from tower data) and from the behavior of w'^2 in Fig. 5.2, one can conclude that there were no dramatic increases in heat flux during the day like those which occur in TKE, $\overline{u'^2}$ and $\overline{v'^2}$. Additionally, only a small change in the parameter g/T occurs across the transition period (see Fig. 4.4c), so that:

$$\frac{g}{T}\overline{w'T'}\,[\text{after}] \approx \frac{g}{T}\overline{w'T'}\,[\text{before}]$$

Thus we have:

$$\frac{w_*^2\,[\text{after}]}{w_*^2\,[\text{before}]} \sim \left(\frac{z_i\,[\text{after}]}{z_i\,[\text{before}]}\right)^{2/3}$$

From Fig. 4.13 b and observations on other days, we can estimate the z_i's: z_i [before] $\sim$ 300 m and z_i [after] $\sim$ 3,000 m.

Thus:

$$\frac{w_*^2\,[\text{after}]}{w_*^2\,[\text{before}]} \sim (10)^{2/3}$$

$$\approx 4.6$$

which falls within the range of 4 to 5 which we found earlier in the ratios of the horizontal variances. Therefore, the observed increase in $\overline{u'^2}$ and $\overline{v'^2}$ is consistent with w_* scaling laws, and the increase in

these variances could be due to the rapid increase in size of the large eddies in the CBL, which happens when the depth of the CBL (z_i) grows very suddenly.

C. Implications of TKE Observations

In the first section of this chapter the magnitude of the horizontal velocity variances in the unstable surface layer was related to the size and intensity of the large thermal eddies in the CBL which were being advected past an Eulerian sensor. Thus adherence of $\overline{u'^2}$ and $\overline{v'^2}$ to w_* scaling thus depends upon the presence of transient thermals in the CBL, moving approximately with the mean speed of the wind in the middle of the CBL.

In the second section the horizontal velocity variances in the surface layer over South Park were shown to be consistent with w_* scaling. It is somewhat surprising that this should be the case over the mountains, since hills and mountains are thought of as warm areas where thermals should be based. In the presence of such supposed "hot spots", one might think that there would be less tendency for thermals to move around and more tendency for them to remain attached to terrain features. The aircraft cross sections in Fig's. 4.18, 4.20, and 4.22 show warm tongues attached to a ridge and thus support this latter view. The applicability of w_* scaling to the horizontal variances, however, implies that at least some of the thermals which transport heat upwards are transient and not attached to terrain features.

The presence of transient thermals in the mountain CBL is not so anomalous as it may at first seem, though. The surface layer itself is a highly turbulent, highly disorganized warm region which cushions

the main portion of the CBL thermally from the ground below. Warner and Telford (1967) used aircraft data to study thermals in the CBL. They reported the following observations:

> ...towards the surface the temperature structure becomes erratic, there are no quiescent regions, and we can no longer speak of organized thermals.
>
> ...although thermals start from within this region close to the surface they are not here recognizable entities, and there is no necessity at all that they should originate at specific terrain features.

Moreover, in discussing the South Park observations presented in the previous section, both Lenschow (personal communication) and Deardorff (personal communication) stated that they were not surprised at the results. Like Warner and Telford their observations indicate that the unstable surface layer near the ground is so highly confused and disorganized that specific terrain features and hot spots do not seem to be important in anchoring thermals. Lenschow's impressions arose from the aircraft data he has analyzed, while Deardorff's were from his water tank observations.

None of the observations or impressions cited above really pertain to mountainous terrain. However, when combined with the observations in Section A of this chapter, these descriptions of the lower part of the surface layer raise questions as to how convection is organized in CBL's over mountainous terrain. It is tempting to hypothesize that dry convection in the mountains should be organized so that the warm ridgetops are at the base of more or less permanent thermals with strong rising air motions. The downward branches of these circulation cells would occur partly in the valleys between mountains, and partly over the plains adjacent to the range. The

observations presented above, however, indicate that this is probably not a completely accurate picture. At least some of the thermals which transport heat upwards seem to be transient--not attached to terrain features. Thus, it is of considerable interest to find out whether both types of thermal (attached and transient) actually exist in mountain CBL's.

D. Aircraft Observations of Thermals

To determine whether both kinds of thermal were present over South Park, the temperature traces of several aircraft flights were plotted. As described in Appendix A, thermals can be identified on an Eulerian temperature trace as follows: thermals appear as regions of elevated, yet highly variable, temperature interspersed among quiescent regions of relatively uniform temperature.

Fig. 5.3 shows an east-west aircraft flight leg flown on 20 July. The upper trace shows the potential temperature trace, with some obvious regions of elevated temperature. The middle trace shows the vertical velocity, with an arbitrary zero value. At the bottom, the terrain is shown as determined by the aircraft's radio altimeter, and the aircraft's flight path relative to the terrain is indicated by a dotted line. The terrain in this region tended to be rather two dimensional, so that the hills on the terrain drawing actually represent north-south ridges in South Park. Looking at the potential temperature data, one can see that the thermals penetrated during this flight leg were mostly associated with specific terrain features, i.e. the ridges.

Fig. 5.4 shows an east-west flight leg flown over a similar region of South Park on a different day, 18 July. The potential

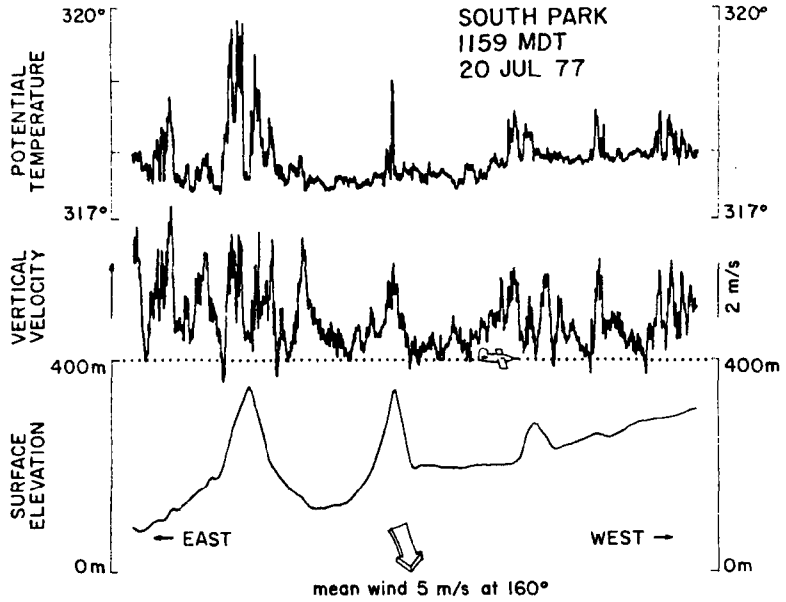

Figure 5.3: Potential temperature and vertical velocity data for a low-level, east-west flight leg of the NCAR Queenair on 20 July 1977. Most of the regions of elevated potential temperature--which indicate regions where thermals may be present--are associated with ridges in this figure.

temperature trace on this figure shows several thermals which are not associated with ridges or other specific terrain features, and some that are based at ridges. Thus, this flight shows that transient thermals, which are not associated with hills or ridges, do exist in the CBL over South Park. This flight leg, as well as the previous one, is representative of several flights which were studied for thermal structure. The overall conclusion that we can draw from the aircraft data is that both transient and attached thermals exist in the CBL over South Park. It is not possible to determine whether the thermals that <u>are</u> associated with terrain features are permanently attached there or may, for example, simply originate and spend some time there.

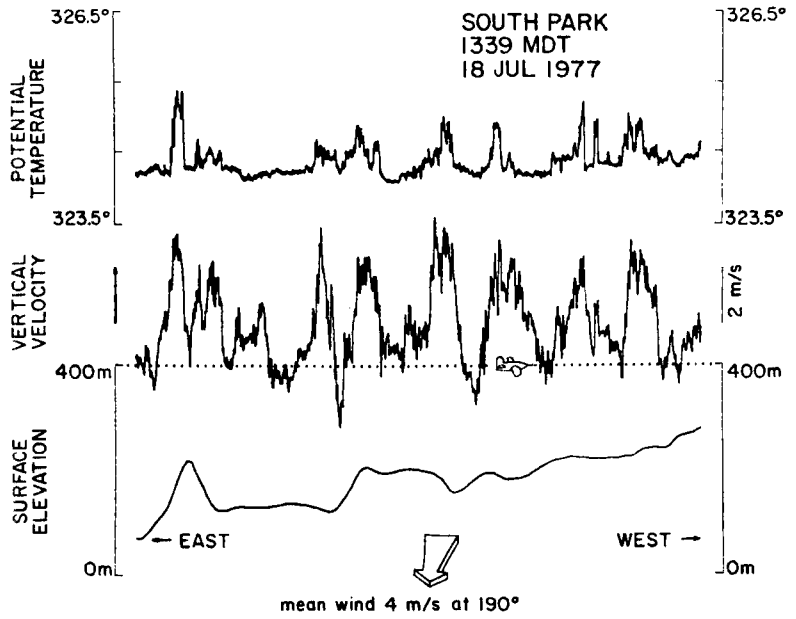

Figure 5.4: Potential temperature and vertical velocity data for a low-level flight leg on 18 July 1977. Many of the regions of elevated θ in this flight leg are not associated with ridges.

E. Discussion

It is well beyond the scope of this study to provide a comprehensive description of convection over mountainous terrain. Such a description will probably need to involve another field project at least, since SPACE-77 was not designed to study dry convection. An important question to be answered in such a study is: what is the role of hills, ridges, and mountains in localizing thermal updraft regions. In the following paragraphs, two impressions of characteristics of convection which were gleaned from the South Park data will be presented.

The peaks of mountains and the tops of hills and ridges are sometimes thought of as regions of warmer temperatures than the surrounding low areas, and this elevated temperature could be

interpreted as indicating the presence of a thermal or updraft region. This situation certainly exists when the cold pool is present in the valleys (although, as shown in Chapter IV, the main updrafts tend to be to the lee of the mountains). In this chapter, on the other hand, we have been discussing turbulence within the CBL rather than discussing organized mesoscale circulations. Even so, when the deep afternoon CBL is established, the mountain regions still seem to be warmer, particularly when aircraft data are studied. Both the author and Hahn (personal communication), however, feel that it remains to be demonstrated conclusively whether the mountains actually are warmer (potentially) than the surrounding surface, and whether the aircraft-observed elevated temperatures actually indicate the presence of any organized atmospheric circulation features. Fig. 5.5 depicts a situation where

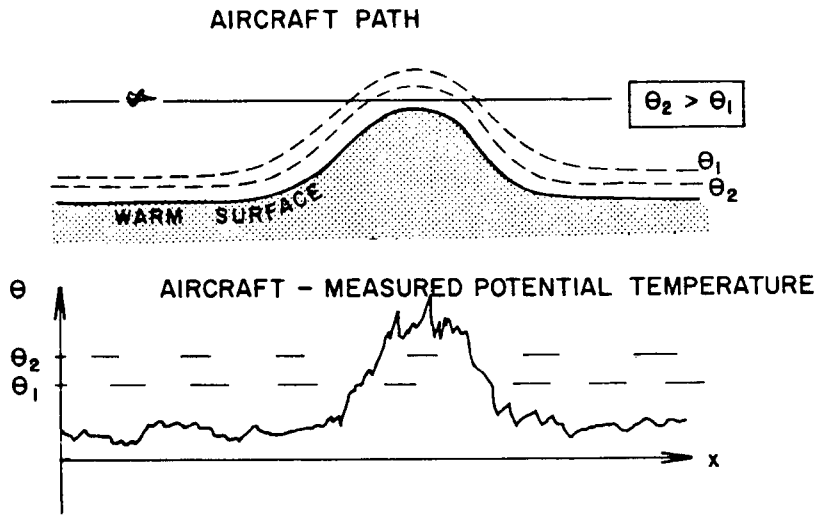

Figure 5.5: Hypothetical aircraft traverse of a ridge, showing how a thermal may appear on the θ trace to be present when in fact there is no thermal.

the surface layer is no warmer (potentially) over the mountains than it is over the valley, yet a level aircraft flight leg would show a much warmer temperature over the mountains. In designing an experiment to investigate convection over the mountains, it will be very important to be able to rule out this effect in determining whether persistent thermals are attached to terrain features.

The second impression is that, while the boundary layer at night and in the morning are extremely inhomogeneous, the deep afternoon boundary layer seems to be somewhat more homogeneous in the horizontal. This agrees with the observations of Lenschow (1981), who compared tower and aircraft measurements over complex terrain in the plains of eastern Colorado. He found that the agreement between tower and aircraft data depended on the extent to which the assumption of horizontal homogeneity held, and he concluded:

> In the unstably stratified boundary layer, the airplane and tower measurements of mean and second moment quantities generally show good agreement. For neutral and stable stratification, however, large horizontal variations in both mean and second moment quantities can exist.

Lenschow (personal communication) also performed spectra on the flight legs for the unstable case. He divided the legs into segments and compared the spectra for each segment with the others. He found that the wavenumbers and spectral densities of the peaks and also the spectral densities in the inertial subrange were similar, thus reinforcing the notion that the turbulence for the unstable case is relatively homogeneous in the horizontal. We performed a similar analysis of several north-south flight legs over South Park, with a similar result: the wavenumbers and spectral densities of the peaks, and the spectral densities in the inertial subrange, were all

comparable for segments of the same flight leg. Thus, as stated at the beginning of this papagraph, the impression that our South Park observations give is that the deep afternoon boundary layer tends to be more horizontally homogeneous than expected, and terrain features seem to have less of an effect in localizing thermals than expected.

The original purpose of this chapter was to explain the gustiness of the afternoon winds, which was noted in Chapter IV. The many topics discussed in this chapter have all been related to that explanation, since the explanation involved a jump in the size of the large (thermal) eddies of the CBL, which in turn was a adjustment to a rapid increase in z_i, the depth of the CBL. But the argument as proposed was incomplete without some evidence that transient thermals do in fact exist in the mountain boundary layer, a point which is moot because heat could be carried aloft entirely by stationary circulations which are held in place by terrain features. Data from South Park showed that at least some thermals are transient.

VI. NUMERICAL MODELING OF FLOW OVER A HEATED RIDGE

The observations which have been presented in previous chapters provide a comprehensive description of processes which accompany local mesoscale flow systems in South Park. Such observational studies, however, are not able to answer many questions which arise concerning the causes of these wind systems. In the first place, the representativeness of the observations themselves in any observational study is always open to question. A second important problem with observational studies is the extreme difficulty in measuring atmospheric pressure and particularly horizontal gradients of pressure, and this is especially difficult in mountainous terrain. This absence of accurate pressure-gradient data prevents any quantitiative descriptions of forces which are important in driving the wind systems. It was hypothesized in previous chapters, for example, that the vertical eddy mixing force was important in producing the reversal to afternoon westerly winds in South Park. It would be desirable to further test this hypothesis by obtaining estimates of the magnitudes of the terms in the horizontal equation of motion. Since the observational data are inadequate to fully describe the balance of forces in this case, another method must be used to estimate the relative importance of the various terms.

In this chapter a numerical model is used to further investigate the problem of flow over a mountain ridge, such as that found at the western edge of South Park. The model used is a dry, two-dimen-

sional, fine resolution version of the Colorado State University Cloud/ Mesoscale Model (Tripoli and Cotton, 1982). The model is used to describe the evolving potential temperature and pressure fields, the terms in the u equation of motion, and other features which are difficult to evaluate by direct measurement. The results give further insight into the processes which are important in driving the meso-scale wind fields found in South Park.

In designing an experiment which is to resemble the situation in South Park, several factors must be considered. The drop in elevation between the peaks of the Mosquito Range to the west and the lower levels of South Park at the latitude of the base site is about 1 km., and this drop is accomplished over 12-15 km. of horizontal distance. Thus, we would like the simulation domain to be around 20 km. wide. The depth of the cold pool was approximately 300-400 m. at the base site, so that farther down in the valley it was probably 500 m. or so. In order to resolve both the cold pool and the shallow CBL which forms below, it will be necessary to have several grid points in the inversion layer. The vertical grid interval, therefore, should be 100 m. at most near the surface.

In the modeling experiments presented in this chapter, these conditions have all been met. These models have 96 grid points in the horizontal, set at 200 m. intervals, so that the width of the domain is a little over 19 km. The vertical grid spacing was not the same in both experiments, but it was on the order of or less than 100 m. in both. The values of these quantities and a fuller description of the terrain used will be given later.

It would have been the most desirable to simulate the South Park case studies fully in three dimensions. However, for a number of reasons, these experiments were carried out in 2-D. In the first place, these were the first exploratory simulations of the CSU Cloud/Mesoscale Model using the terrain co-ordinate transform, particularly with fine resolution and surface heating. It was deemed unwise to jump immediately to 3-D before these features were tested on a somewhat simpler, 2-D version. Second, the nature of the terrain and certain aspects of the flow in the vicinity of the Mosquito Range near the Base Site are relatively homogeneous in the north-south direction. This suggests that an east-west, 2-D model may well capture the essential physics of the developing flow systems in that region. Finally, a 3-D model covering even a reasonable portion of South Park would have to have quite coarse resolution compared to that selected for the 2-D model. In order to be able to use the finer resolution which we regarded as important for a successful simulation, it was necessary to use a 2-D version of the model.

A. Some Numerical Models of Flow over Complex Terrain

A wide variety of numerical models has been used to study the problem of flow over mountainous terrain. Reviews of such studies have been compiled as part of ASCOT (1980) and by Pielke (1981). The purpose of the present section is to briefly mention a few of these modeling studies in order to establish where the current study fits in.

Many of the mesoscale models which have been developed to date have domains and grid intervals which are much larger than those used in this study. For example, Mahrer and Pielke (1976, 1977) used a hydrostatic model with surface heating and horizontal grid intervals of 5 km. to

simulate the air flow over the island of Barbados and over the mountains near White Sands, New Mexico. Also, using an earlier version of the same model, Hughes (1978) simulated the diurnal cycle of air flow over mountains in Colorado. In none of these experiments which has winds aloft did thermally-forced upslope ever actually develop, although deflections of the flow in the vicinity of terrain features show that the thermally-induced horizontal pressure gradients are in the right directions. A similar type of model was developed by Yamada (1978), except that the vertical turbulent fluxes were computed using a simplified second-moment (or "second-order") closure scheme. A number of mesoscale models have been used to study the problem of mountain waves and severe downslope windstorms, e.g. Klemp and Lilly (1975, 1978) and Peltier and Clark (1979). However, since these studies do not address the problem of a heated boundary layer, they will not be further discussed here.

A number of modeling studies of thermally-forced slope and valley winds have appeared. Among these, Orville (1964) and Gal-Chen (1975) studied the circulations which developed over a symmetric, two-dimensional, heated ridge, and the latter study also included results from cases where the hill was heated asymmetrically. The grid interval used in these studies (approximately 100 m. by 100 m) was comparable to that used in the present study, although the domain sizes (3 km. square and 7 km. square, respectively) were smaller. Thermally-forced flow in deep mountain valleys has been simulated by Thyer (1966), McNider and Pielke (1979,1981) and Bader (1981). In each of the above cases, the thermally-forced flow was simulated in a quiescent environment (i.e., there was no flow aloft).

Cases where slope winds form in the presence of flow aloft are of considerably more interest than those where the slope winds form in a still environment, since ridgetop-level winds are very seldom calm--or even nearly so--in nature. Two such studies were presented by Orville (1968) and Tang (1976). In the former study, Orville modeled the generation of mountain upslope as a precursor to cumulus formation in the mountains. In the latter, Tang used series expansions to evaluate a diagnostic set of the primitive equations, to find steady-state solutions for both the upslope and the downslope cases with flow above the ridgetops.

The model to be described in the following chapter is a relatively fine-resolution model of upslope winds which form in the presence of ridgetop flow aloft, a situation which only a few modeling studies to date have addressed. The resolution of the model allows us to study the growth of the CBL in addition to the development of thermally-driven upslope flow; this is important since we have seen that both processes occur simultaneously in South Park. There are two important meteorological effects which are included in the following study that have not been modeled in similar previous studies. They are: an initial temperature structure which includes a stable cold pool and a deep neutral layer aloft, and a stability-dependent eddy-mixing coefficient (K_z). The latter effect reduces the mixing in the stable region at the top of the cold pool (thus allowing upslope to form below) and also enhances mixing when the deep CBL forms, with K_z values of 100 m^2/s and even greater being developed in this region.

B. Brief Description of the Numerical Model

As mentioned previously, the model used in this study is a version of the Colorado State University Cloud/Mesoscale Model. This model has been described in detail by Tripoli and Cotton (1982), and the major dynamic and thermodynamic equations are presented in Appendix B of this paper. The first part of this section consists of a brief review of the characteristics of the basic model. The second part contains specific adaptations which have been made to the model for the current experiments.

1. Characteristics of the CSU Cloud/Mesoscale Model

The major hydrodynamic relationships in the model consist of equations for perturbation quantities about a hydrostatic base state. The model is elastic (and non-hydrostatic), with the solution for perturbation density (and pressure) being obtained in conjunction with the solutions for the velocity components, using an abbreviated set of equations. The abbreviated set consists of terms which are acoustically active, and thus they describe the mass and energy redistribution accomplished by sound waves. Because of the very fast propagation speed of sound waves, these acoustic equations are solved on a very small time step (in the following studies .05s was used). The other terms in the equations, which vary on a longer time scale characteristic of meteorological phenomena, are computed only at longer time intervals; in our case the long time step was 2s. Because the hydrodynamic equations are divided into two sets of terms, one of which is evaluated on a longer (meteorological) time step and the other, on a shorter (acoustic) time step, this method of solution has been called "time-splitting" (Klemp and Wilhelmson, 1978).

Other important features of the model include a terrain-following "sigma-z"-type co-ordinate system and the use of a staggered grid to increase the effective resolution of the model. The terrain-following co-ordinate system in effect compresses the vertical grid interval (Δz) over hills or mountains. The staggered grid configuration is shown in Fig. 6.1. The moisture and cloud-microphysical aspects of

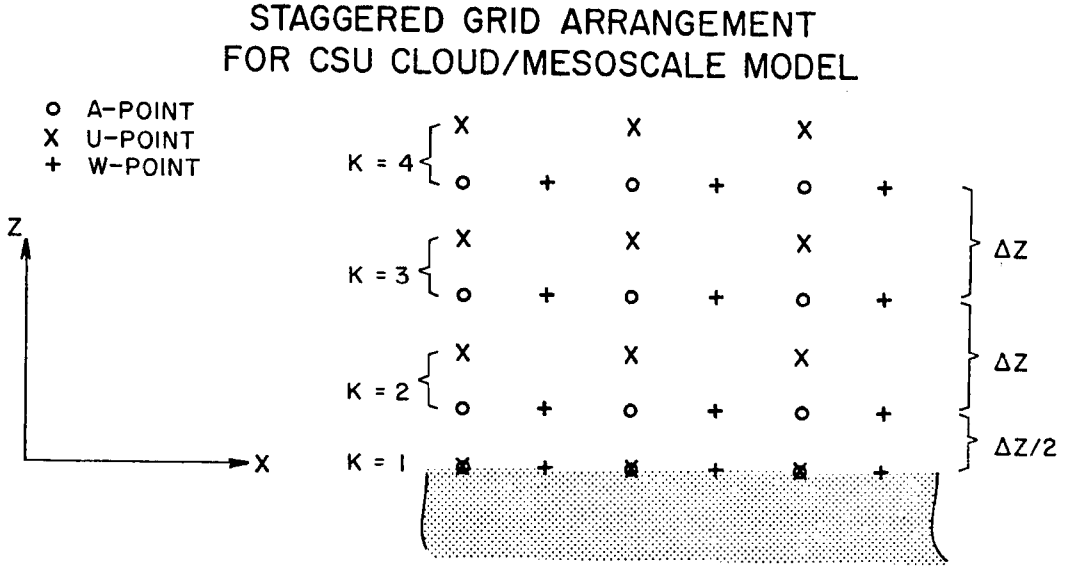

Figure 6.1: Staggered grid arrangement of CSU Cloud/Mesoscale model.

the model described by Tripoli and Cotton (1982) were not used in the following simulations and so will not be discussed here.

The more detailed aspects of the model and model equations are discussed in Appendix B . One detail which should be mentioned here, however, is the parameterization for the eddy mixing coefficient, K_m. This quantity is parameterized as being proportional to the magnitude of the deformation and a factor which is dependent on the static stability, expressed by the Richardson number, as recommended by Lilly (1962) and tested by Cotton (1975):

$$K_m = \frac{(0.25)^2}{\sqrt{2}} \; D \; \ell^2 \left(1 - (K_H/K_m)\; Ri\right) \quad , \tag{6.1}$$

where the square of the deformation, D, is:

$$D^2 = \sum_j \sum_k \left(\frac{\partial \bar{u}_j}{\partial x_k} + \frac{\partial u_k}{\partial x_j}\right)^2$$

and the Richardson number, Ri, for our dry case is:

$$Ri = \frac{g\partial\theta/\partial z}{\bar{\theta}\; D^2}$$

The mixing coefficient for heat (i.e. potential temperature) is calculated using the relationship recommended by Deardorff (1971) and Cotton (1975):

$$K_H = 3\; K_m$$

The mixing length in (6.1), ℓ, is taken to be equal to the grid interval in the direction of diffusion, either Δx or Δz.

The basic boundary conditions of the model could be described briefly as follows: The lateral boundary conditions are of the radiation type, which allow gravity waves to propagate outwards. Additionally, beyond these boundaries and exterior to the primary domain of simulation, there is an extra, larger grid volume representing a "mesoscale compensation region" or MCR. This MCR simulates the larger-scale feedback when circulations originating within the domain extend past the boundaries and outside the domain. The upper boundary is a lid with a Rayleigh friction zone just below, and the upper boundary also has a radiation condition which allows acoustic waves to pass through. At the lower boundary, velocities are assumed zero

and the fluxes of momentum and θ are computed using a diabatic surface-layer formulation similar to that described by Louis (1979), which is based on the Businger-Dyer surface-layer equations. The surface-layer formulation is further discussed in Appendix B .

2. Adaptations for the South Park simulations

A number of adaptations and adjustments to the model were made for the following model runs. The v component of velocity was set to zero, and Coriolis force was neglected. As mentioned above, these model runs were dry, so that the water-vapor mixing ratio was set to zero. An exception to this were some later model runs, where very small values of water vapor mixing ratio were used as a passive tracer. At any rate, no condensation ever occurred in these model runs, so the thermodynamic variable $\theta_{i\ell}$ (the "ice-liquid water potential temperature") was always the same as θ, the potential temperature, defined in the usual way. With the vertical grid spacing, Δz, being 100 m. or less, the longer time step used was 2s. and the shorter time step was 0.5s., as mentioned above.

Because the grid spacing for these experiments was much smaller than had been used in previous cloud modeling experiments, the value of K_m computed from (7.1) was too small to suppress numerical noise. For this reason the eddy mixing coefficient computed from (7.1) was enhanced by a factor of 30. Because of the time and expense of running this model, it has not been possible to test the model results for sensitivity to this parameter. However, from earlier model runs it appears that a factor of 10 is too small to suppress numerical noise during the early phases of the model runs--about the first 3600s. or so--since the model became unstable if the factor was too small.

It should be pointed out that although the factor of 30 seems rather arbitrary and excessive, the following points should be made: (1) The factor ℓ^2 in (6.1) is equal to the grid spacing. Since Tripoli and Cotton (1982) used vertical grid intervals of 750 m. the actual values of K_m used in this study are comparable to or less than the values used by Tripoli and Cotton. (2) Values of K_m computed for the central portions of the CBL's are of the same magnitude as those observed in the central portions of a horizontally-homogensous CBL. Although K values for a 2-D model of this type should be smaller than for a 1-D (horizontally-homogeneous) case, the larger K values probably indicate that the sub-resolution scale processes are performing the transport which should be accomplished by thermals.

The terrain which was used to simulate the ridge of the Mosquito Range was an asymmetric hill, depicted in Fig. 6.2 with an exaggerated vertical dimension. The steeper upwind (western) side is represented by the mathematical formula:

$$z_s(\xi) = (h-\beta)\,\frac{\alpha^2 - \xi^2}{\alpha^2 + \xi^2} \qquad \xi < 0$$

and the downwind side by the formula

$$z_s(\xi) = \text{MAX}\left[h\left(\frac{\alpha}{\alpha + \xi}\right) - \beta,\ \ 0\right], \qquad \xi \geq 0$$

where $\xi = x - x_{mid}$ and x_{mid} is the top of the hill.

The model was initialized by specifying a vertical sounding of θ and u. The θ sounding was chosen as a compromise between those taken on the mornings of 2 and 3 August, two of the "more typical" of the

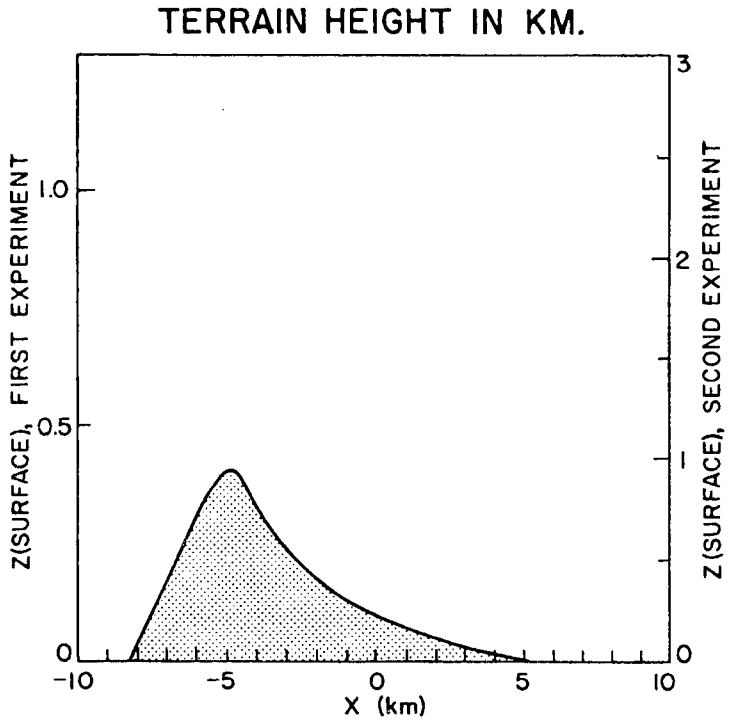

Figure 6.2: Terrain configuration for 2-D numerical experiments. Height scale for first (smaller hill) experiment is on left hand ordinate, and scale for second (larger hill) experiment is on the right.

typical dry days during SPACE-77. Ridgetop wind speeds of 4 m s^{-1} were chosen, with wind speeds of 0.4 m s^{-1} below about 1 km. This sounding is shown in Fig. 6.3. The initial θ field is specified so that the isentropes are level (see Fig. 6.4), and similarly the winds at levels above the ridgetops are specified to be horizontally homogeneous. The remainder of the wind sounding is input gradually over a given time interval as a band of winds a certain number of gridpoints deep. By adding the winds in this manner, the horizontal mass flux through all vertical columns is kept equal and the winds have a chance to adjust to the flow over the terrain. In the model runs to be presented, the low-level band of winds was added in over a 10-min. time period and then allowed to settle for 5 min. until heating was initiated.

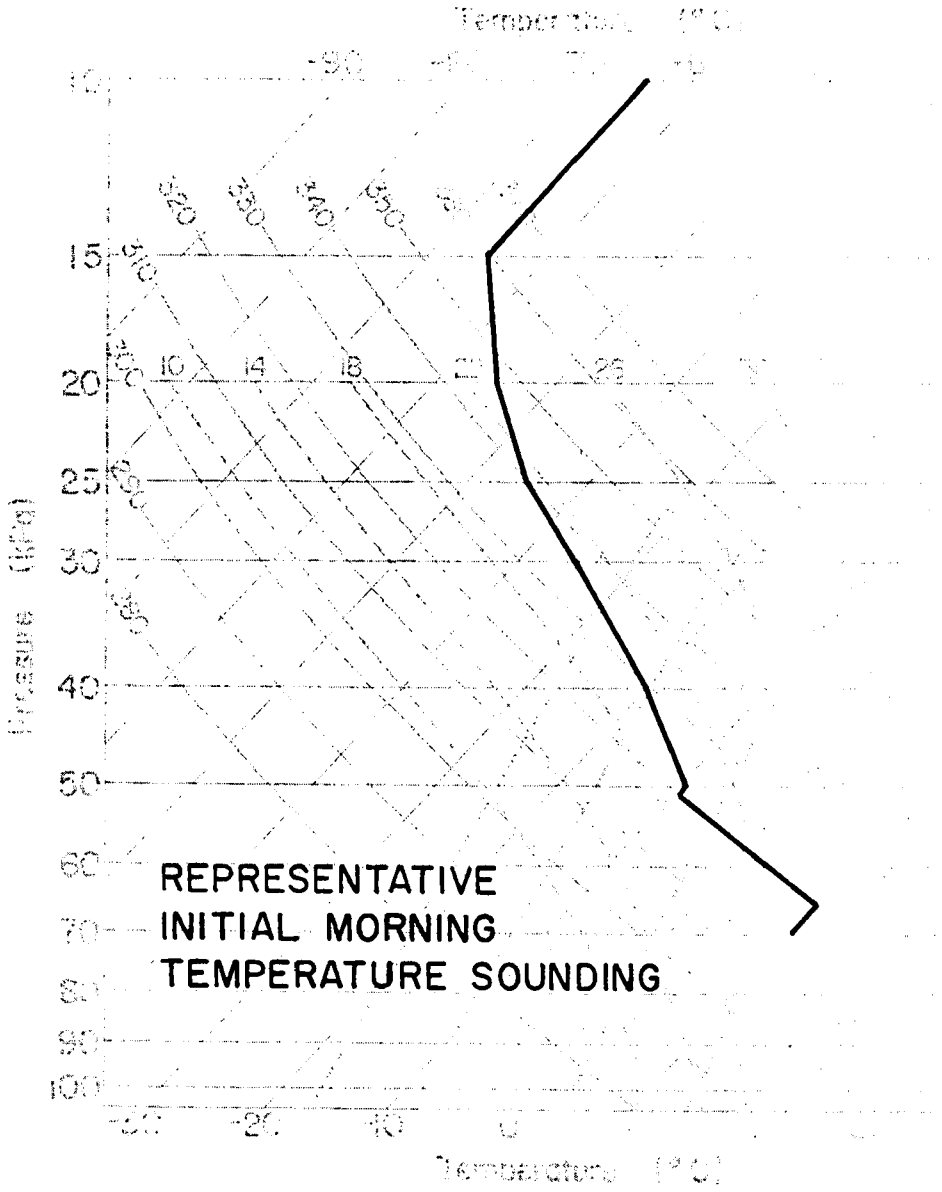

Figure 6.3: Skew-T, log-p diagram of temperature sounding used in the second numerical simulation. Sounding for first experiment is identical except sounding starts 10 mb. higher.

Heating at the lower boundary of the model was started gradually, going from 0 at 900 s. (15 min.) to its maximum value at 1800 s. (30 min.) in a sinusoidal manner. The input to the heating fuction was specified to be the same at each point along the surface, regardless of elevation, etc., so that the heat flux was nearly uniform everywhere along the surface. Further information on the heating function is given in Appendix B with the discussion of the surface-layer formulation.

The results of two numerical experiments are presented below, using two different maximum ridge heights. In the first experiment, the ridge reaches a height of 407 m. Since this is less than half the proper ridge height for South Park, this experiment is described only briefly. However, in spite of this lack of geometric similarity to the situation in South Park, this simulation did reproduce many of the events which were found to occur in the field. The maximum ridge height in the second experiment was 949 m, which is close to that observed in the Park. In this case again, many of the features of boundary-layer growth and local wind development found in the field were reproduced by the model. This experiment is analyzed in more detail than the first experiment.

C. Small Hill Experiment

1. Description

In the first experiment, where the maximum hill height was just over 400 m., the domain consisted of 48 grid points in the vertical. The basic vertical grid spacing was 100 m. (becoming about 90 m. over the highest terrain point), so that the top of the domain extended to 4.7 km. The initial basic sounding from the reference level height (z_s = 0.0) is given in Table 6.1, and shown in Fig. 6.4a.

TABLE 6.1 Base State for First Experiment

K	Z (km. AGL)	p (kPa)	θ (^{o}K)	u (m/s)
1	.000	68.00	315.6	0.4
2	.050	67.59	316.2	0.4
3	.150	66.78	317.3	0.4
4	.250	65.98	318.4	0.4
5	.350	65.19	319.5	0.4
6	.450	64.40	319.9	0.4
7	.550	63.63	319.9	0.8
8	.650	62.86	319.8	2.4
9	.750	62.10	319.8	3.6
10	.850	61.34	319.8	4.0
11	.950	60.59	319.8	4.0
12	1.05	59.85	319.8	4.0
13	1.15	39.11	319.8	4.0
14	1.25	58.38	319.8	4.0
15	1.35	57.65	319.8	4.0
16	1.45	56.94	319.8	4.0
17	1.55	56.22	319.8	4.0
18	1.65	55.52	319.8	4.0
19	1.75	54.82	319.8	4.0
20	1.85	54.13	319.9	4.0
21	1.95	53.44	319.9	4.0
22	2.05	52.76	319.9	4.0
23	2.15	52.09	320.4	4.0
24	2.25	51.43	321.0	4.0
25	2.35	50.77	321.8	4.0
26	2.45	50.12	322.8	4.0
27	2.55	49.48	323.5	4.0
28	2.65	48.84	324.1	4.0
29	2.75	48.21	324.5	4.0
30	2.85	47.59	324.8	4.0
31	2.95	46.98	325.1	4.0
32	3.05	46.37	325.4	4.0
33	3.15	45.76	325.6	4.0
34	3.25	45.17	325.9	4.0
35	3.35	44.58	326.2	4.0
36	3.45	43.99	326.5	4.0
37	3.55	43.41	326.8	4.0
38	3.65	42.83	327.2	4.0
39	3.75	42.27	327.5	4.0
40	3.85	41.71	327.9	4.0
41	3.95	41.16	328.2	4.0
42	4.05	40.61	328.6	4.0
43	4.15	40.06	329.0	4.0
44	4.25	39.53	329.3	4.0
45	4.35	39.00	329.6	4.0
46	4.45	38.47	329.9	4.0
47	4.55	37.95	330.3	4.0
48	4.65	37.43	330.6	4.0
49	4.75	36.92	331.0	4.0

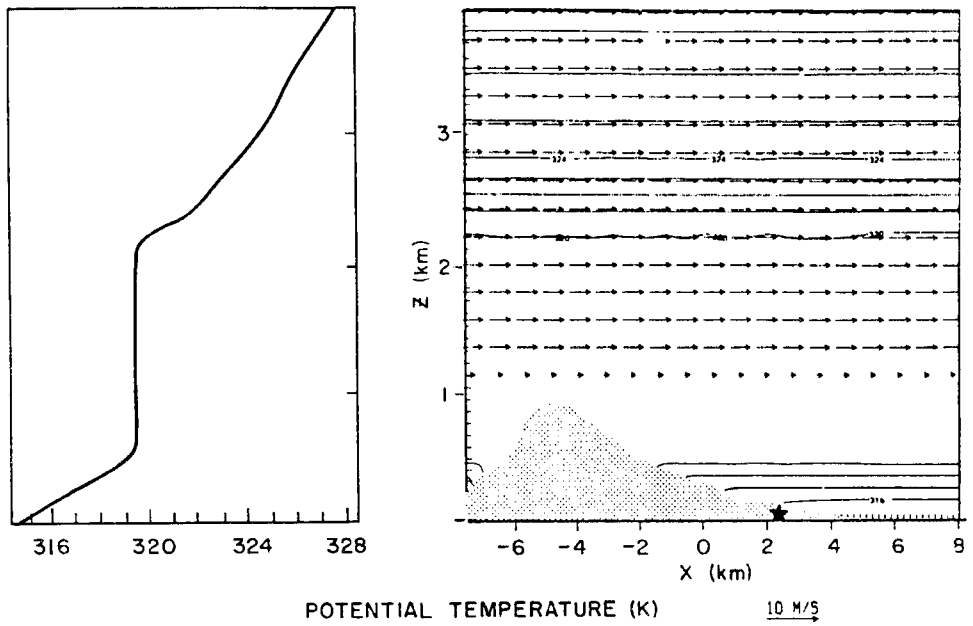

Figure 6.4: (a) Initial θ sounding for a location over the plain. (b) Initial field of θ and horizontal winds for second experiment before low-level winds were added in. Note that isentropes were initialized to be horizontal, except for some minor wiggles resulting from the hydrostatic adjustment in the intialization process.

The heating function is determined by specifying a value for $\Delta\theta$, which represents the difference in θ between the surface and the first gridpoint above the surface. For this experiment $\Delta\theta$ was set at 4.0 K, which produced values of the kinematic surface heat flux, $\overline{w'\theta'}_o$, of 15-17 cm K/s. This heat flux was not allowed to exceed 17 cm K/s.

2. Results

The resulting potential temperature and perturbation pressure fields generated by the model are shown in Figs. 6.5-6.10, with isentropes at intervals of 1 K and isobars at 50 x 10^{-3} mb. The star in the terrain on these figures indicates the location of a "Base Site" from which soundings will be obtained later. Fig. 6.5 shows the initial θ field before heating but after the initialization of the

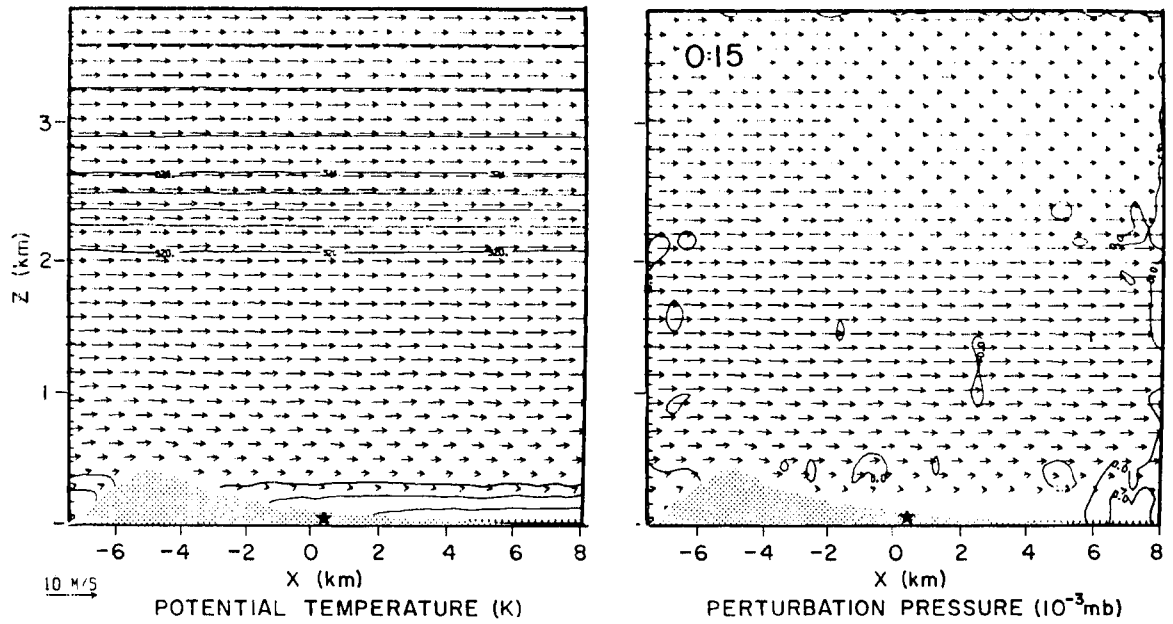

Figure 6.5: Model-generated potential-temperature and perturbation-pressure cross sections for smaller-ridge experiment after 15 min. of simulated time, which is the time when surface heating begins. Isentropes are at intervals of 1K, and perturbation isobars at 50 dyne/cm^2.

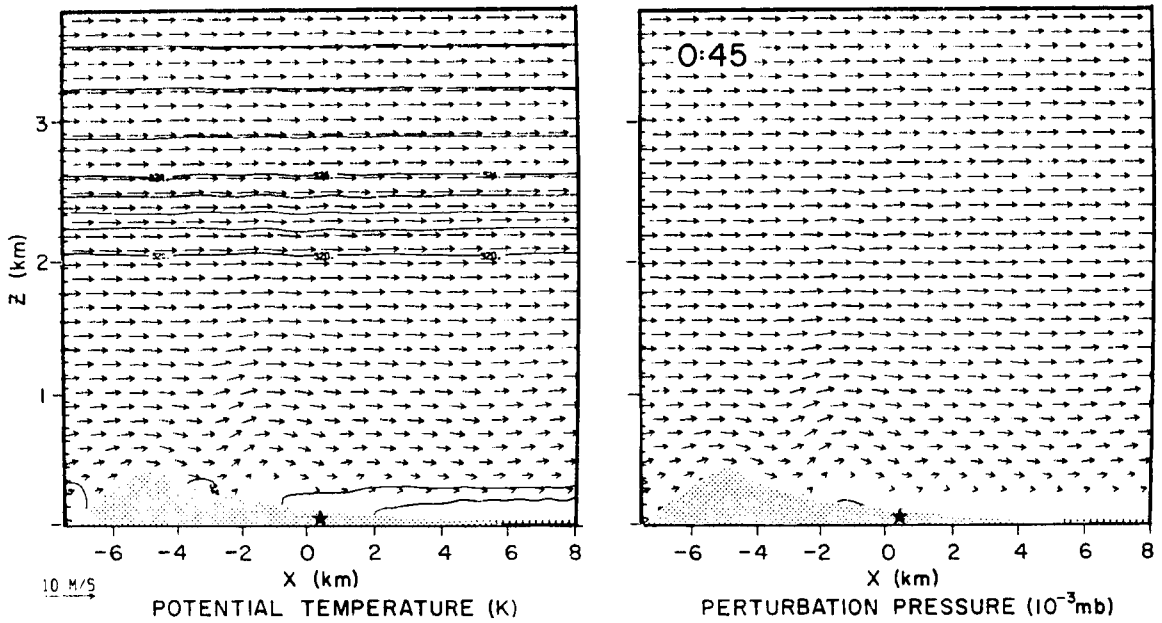

Figure 6.6: Model-generated potential-temperature and perturbation-pressure cross sections for smaller-ridge experiment after 45 min. of simulated time, which is 30 min. after the start of heating. Isopleth intervals are the same as in Fig. 6.5.

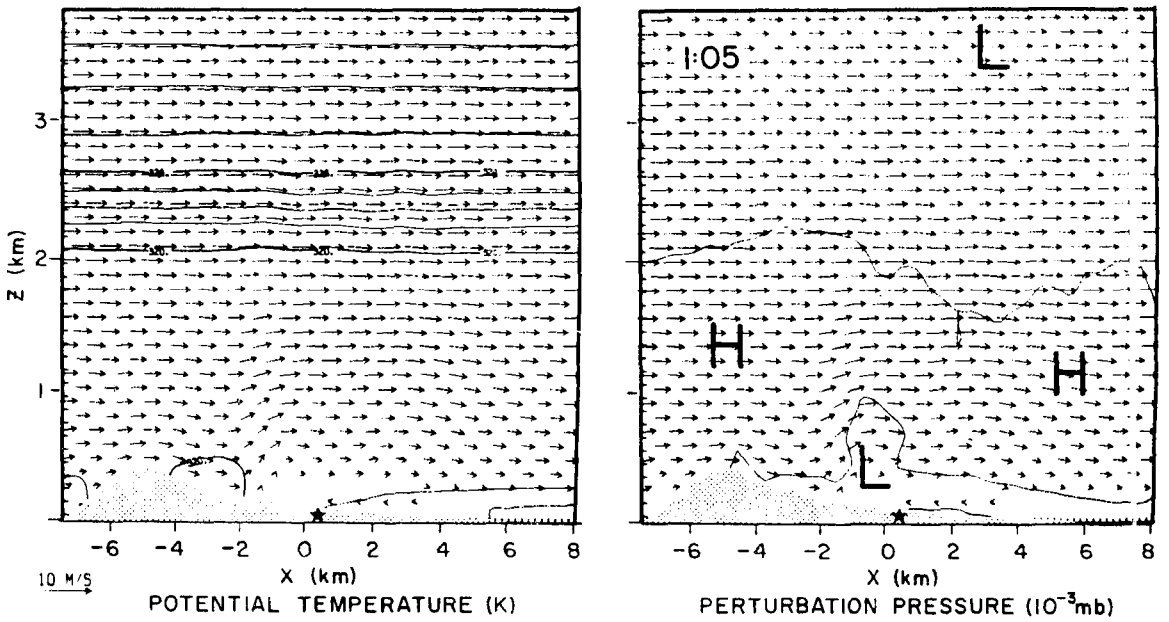

Figure 6.7: Model-generated potential-temperature and perturbation-pressure cross sections for smaller-ridge experiment after one hour, five minutes of simulated time. Isopleth intervals are the same as in Fig. 6.5.

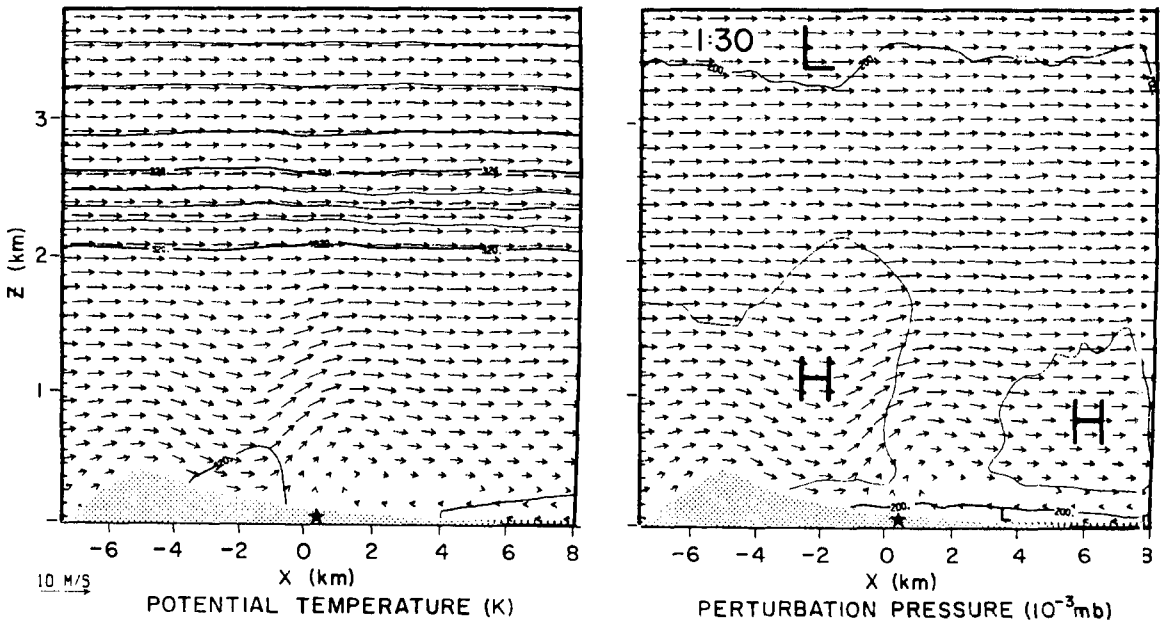

Figure 6.8: Model-generated potential-temperature and perturbation-pressure cross sections for smaller ridge experiment after 1½ hour of simulated time. Isopleth intervals are the same as in Fig. 6.5.

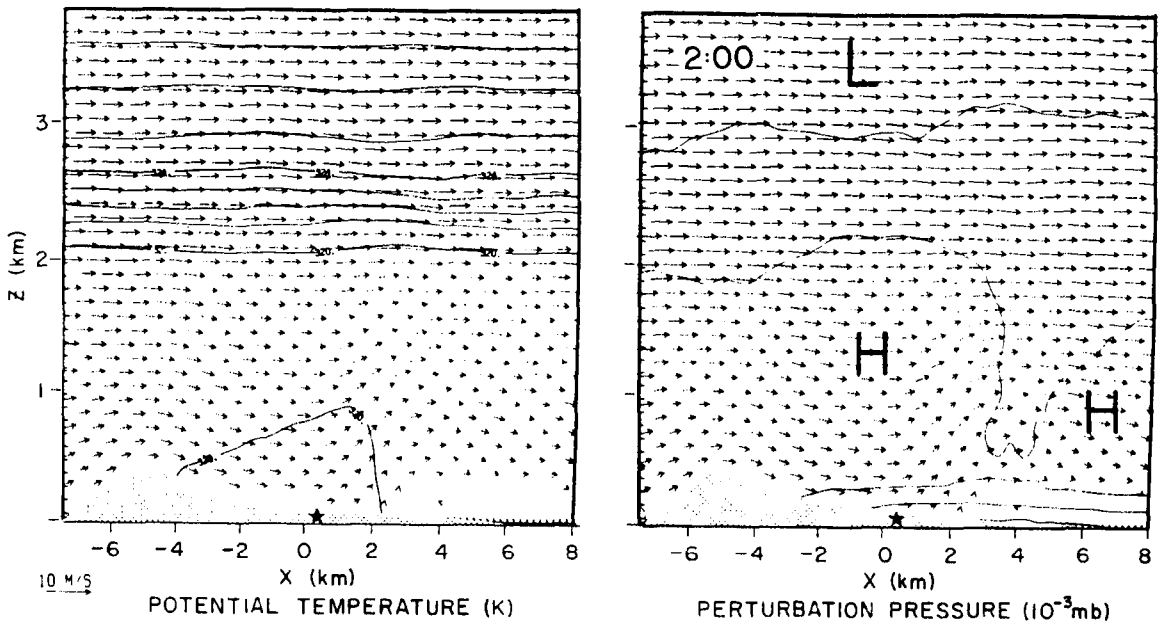

Figure 6.9: Model-generated potential-temperature and perturbation-pressure corss sections for smaller ridge experiment after 2 hours of simulated time. Isopleth intervals are the same as in Fig. 6.5.

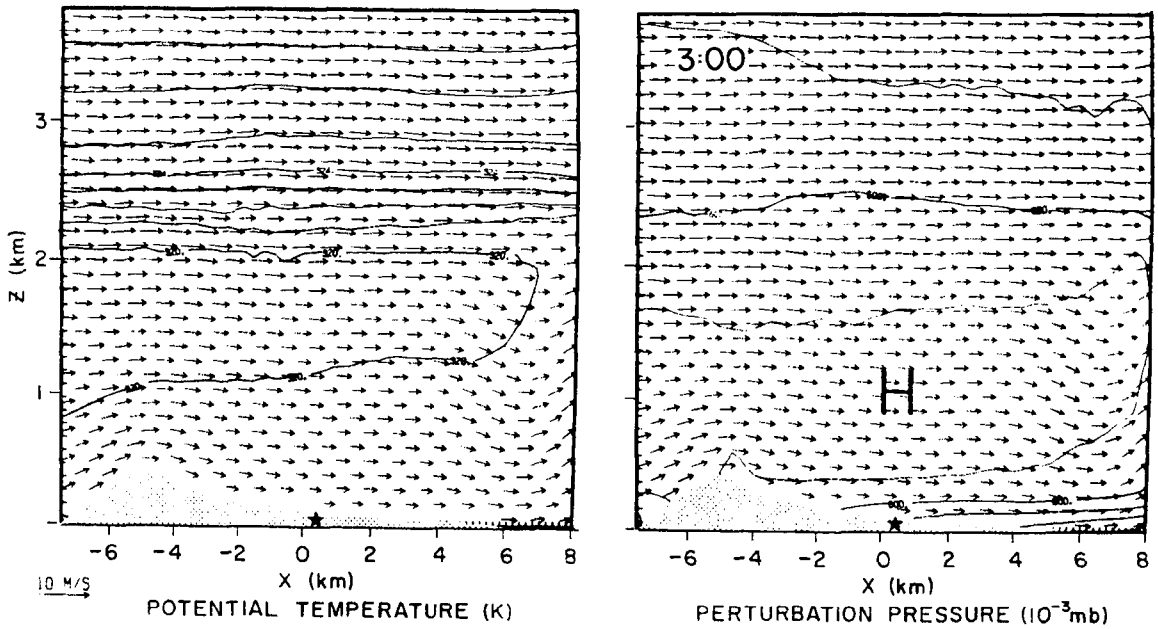

Figure 6.10: Model-generated potential-temperature and perturbation-pressure cross sections for smaller ridge experiments after 3 hours of simulated time. Isopleth intervals are the same as in Fig. 6.5.

wind field. The stable cold pool is evident at lower levels, and the absence of isopleths between z = 0.5 and 2.0 km. indicated a dry adiabatic region corresponding to the neutral layer aloft. Above 2 km., θ again increases with height in the stable "free atmosphere." In Fig. 6.5b the random pressure fluctuations indicate that there are no organized pressure patterns which have developed to this point.

After 45 min. of simulated time (30 min. after the heating was turned on), the surface begins to warm as shown in Fig. 6.6a. There is a warm bubble at the surface between x = -4 and -3 km., and the cold pool has a neutral region near the ground (this region should actually be shown as superadiabatic in this and subsequent θ cross sections, but the early version of the program which generated these analyses did not plot the superadiabatic region properly). The velocity field shows upward motion just downwind of the warm region at the surface, and in the pressure field there is a small bubble of low pressure at the surface just upwind of the base site (star) at about x = -1 km.

By an hour and 5 min. (Fig. 6.7) a distinct upslope flow has begun to form at the surface between x = 0 and 4 km. The warm region just to the lee of the ridgetop has expanded, and the cold pool shrinks as the isentropes continue to retreat downhill with heating. The region of upward motion is broader and more intense than in the previous figure, and it is now above a distinct region of surface convergence. In the pressure field, there is a region of relative low pressure nearly 1 km. deep above the low-level convergence region. The surface itself is an area of low pressure, and downwind (and

downhill) of the deep low, the isobars slope downhill, producing a pressure gradient favorable to upslope accelerations (note that the isobars represent perturbation - not total - pressure.

The cross-sectional analyses for 1½ hr. (Fig. 6.8), 2 hr. (Fig. 6.9) and 3 hr. (Fig. 6.10) show a continuation of the processes just described for 1:05. The warm region to the lee of the ridge continues to expand, the cold pool continues to shrink as the boundary layer warms, and the upward motion above the convergence zone continues to increase. In the pressure field, the low pressure associated with the convergence zone deepens to include the entire boundary layer up to 2 km., and the low pressure near the ground continues to intensify. Also near the surface the isobars tend to form a dome over the convergence region, sloping downhill on the downhill side to produce an upslope pressure-gradient force, but sloping the other direction on the uphill side. Thus, on this uphill side, the pressure gradient actually favors downslope accelerations in spite of the presence of a warm surface (which should produce an upslope pressure gradient force).

A significant phenomenon which can be found by comparing Fig. 6.8-10 is the downhill, downstream propagation of the convergence region. The cold pool and the associated upslope region can be seen to shrink and move to the right, out of the domain. As this occurs, the convergence zone proceeds from near x = -1 km. on Fig. 6.7, to x = 0 on Fig. 6.8, to x = 3 km. on Fig. 6.9, and out of the domain on Fig. 6.10. Thus the speed of propagation of the convergence zone increases from about 2 km/hr (0.6 m/s) before 1½ hr. to about 7 km/hr. (2 m/s) between 2 and 3 hr. Behind (i.e. upwind) of the convergence zone there are well-mixed "westerly" (downslope) winds

from heights of 1 to 2 km. all the way down to the surface. By 3 hours of simulated time (Fig. 6.10), these downslope winds have taken over almost all of the domain, and there is no tendency for another region of convergence to form anywhere along this slope.

These model results bear a strong resemblance to the events which were described to occur in South Park earlier in this dissertation. Upslope winds formed at the underside of a stable cold pool. In the higher elevations where there was no stable layer next to the ground, a deep CBL formed. On the lee slope, well-mixed downslope winds existed down to the surface. Between the upslope and downslope winds there was a zone of convergence, with a region of strong updrafts above it. This zone, earlier called the leeside convergence zone, propagated down the slope as heating persisted and as the edge of the cold pool retreated.

3. Analysis

Two kinds of further analysis were performed for this experiment. The first consisted of vertical soundings of θ, u, and K_z (the vertical eddy mixing coefficient for momentum) at the site indicated by the star on the cross sections, which corresponds to about where the base site was located in South Park. The second type of analysis is an evaluation of the terms in the u equation of motion at the first grid point off the surface at the starred "base" site.

The vertical profiles are presented in Fig. 6.11. The initial potential temperature field (before heating starts) has a stable inversion layer below about 300 m., and then a deep neutral layer aloft up to 2 km. After 60 min. there is a shallow CBL beneath the inversion and a superadiabatic surface layer. By 90 min. the shallow CBL has grown past the top of the inversion layer (note that Fig. 6.8 shows

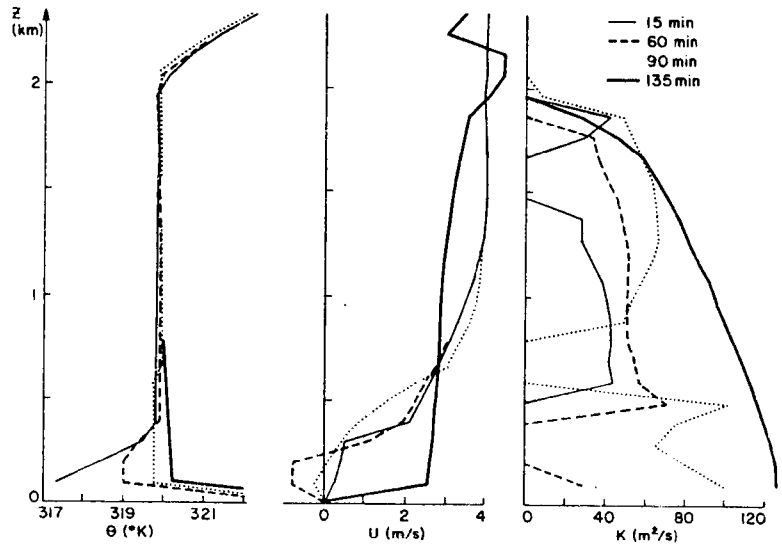

Figure 6.11: Model-generated profiles of potential temperature horizontal winds, and vertical eddy-mixing coefficient (k_z) for the smaller-rideg experiment. The location of the profiles is the "Base Site" indicated by the star in the above cross sections. Times of the profiles are as follows: light solid line-15 min.; dashed line-1 hr.; dotted-1½ hr.; dark solid line-2 hr., 15 min.

that the low-level winds are blowing nearly straight up just above the "base" at this time), and only a very thin remnant of the inversion remains near 600 m. Finally by 135 min. (2 hours and 15 min.) a deep CBL has formed from the surface to 2 km.

The initial horizontal wind profile shows stronger winds (2-4 m/s) above the cold-pool inversion and weaker winds (0.4 m/s or less) within the inversion layer, all downslope. By 60 min. the winds in the shallow CBL which has formed below the inversion are blowing in an upslope direction at about 1 m/s, with little change in the winds above the inversion. At 90 min. a strong downward diffusion of westerly momentum is indicated by the curvature in the u profile below 600 m., and the wind speeds below 300 m. are very small. Finally, after the deep afternoon mixed layer has formed (135 min.), the winds are rather

well mixed with speeds of 2½ to 3½ m/s from just off the surface up to the top of the mixed layer.

The profiles of the eddy mixing coefficient show regions where vertical diffusion is strong, and where it is suppressed. Initially (i.e. at 15 min.) K_z is negligible everywhere in the cold-pool inversion layer. In the neutral layer aloft, however, the potential for mixing is strong with $K_z \sim 40\ m^2/s$. Because of some minor wiggles in the initial θ profile, there is a layer just above 1.5 km. where mixing is suppressed. K_z is also negligible, as expected, in the stable free atmosphere above 2 km. Later, when the shallow CBL forms at 60 min, the CBL can be seen as a low-level region of enhanced mixing. K_z continues to be large in the neutral layer aloft, and the continuity of K_z from 0.5 to 1.8 km. shows that the initial stable wiggle in the θ profile has been smoothed out. The two layers of large K_z--the shallow CBL and the neutral layer aloft--are separated by an area of negligible K_z, so that these layers are not convectively coupled at this time in the model. The profile at 90 min. shows a much deeper low-level region of strong mixing still separated from the layer of strong mixing aloft. Finally, the deep afternoon CBL at 135 min. is seen to be a region of very strong mixing throughout its depth.

The profiles presented in Fig. 6.11 again strongly resemble many features of our analyses of observational data. The θ and u profiles are similar to those presented in Fig. 4.15, and the K_z profiles show that the model has simulated the decoupling of the shallow CBL from the neutral layer aloft by the nocturnal inversion layer. The major feature which was not anticipated in the observational analysis were the 90 min. profiles through the convergence zone, which was a region of

upward advection. The model results show what a sounding through this transitional feature might look like, if it were available from the observations.

The second analysis of this experiment is the evaluation of terms in the u equation of motion. This type of analysis, shown in Fig. 6.12, is not available from the analysis of field data for reasons discussed at the beginning of this chapter. It is of considerable interest, however, to determine which forces are important in driving the local

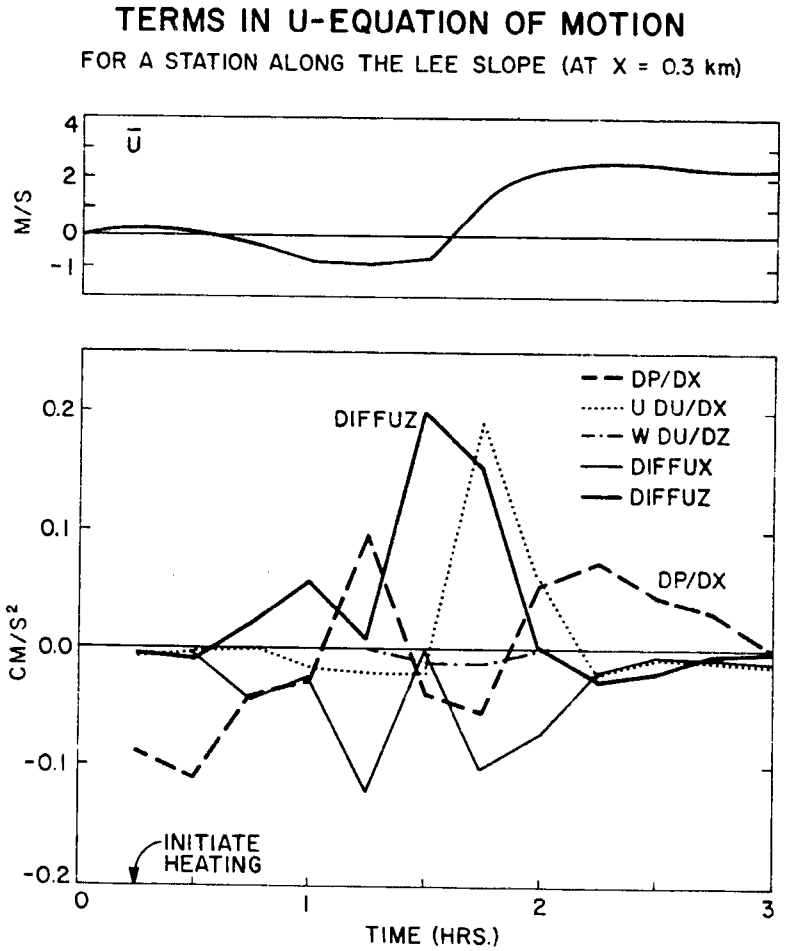

Figure 6.12: Terms in horizontal equation of motion plotted at 15-min. intervals for the first grid point above the surface (z ~ 50 m.) at the starred "Base Site" in the cross sections.

wind systems. This is because such information is crucial in determining under what circumstances simplified models, such as the Wagner-Defant model discussed in Chapter II, might be valid.

The time series graphs presented in Fig. 6.12 are drawn from instantaneous values of the terms at 15 min. intervals. The point selected for this analysis was the first grid point above the ground at the starred "base" site in the cross sections; the height of these "observations" was about 50 m above the ground. The acoustically-active term (i.e. the pressure force term, DP/DX) was averaged over the 80 short time steps to eliminate the acoustic noise. The magnitude of the terms are expressed in terms of accelerations to the u component, so that for the lee slope station involved, a positive term indicates an acceleration down the slope (in the positive x direction), while a negative term indicates upslope acceleration.

The upper portion of Fig. 6.12 shows the time sequence of u. When the heating starts at 15 min., u is very weak and positive. After 30 min. upslope forms, reaching a nearly steady-state magnitude of 1 m/s between 1 and 1½ hrs. After 1½ hrs. there is an abrupt shift to downslope winds, and these reach a nearly steady-state value of just over 2 m/s from 2 to 3 hr.

The lower figure shows the terms as a function of time. In the initial phase of heating, up to around 1 hr., the pressure gradient term is relatively large and negative, as expected. Toward the end of this period the diffusion terms also become large, with horizontal (x) diffusion tending to bring in upslope and vertical (z) diffusion tending to oppose it. By 1 hour these three terms along with the u advection of upslope momentum tend to cancel each other out, as steady-

state persists, except the pressure gradient and the x diffusion. These two terms are very large during this time period and tend to cancel each other, meaning that taken together they are of little dynamic consequence. In the analysis of the next section it will be shown that they occur in a limited region of opposing $2\Delta x$ fluctuations, but the ultimate cause of these fluctuations remains in doubt. At any rate the time period from about 1 hr. to just before 1½ hr. is a time period of little significant dynamic activity. Up to this point it is as though the pressure gradient force gave the winds a push before 1 hr. and then the winds were allowed to coast in steady state until something else happened.

The "something else" was the enhancement of the vertical diffusion of downslope momentum (DIFFUZ), which occurred at 1½ hr., the time of Fig. 6.8 and the time of the 90 min. profiles in Fig. 6.11. The u component (shown in the upper portion of the figure) experiences a sudden positive (downslope) acceleration at this time. The diffusion term remains large for the next 15 min., but the horizontal advection of downslope momentum becomes even larger, as stronger westerly winds push their way past the starred site. After 2 hr. the low pressure and the low-pressure "dome" of isobars in the cross sections have both passed downwind of the site, and the pressure gradient force now enhances the downslope accleration, while the vertical diffusion acts in its traditional role of frictionally retarding the flow. From 2 to 3 hr., the terms cancel each other with the u velocity in steady state. The magnitudes of all the terms gradually die out as 3 hr. is approached, indicating that u must continue at its steady-state velocity.

Many aspects of this time sequence of the balance of forces were anticipated in our analyses of South Park data, but others were not. We hypothesized that the thermally-generated pressure gradient force was important in driving the upslope flow and that the reversal to downslope flow was driven primarily by the vertical eddy diffusion term, in agreement with the results presented here. On the other hand, we did not anticipate the important role of the horizontal advection of downslope momentum after vertical diffusion had started the process, nor did we anticipate that the forces driving the local winds would consist of two dynamically active periods followed by quiet periods of near-steady-state winds.

The results presented above, although they resembled the sequence of events in South Park, were obtained with a ridge that was considerably smaller than that found at the western edge of South Park. In the following section, results are presented for a case in which the ridge was comparable in size to the Mosquito Range west of the Park.

D. Large Hill Experiment

1. Description

In the second experiment a ridge height of almost 1 km. was used. Since this produced a sizeable obstacle to the flow (especially considering that the neutral layer aloft extended only to 2 km.) there was some concern that the upper boundary might be too low. To assure that the upper boundary did not adversely affect the solution, two changes were made: (1) the number of grid points in the vertical was doubled to 96, and (2) grid points were set initially at constant pressure increments of 7 mb. (0.7 kPa). Once the vertical z heights of the grid points were set during program initialization, the points then

retained those z values for the entire experiment. This placement of grid points is well suited for the present experiment because it both removes the upper boundary to an extreme height and gives the finest resolution near the surface where the solution is of greatest interest. Table 6.2 shows the placement of the grid points in the vertical. The resolution near the surface is about 80 m. and the top of the model is above 21 km.

The cold pool was somewhat deeper in this experiment, so the sequence of events occurred somewhat more slowly. In the first experiments a numerical instability occurred near the top of the domain before the afternoon winds were established. So in the following experiment the sequence of events was speeded up by increasing the surface heat flux. The input to the heating function, $\Delta\theta$, was set at 6 K, and this produced surface heat flux values of 20 to 25 cm K/s (25 cm K/s was the maximum value allowed).

2. Results: Cross sections

The potential temperature and pressure cross sections for the second experiment are presented in Figs. 6.13-6.18. Fig. 6.13 shows that the cold pool initially extends up to over 560 m. above the basic surface level of the model, and that there is little organization to the pressure field before heating commences. At 30 min. (Fig. 6.14)--fifteen minutes after the heating started--a warm cap has formed over the hill and a shallow CBL has started to form at the underside of the cold pool. The pressure cross section at this time shows a general region of low pressure along the slope next to the ground.

By 1 hr. (Fig. 6.15) the shallow CBL grows in depth to 200-300 m. and a warm tongue can be seen extending downwind from the ridge. A

TABLE 6.2: Base State for Second Experiment

(km.)	p (kPa)	θ (°K)	u (m/s)	K	Z (km.)	p (kPa)	θ (°K)	u (m/s)	K	Z (km.)	p (kPa)	θ (°K)
.000	69.00	313.9	0.4	33	3.075	46.95	325.1	4.0	65	7.717	24.55	339.7
.042	68.65	314.6	0.4	34	3.190	46.25	325.4	4.0	66	7.909	23.85	340.4
.127	67.95	315.7	0.4	35	3.306	45.55	325.7	4.0	67	8.105	23.15	341.2
.213	67.25	316.6	0.4	36	3.424	44.85	326.1	4.0	68	8.307	22.45	342.0
.299	66.55	317.6	0.4	37	3.543	44.15	326.4	4.0	69	8.513	21.75	343.0
.387	65.85	318.6	0.4	38	3.664	43.45	326.8	4.0	70	8.725	21.05	344.0
.475	65.15	319.6	0.4	39	3.786	42.75	327.2	4.0	71	8.942	20.35	345.2
.565	64.45	319.9	0.4	40	3.910	42.05	327.7	4.0	72	9.166	19.65	346.4
.655	63.75	320.0	0.4	41	4.036	41.35	328.1	4.0	73	9.396	18.95	347.8
.746	63.05	319.8	0.4	42	4.163	40.65	328.6	4.0	74	9.634	18.25	349.3
.837	62.35	319.8	0.4	43	4.292	39.95	329.1	4.0	75	9.879	17.55	351.0
.929	61.65	319.8	0.4	44	4.423	39.25	329.5	4.0	76	10.13	16.85	352.8
.022	60.95	319.8	0.8	45	4.555	38.55	329.9	4.0	77	10.40	16.15	354.8
.116	60.25	319.8	2.4	46	4.690	37.85	330.3	4.0	78	10.67	15.45	356.9
.211	59.55	319.8	3.6	47	4.826	37.15	330.8	4.0	79	10.95	14.75	359.9
.306	58.85	319.8	4.0	48	4.965	36.45	331.3	4.0	80	11.25	14.05	365.0
.402	58.15	319.8	4.0	49	5.105	35.75	331.8	4.0	81	11.56	13.35	370.4
.499	57.45	319.8	4.0	50	5.248	35.05	332.4	4.0	82	11.89	12.65	376.2
.597	56.75	319.8	4.0	51	5.394	37.35	332.8	4.0	83	12.23	11.95	382.3
.695	56.05	319.8	4.0	52	5.541	33.65	333.2	4.0	84	12.60	11.25	389.0
.795	55.35	319.8	4.0	53	5.691	32.95	333.7	4.0	85	13.00	10.55	396.2
.895	54.65	319.9	4.0	54	5.843	32.25	334.2	4.0	86	13.42	9.84	404.1
.997	53.95	319.9	4.0	55	5.998	31.55	334.8	4.0	87	13.87	9.14	412.7
.099	53.25	319.9	4.0	56	6.156	30.85	335.4	4.0	88	14.35	8.44	422.2
202	52.55	319.9	4.0	57	6.317	30.15	336.0	4.0	89	14.88	7.74	432.9
307	51.85	320.6	4.0	58	6.480	29.45	336.4	4.0	90	15.46	7.04	444.8
413	51.15	321.3	4.0	59	6.647	28.75	336.7	4.0	91	16.10	6.34	458.3
520	50.45	322.3	4.0	60	6.816	28.05	337.0	4.0	92	16.81	5.64	473.9
628	49.75	323.2	4.0	61	6.989	27.35	337.5	4.0	93	17.62	4.94	492.3
738	49.05	323.9	4.0	62	7.166	26.65	337.9	4.0	94	18.56	4.24	514.4
849	48.35	324.4	4.0	63	7.346	25.95	338.5	4.0	95	19.66	3.59	541.8
961	47.65	324.8	4.0	64	7.529	25.25	339.0	4.0	96	21.02	2.83	577.4
									97	22.37	2.26	615.3

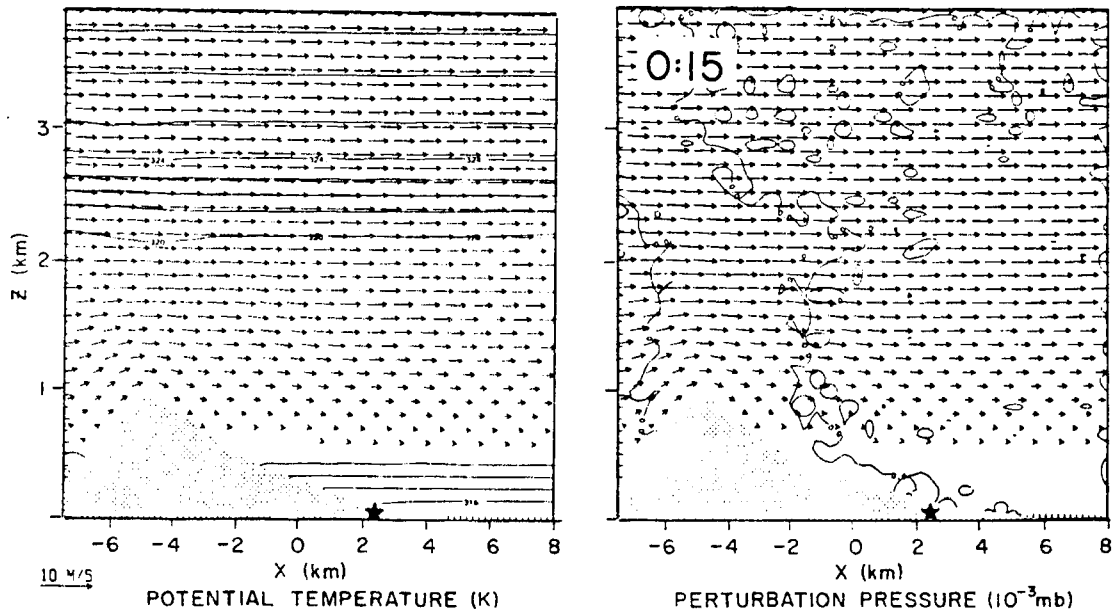

Figure 6.13: Model-generated potential-temperature and perturbation-pressure cross sections for larger-ridge experiment after 15 min. of simulated time, which is the time when surface heating was turned on. Isentropes are at intervals of 1K, and perturbation isobars at dyne/cm^2.

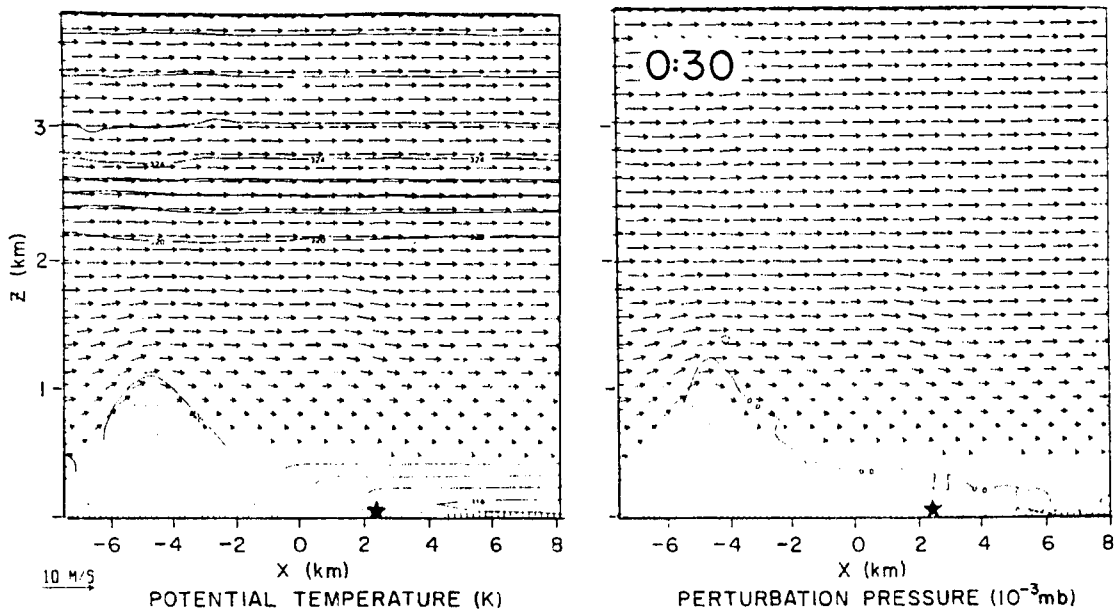

Figure 6:14: Model-generated potential-temperature and perturbation-pressure cross sections for larger-ridge experiment after 30 min. of simulated time, which is 15 min. after the start of heating. Isopleth intervals are the same as in Fig. 6.13.

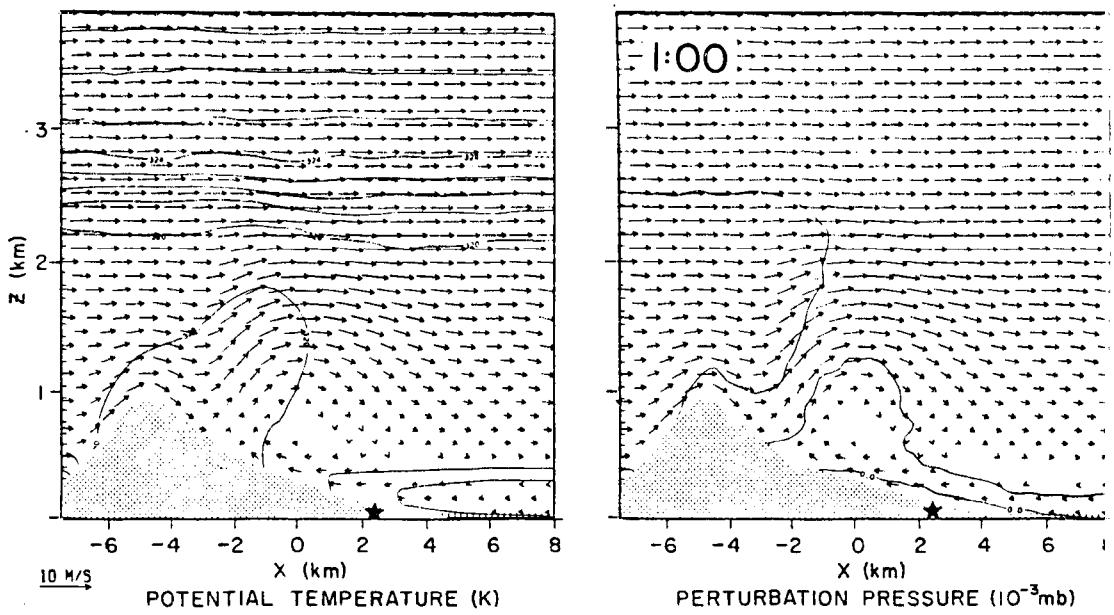

Figure 6.15: Model-generated potential-temperature and perturbation-pressure cross sections for larger-ridge experiment after 1 hr. of simulated time. Isopleth intervals are the same as in Fig. 6.13.

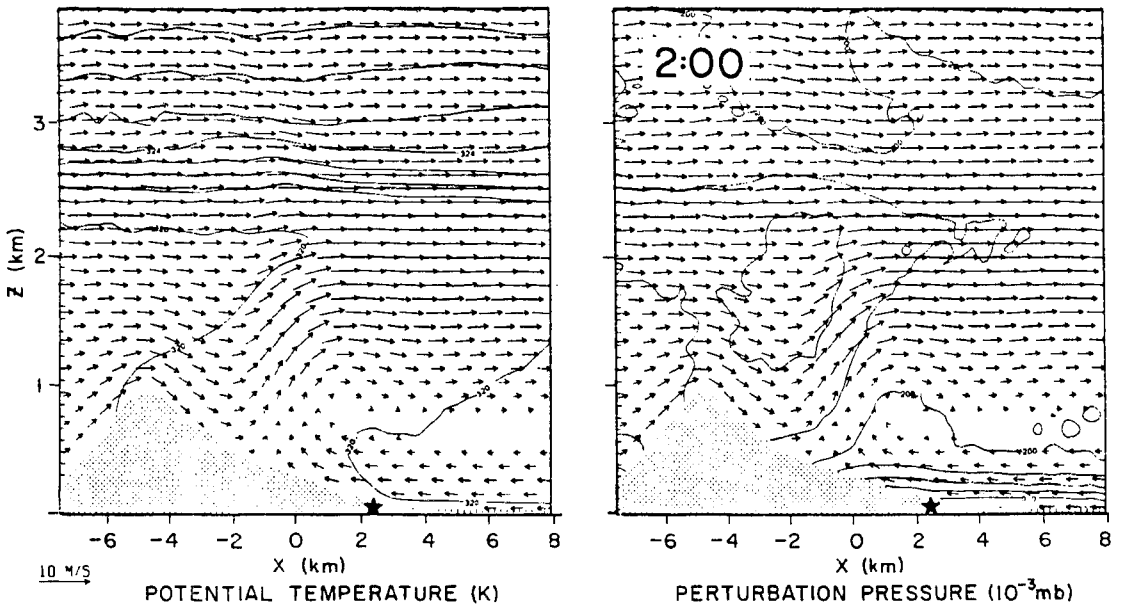

Figure 6.16: Model-generated potential-temperature and perturbation-pressure cross sections for larger-ridge experiment after 2 hrs. of simulated time. Isopleth intervals are the same as in Fig. 6.13.

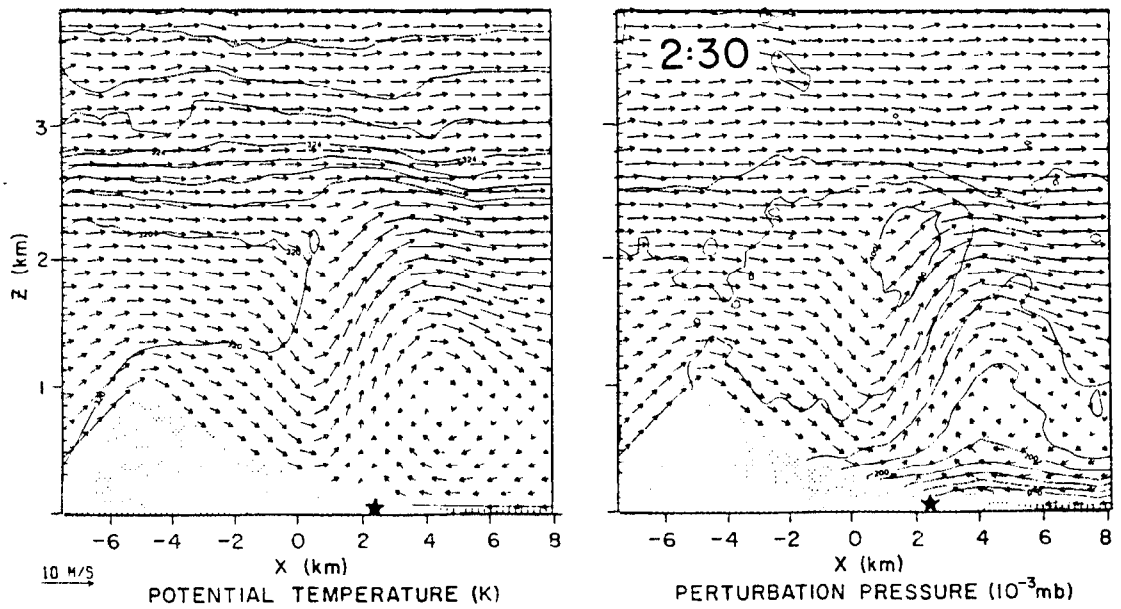

Figure 6.17: Model-generated potential-temperature and perturbation-pressure cross sections for larger-ridge experiment after 2½ hrs. of simulated time. Isopleth intervals are the same as in Fig. 6.13.

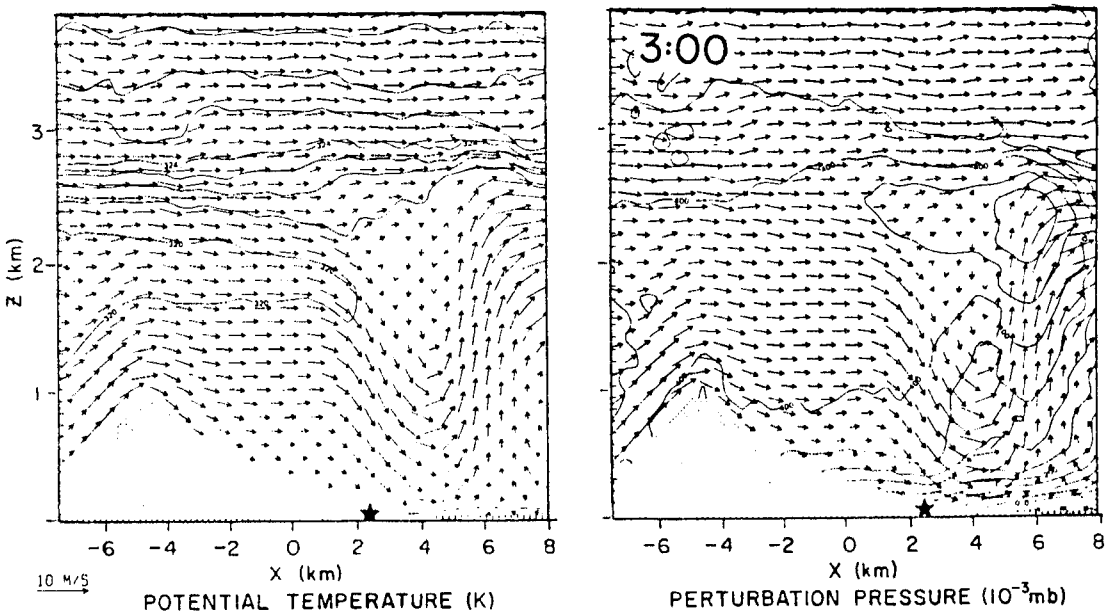

Figure 6.18: Model-generated potential-temperature and perturbation-pressure cross sections for larger-ridge experiment after 3 hrs. of simulated time. Isopleth intervals are the same as in Fig. 6.13.

distinct, organized region of upslope has formed in the shallow CBL, and a zone of convergence exists near x = -2.5 km., where these upslope winds meet downslope winds coming over the top of the ridge. An interesting feature of the velocity field at this time is a closed horizontal vortex centered approximately over x = 0. Both the upslope winds beneath it and the westerlies above it are blowing at faster speeds than other winds at their level, indicating some dynamic enhancement by the eddy. The pressure field shows that this vortex is at the center of a region of low pressure, which is similar to the region of low pressure in the first experiment. Also as in the first experiment, the surface is a region of low pressure on the lee slope, and the isobars have a strong downhill slant, favoring upslope accelerations of the wind. A region of high pressure has formed over the ridge and contributes to the acceleration of the winds over the top of the horizontal vortex.

Fig. 6.16 shows a deeper and stronger layer of upslope flow at 2 hr., and the convergence zone has moved downhill to about x = -1 km. The warm plume has grown to become a large warm region extending from the upper lee slope of the ridge up to the top of the deep CBL several kilometers downstream. The θ structure above the upslope flow shows that the remnant of the stable layer at the top of the shallow CBL is very thin at this time and less than $1^{o}K$ in intensity. The vortex, centered near x = 2 km., is not obviously closed at this time (in fact at 1:30 it appeared not to be closed at all). The pressure field shows a low associated with the vortex, very intense low pressure at the surface, and an independent center of high pressure which seems to have blown over the ridge.

The model results up to 2 hr. of simulated time bear a reasonable resemblance to the results in the first experiment, considering the difference in the size of the ridge. The observed phenomena are reasonably well explained as they were in the previous case, and are much the same as in the observations. After 2 hr., however, the solution changes character rather dramatically.

The situation at 2½ hr. is shown in Fig. 6.17. A closed horizontal vortex has again formed, but this time the vortex is considerably stronger than before and it is the dominant feature of the cross sections for the remainder of the simulation. The vortex still has low pressure at its center, and it has moved to a location three kilometers downstream from where it had been a half hour previously.

In the rest of the domain, the low pressure at the surface is even more intense than it was, and a high aloft exists in the divergent region above an intense updraft which has formed. The potential temperature field shows that a deep well-mixed CBL is present over almost all of the domain, except possibly at the extreme lower right of the figure where a very thin remainder of the inversion layer may still be present.

At 3 hr. this system has propagated to the edge of the domain, where it can interact with the boundary conditions; thus the solution at this point must be viewed with some skepticism. Fig. 6.18 shows the solution at this time. The system remains intact and continues to intensify as it propagates out of the domain (which actually extends to 9.3 km.). The surface convergence, the updraft, and the upper level high have all increased in intensity, and a second region of low pressure has formed upstream of the system.

From the above sequence of cross sections, the development of the winds and boundary layer structure can be divided into three phases. The first phase is the initiation phase, which extends up to ½ hr. or so. During this phase heating begins and a region of low pressure starts to form next to the lee slope of the ridge. There is little deflection of the initial flow at this point except right next to the surface. The second phase of the simulation is the formation and deepening of the thermally-produced shallow CBL/upslope layer. It occurs between about ½ hr. and 2 hr. of simulated time. Thermally-forced flow and mixing processes are important during this phase, and a convergence zone forms near the surface between the thermally-forced upslope flow and the well-mixed downslope flow which occurs at the higher elevations of the lee slopes. The convergence zone during the latter stages of this phase moves down the slope at a rate of approximately 1½ km/hr.

The third phase of this experiment is the phase during which the dynamics of the large horizontal vortex dominate the dynamics of the domain. The vortex forms, intensifies, and moves rapidly out of the domain. During the hour between 2:00 and 3:00, the convergence zone propagates more than 7 km down the hill (i.e. at a speed of over 7 km/hr. or 2 m/s). This third phase, with the appearance of an intense horizontal vortex which seems to have its own dynamics, is the major difference between this experiment and the first experiment. Thus, a major contribution to the formation of this eddy is apparently the size of the obstacle (ridge) over which the air must flow.

To supplement the observation of pressure in the cross sections presented above, cross sections of the horizontal pressure-force term

in the u equation of motion were prepared. Cross sections for the second phase of the simulation are given in Fig. 6.19, and for the third phase, in Fig. 6.20. These values represent the actual term in the u equation, averaged over the 80 acoustic time steps. Thus, they are in units of cm/s^2, with contour intervals of 0.2 cm/s^2. Looking at plots of pressure gradient can be advantageous for two reasons: first, it is not always evident from cross sections of pressure itself which direction the pressure gradient actually points, and second, by looking at the zero line one can tell the exact location of pressure extrema (i.e. highs and lows) in the horizontal.

The cross sections for the second, thermally-forced phase of the experiment are presented in Fig. 6.19a and b. The first figure, representing the pressure gradients after 1 hr., shows a broad region of upslope (negative) gradients along the slope up to the convergence zone, with maximum values near the surface. The location of the zero isopleth at the upslope edge of this negative area shows that the actual location of the lowest pressure is at the uphill side of the horizontal vortex. Uphill from this there is a region of positive (downslope) pressure gradient. Even higher up the slope, just to the lee of the ridge top, there is another region of negative pressure gradient. A region of especially large magnitudes occurs at the surface and immediately downwind of the ridge top. This region appears in all the cross sections, and the intensity of its maximum increases as the wind speeds blowing over the ridge increase. Thus, this position of the flow represents flow over an obstacle, and in this region the pressure pattern resembles that for potential flow around a cylinder, for example .

Fig. 6.19b shows the pressure-gradient force at 2 hr. The region of posi-

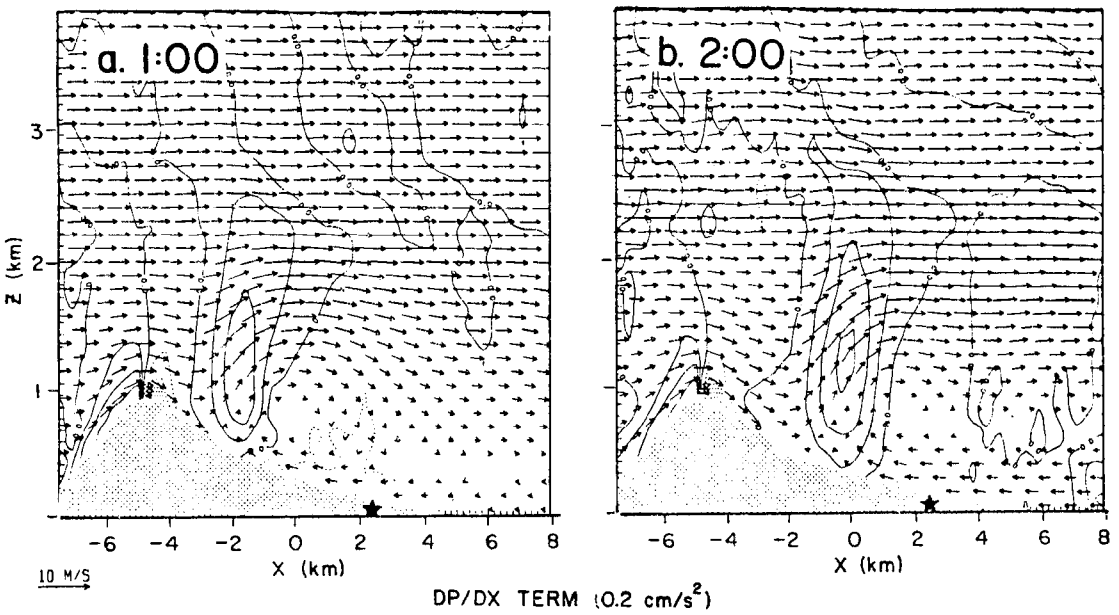

Figure 6.19: Model-generated cross sections of the horizontal pressure-gradient term in the u equation of motion at (a) one hour and (b) two hours of simulated time.

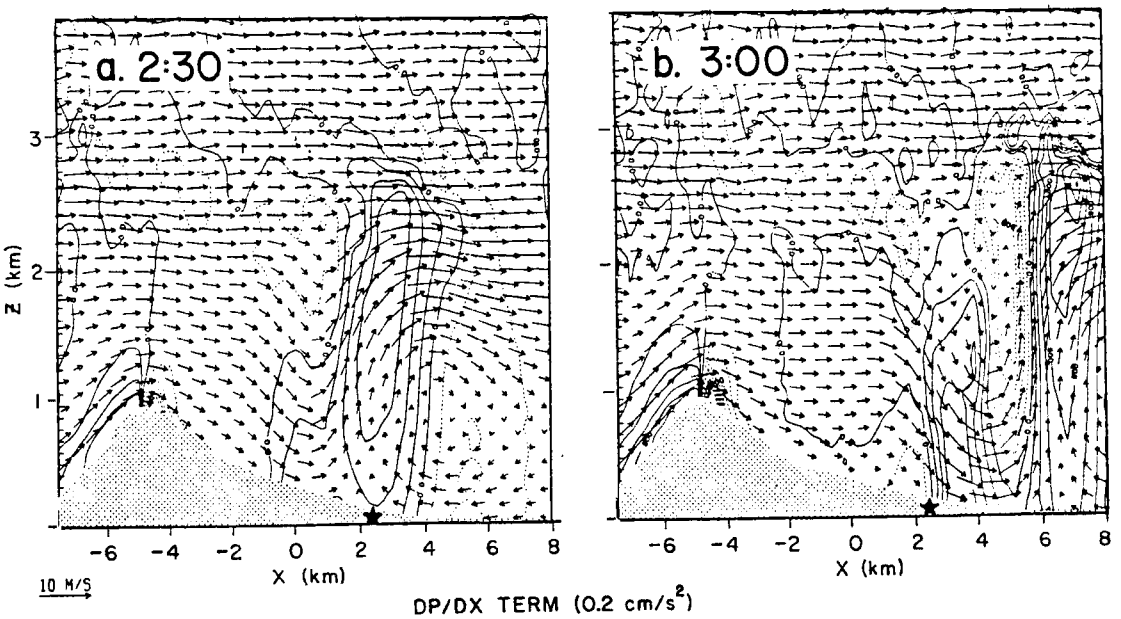

Figure 6.20: Same as Fig. 6.19 except for simulated times of (a) 2½ hr. and (b) 3 hr.

tive (downslope) pressure force has expanded and the region favoring upslope has diminished in size and intensity.

The pressure forces accompanying the intensified horizontal vortex are shown in Figs. 6.20a and b. As expected the patterns show considerable amplification over the previous patterns. Additionally, large values occur all the way to the top of the deep CBL, and in the last figure, the largest values in general do not appear at the surface.

3. Further Analysis

For further analysis of the data generated by this experiment, a somewhat different approach was used from that of the first experiment. Instead of using instantaneous values of the variables of interest to form profiles or other analyses, the variables were first smoothed by averaging over a volume of space and time. This procedure is intended to be analogous to the horizontal ensemble averaging approach used over flat terrain in analyzing both aircraft data (e.g. Lenschow, 1970, 1974 and Coulman, 1978) and model-generated data (e.g. Deardorff, 1974, and Sommeria, 1977).

According to this latter approach, the flight leg (of usually 10-20 km or more) or the modeling domain is assumed to be horizontally homogeneous. Means are computed over the entire flight leg or over an entire horizontal level of the model, and vertical profiles can then be defined with respect to those horizontal means for the purpose of computing turbulence quantities, such as variances and fluxes, and vertical profiles of these turbulence quantities can then be constructed.

In a region which is not horizontally homogeneous, however, the situation is more complicated. Horizontally-averaged values of a quantity often end up being a compromise between a general region of

higher values and a general region of lower values (as for example measurements of θ over mountains and over an adjacent plain). Additionally, the fluctuations measured in this way from the compromise "mean" value tend to be dominated by the large differences between the two regions. Thus, this is not a very useful way to define fluctuations.

In order to avoid these problems, the quantities presented below (except where noted) have been subjected to a running-mean filter in space and time. The variables were averaged over seven points (1.4 km) in the horizontal, 2 points (200 m) in the vertical, and over the five previous one-minute time levels (the data were stored on the analysis tape at one-minute intervals). These values were chosen to give a reasonably large number of data points (70), yet to provide a region of space and time that was small enough to be relatively homogeneous over much of the domain. Over these 70 points, then, we could determine fluctuations from the mean and compute turbulent variances and fluxes.

The averaging operator defined in the preceding paragraph is thus a discrete version of the space-time averaging operator (~) defined and discussed by Cotton et al. (1978)

$$\tilde{\phi} = \frac{1}{\tau L_x L_y L_z} \int_{z-\frac{L_z}{2}}^{z+\frac{L_z}{2}} \int_{y-\frac{L_y}{2}}^{y+\frac{L_y}{2}} \int_{z-\frac{L_z}{2}}^{z+\frac{L_z}{2}} \int_{t-\frac{\tau}{2}}^{t+\frac{\tau}{2}} \phi(x,y,z,t)\,dx\,dy\,dz\,dt \quad ,$$

where ϕ is an arbitrary variable to be averaged over time and space, and L_x, L_y, L_z and τ represent the length and time intervals or scale over which the averaging is to be performed. For example, in the present example L_x = 1.4 km., L_z + 200 m., and τ = 5 min. (The ensemble

averaging procedure included in the definition of Cotton et al. has been omitted from the above definition, since we are dealing with numerical modeling data rather than realizations of actually-observed data.)

a. Profiles of mean quantities

The "Base Site" for this experiment, from which profiles were determined, was located at x = 2.2 km. The local terrain height at this point is about 100 m. Profiles of potential temperature, averaged in the manner described above, for the second experiment are presented in Fig. 6.21. The profile at 30 min. shows that the stable nocturnal inversion layer extends to above 450 m and a warm, unstable surface layer has formed at its underside. By 1 hr. the shallow CBL grows to over 200 m thick, and by 1:45 it is more than 300 m thick, as the strength of the inversion diminishes. The height of the inversion drops somewhat at 1 hr. in response to the subsidence over the site at that time (see Fig. 6.15), but by 1:45 it is back to its original level. By 2½ hr. the deep CBL has formed, with a slightly unstable θ profile up to a height of 2.2 km.

The profiles for filtered values of u are shown in Fig. 6.22. Very small negative (upslope) values begin to appear at the lowest levels by 30 min. A half-hour later, at 1 hr., a shallow region of well-mixed upslope extends from the surface to over 200 m, and by 1:45 the depth of this region grows to over 300 m; both of these depths correspond to the thickness of the shallow CBL. By 2½ hr. the upslope layer has diminished in speed and is no longer well mixed, but it has not disappeared because of the resurgence of the large horizontal vortex downwind of the site (see Fig. 6.17).

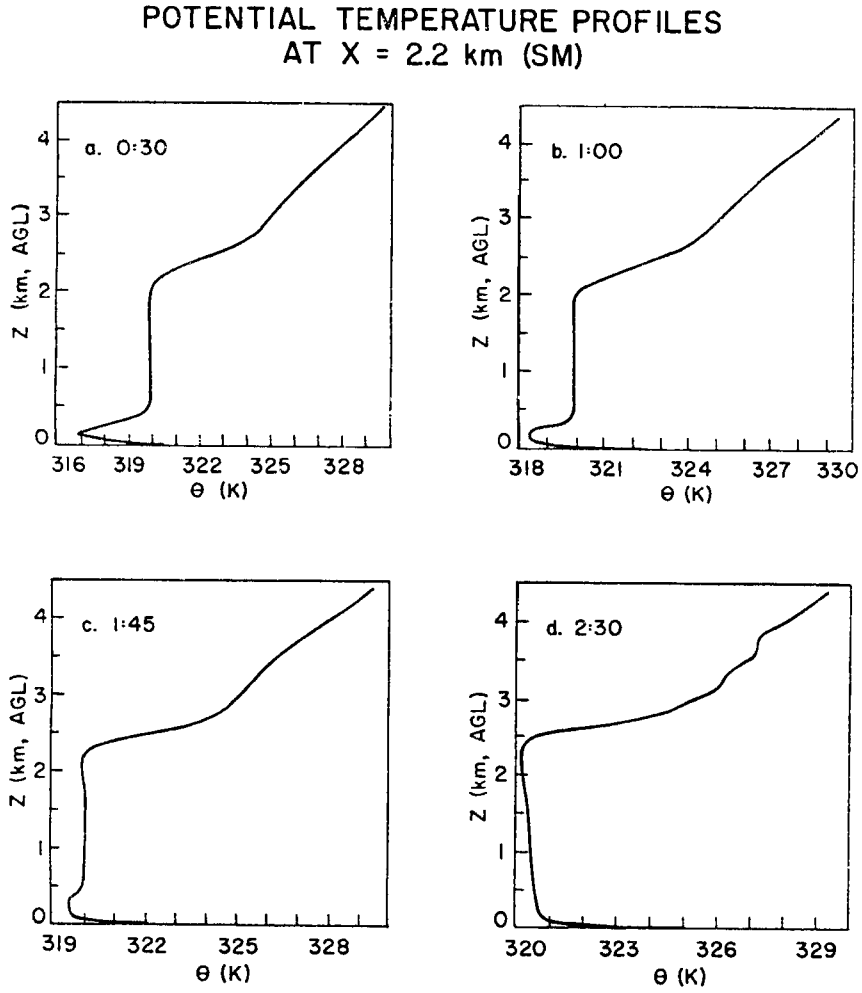

Figure 6.21: Model-generated vertical profiles of filtered potential temperature for (a) ½ hour, (b) 1 hour, (c) 1 hour, 45 min., and (d) 2½ hours. Profiles are at starred "Base Site" in the previous cross sections.

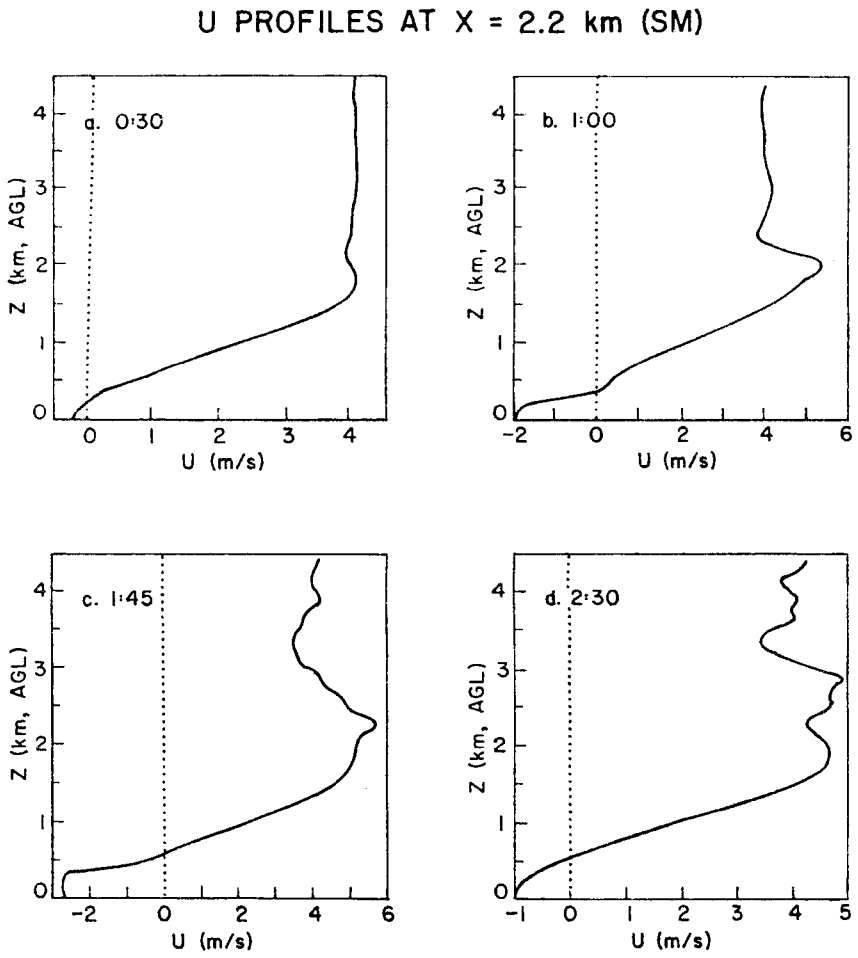

Figure 6.22: Model-generated vertical profiles of filtered horizontal wind speed (u) for (a) ½ hour, (b) 1 hour, (c) a hour, 45 min., and (d) 2½ hours. Note the change in horizontal scale among the four profiles. Profiles were obtained from data at the location of the "Base Site" (star) on the previous cross sections.

Profiles of smoothed w values are given in Fig. 6.23. Subsidence in the neutral layer aloft over the site grows from a maximum of 14 cm/s at 30 min. to 33 cm/s at 1 hr. These downward velocities diminish, and their pattern becomes more complex, as the horizontal vortex passes over the site at 2 hr. At all three of these times, upslope in the shallow CBL produces upward velocities near the surface. At 2½ hr. the convergence zone is almost directly over the site. At this time the w profile shows upward motion reaching a maximum of 1.8 m/s in the middle of the deep CBL.

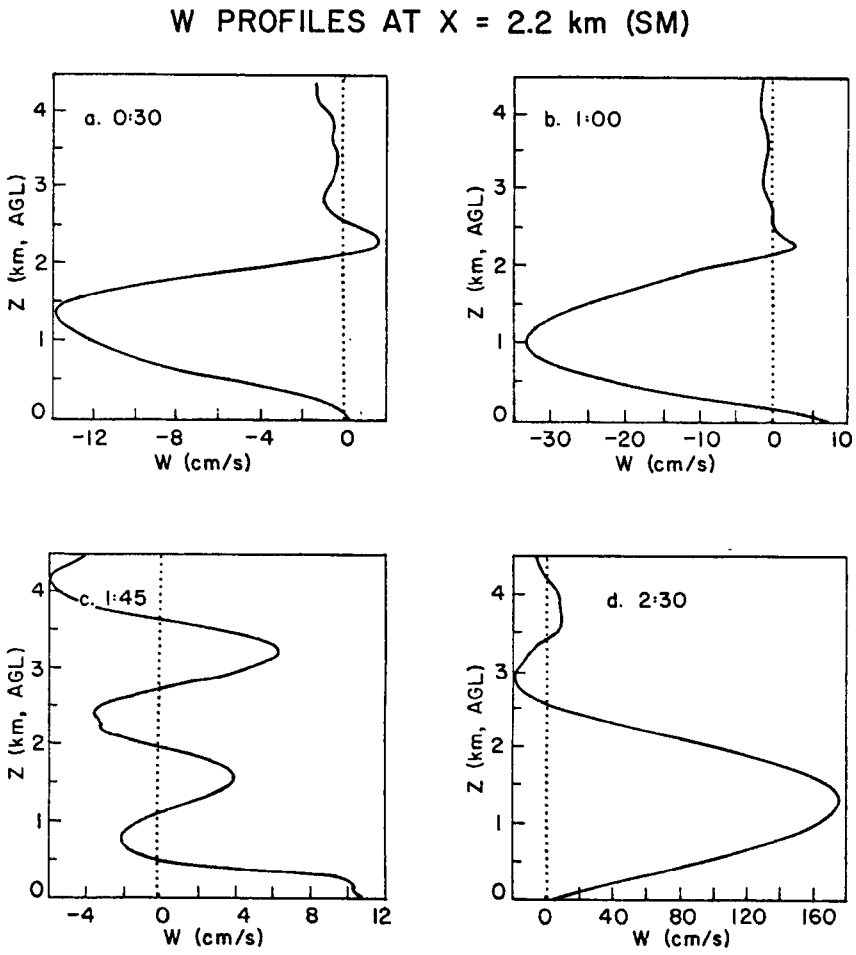

Figure 6.23: Model-generated vertical profiles of filtered vertical wind speed (w) for (a) ½ hour, (b) 1 hour, (c) a hour, 45 min., and (d) 2½ hours. Note change in horizontal axes. Profiles are from the "Base Site" indicated by a star in the previous cross sections.

b. Terms in the u equation of motion

As in the previous (small hill) experiment instantaneous values for the terms in the u equation of motion were evaluated at 15-min. intervals. In this section only the raw values of u and of the terms in the equation have been used, viz. no smoothing has been applied (except, of course, that the acoustically-active terms have been averaged over one "long" x, or 2 s., time step).

Time plots of the terms are given in Fig. 6.24 for the first grid point off the surface (at K=2) at the "base site" from the previous section (x = 2.3 km). The height of this point is about 40 m above the ground. It is immediately obvious that all the terms for this larger hill experiment seem to have greater amplitudes than they did in the small-hill experiment.

In describing this figure it is again convenient to refer to the three phases of this experiment. During the first phase--up to 30 min.--the pressure gradient is building up but still small, and upslope flow has just started to form. The second phase of the experiment lasts from about ½ hr. to over 2 hr. At this particular point along the slope, the entire duration of this phase is spent in upslope, since here upslope ends only after the horizontal vortex has intensified.

The upslope pressure force builds to a maximum at 1 hr. and helps to establish strong upslope winds of 3 m/s. After this, however, the pressure force diminishes. Two reasons why this happens are: first, that the strong upslope flow is advecting cooler air up the slope, and second, that the strong subsidence noted previously over the site is pushing down warmer air in the atmosphere over the lower areas of the slope and over the plain. Both of these effects reduce the horizontal

temperature gradient, which in turn reduces the pressure gradient. The upslope continues to blow at around 3 m/s, however, largely because of horizontal diffusion of upslope momentum. Horizontal advection acts at various times to either enhance or diminish the upslope during this phase.

The vertical diffusion term acts to oppose the upslope at all times during this phase of the simulation. While this is the traditional role of this "friction" term, the maximum value reached at 1 hr.--before the largest upslope values of u are achieved--seems contradictory. However, the explanation for the rapid increase of this term at this time is that upslope is initiated near the surface where the pressure gradient is largest. This produces a nose (i.e. maximum) in the upslope wind profile at the point being analyzed, and this shape of profile produces both an upward and a downward flux of upslope momentum, maximizing the diffusion. As the heating processes continue, upslope develops at the point above the one being analyzed. The (negative) value of u at K=3 catches up with the value at K=2, and this produces a profile with smaller values for the diffusion term.

As this second phase of the simulation draws to a close, the vertical diffusion term does not have an opportunity at the location of this site to play the same role as it did in the first experiment, namely that of mixing the westerlies downward after the nocturnal inversion layer is completely eroded. The reason is that by the time the inversion layer disappears and the convergence zone reaches the site, the horizontal vortex is already fully formed, and the simulation is already in its third phase. Fig. 6.20a shows that at 2:30 the site is at the edge of a region of large values of downslope pressure forces

generated by flow around the vortex. According to the present figure (Fig. 6.24) this is also the time during which the flow at this point is undergoing its transition to downslope winds. Thus, in this case the downslope is brought in by large pressure forces associated with the vortex rather than by downward diffusion as in the small hill experiment.

We should remark here that similar analyses were performed at other points in the domain (all at the first grid point off the surface), among them a point higher on the slope at x = -1.7 km. At this point the upslope disappears during the second phase of the experiment, before the intensified vortex forms. There are two observations of interest about the vertical diffusion term. First, this term becomes very large (+0.38 cm/s^2) by 45 min. because of the "nose in the profile" effect described above, and second, vertical diffusion is the dominant term during the transition to downslope flow, as it was in the first experiment. In fact, during the latter stages of the transition at this site, the horizontal advection of downslope momentum also becomes important, as it had in the earlier experiment.

Returning briefly to Fig. 6.24, we merely note that during the third phase of the experiment after 2¼ hr. or so, this site is under the influence of flow and pressure patterns associated with the vortex, although the effect dies off toward the end of the run. The result of this influence is large-amplitude fluctuations in all terms during this time period.

Finally, while discussing terms in the u equation of motion, it was mentioned in the first experiment that an unexplained fluctuation between the pressure force and the horizontal u diffusion terms occurred, which

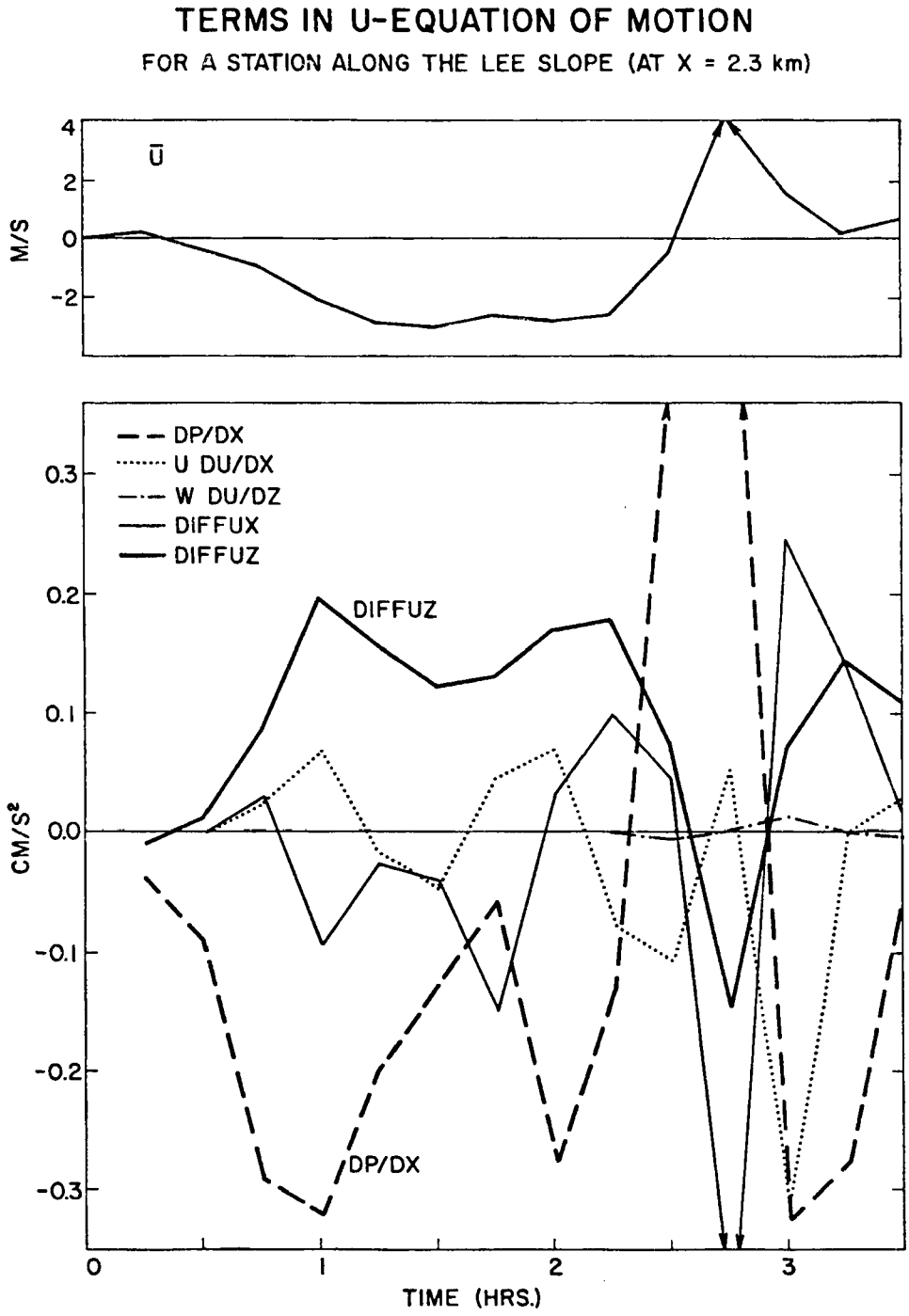

Figure 6.24: Terms in horizontal equation of motion plotted at 15 min. intervals for the larger-ridge simulation. The location at which the terms were evaluated was the first grid-point above the surface (z ~ 50 m.) at the "Base Site" (star) in the previous cross sections.

believed to be dynamically insignificant. Similar fluctuations were observed in the analysis of u-equation terms at x = 0.3 km in this experiment. Since better analysis routines are available for this experiment, the characteristics of these fluctuations are further investigated, although their cause remains unexplained.

Fig. 6.25 shows several variables plotted as a function of x

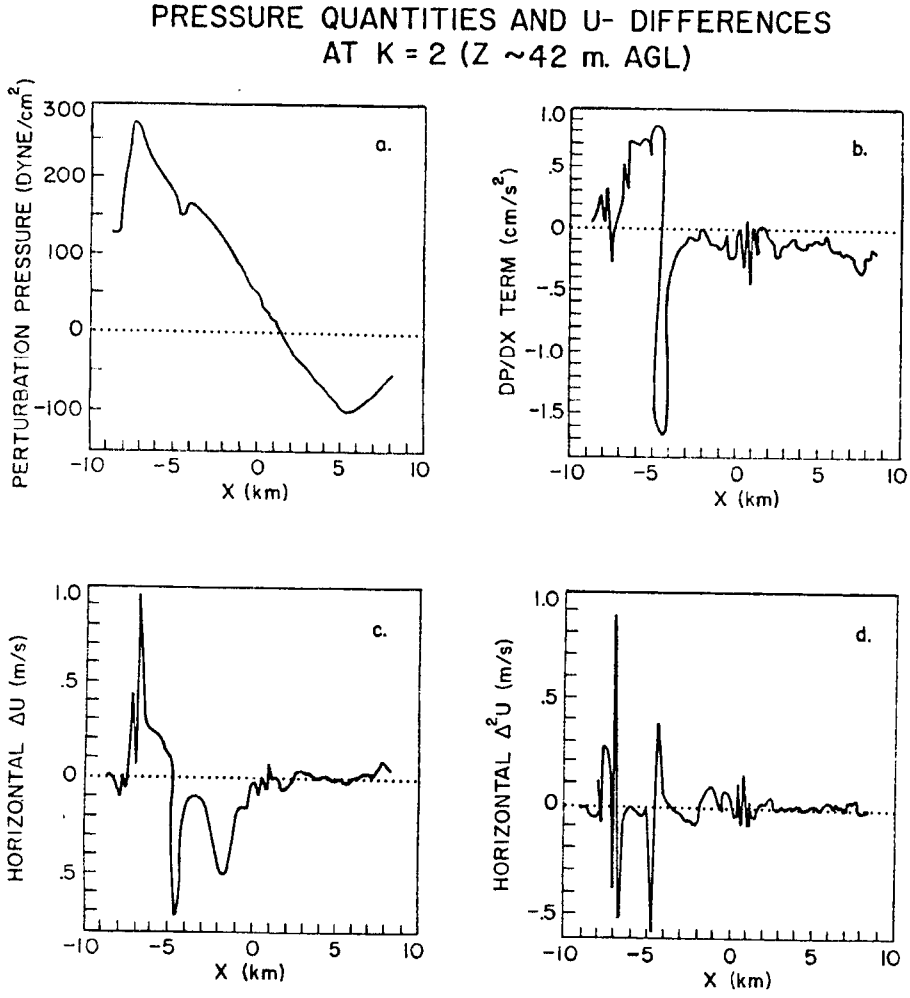

Figure 6.25: Horizontal plots, evaluated at the 42 m. level above the terrain, of the following quantities: (a) perturbation pressure, (b) horizontal pressure gradient term in the u equation of motion, (c) Δu, and (d) $\Delta^2 u$.

distance at a level approximately 40 m off the ground at a simulated time of 1½ hr. Fig. 6.25a gives the unfiltered perturbation pressure and 6.25b the pressure gradient force in the u equation (note, however,

that the horizontal pressure derivative used in computing the latter term contains a transform term so it is not strictly the slope of the former term). In Fig. 6.25b there is a region between x = 0 and 1 km where there is a strong $2\Delta x$ fluctuation in the pressure force term. The corresponding region in Fig. 6.25a shows some small wiggles in the pressure field but no sharp singularities. Figs. 6.25c and d show the first and second horizontal differences in the unsmoothed, uninterpolated u field, Δu and $\Delta^2 u$. The former quantity is proportional to the horizontal divergence, and the minimum in divergence near x = -2 km represents the convergence zone. The latter quantity is nearly proportional to horizontal diffusion in this case, and it represents the horizontal difference of the former quantity. Of interest here is the fact that both quantities show significant $2\Delta x$ fluctuations between x = 0 and 1 km, with the second difference showing worse behavior than the first, as expected. Thus, Figs. 6.25b and 6.25d show that in a limited region of the solution, the pressure force and horizontal diffusion terms in the u equation develop some sharp $2\Delta x$ fluctuations--the diffusion presumably in response to the accelerations in u produced by the fluctuating pressure force. These fluctuations eventually damp out and do not seem to have any significant lasting effect on the simulation, so as hypothesized previously they do not seem to be dynamically important. It is of interest and possible significance that these fluctuations occur during the time when the upslope seemed to have "overshot" and the horizontal pressure gradients near the surface were diminishing in magnitude.

c. Turbulence quantities

As described at the beginning of this section, fluctuations can be defined with respect to the mean value computed in our space and time averaging volume. The squares of these fluctuations can be averaged over the volume to obtain variances, and products of fluctuations of different quantities can be averaged to obtain covariances, or "fluxes" if the covariance includes a velocity component. In this section the overbar ($\bar{}$) will refer to a mean over the averaging volume, and the prime (') will denote a deviation at an individual grid point in that volume from the volume mean.

A consequence of this averaging procedure, in which the horizontal length scale of the averaging operator is limited, is that w fluctuations tend to be small, and most of the vertical transport of quantities occurs through the mean w, i.e. by vertical advection, since in general $\bar{w} \neq 0$. This is generally the case for this experiment, except during the third phase of the experiment when the horizontal vortex produces large magnitude w fluctuations.

An example of this kind of behavior is shown in Fig. 6.26. In this figure profiles of $\overline{w'^2}$, the vertical velocity variance over the space-time averaging volume, are presented for the "Base Site" of the previous section. Fig. 6.26a shows the profile for 1 hr. of simulated time. Maxima are apparent at the bottom and top of the neutral layer aloft, probably because of gravity waves. The magnitudes of $\bar{w}'^2$ are small at all levels and are fairly characteristic of the values seen when the convergence zone or the horizontal vortex are not present. In contrast Fig. 6.26b shows the $\bar{w}'^2$ profile at 2:45 when the vortex is well formed

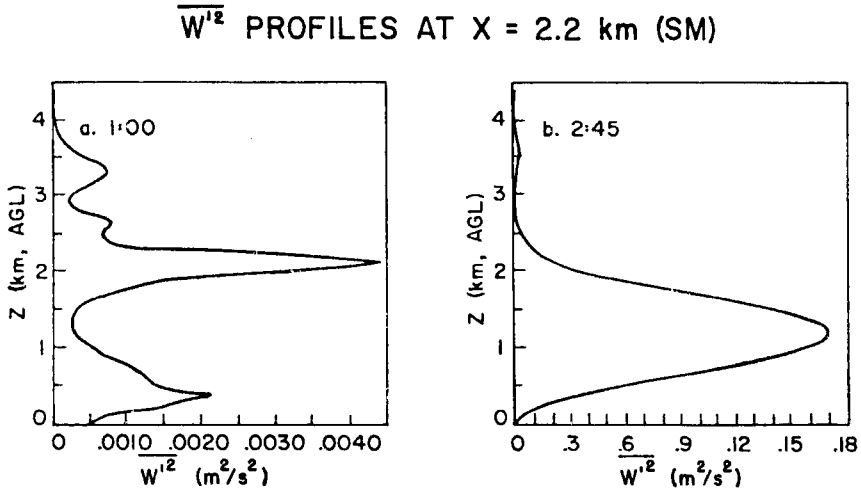

Figure 6.26: Model-generated vertical profiles of vertical velocity variance ($\overline{w'^2}$) at the starred "Base Site" for (a) 1 hr. and (b) 2 hr., 45 min. Note the change in horizontal scale.

and the convergence region is over the site. The peak magnitude of in the middle of the CBL is 1.7 m^2/s^2. The latter value is more in line with values of TKE (which includes $\overline{w'^2}$) which were found by Hahn (1980) in the middle of the CBL over South Park. Hahn's values were based on 1-km. averages of aircraft flight-leg data.

Profiles of $\overline{\theta'^2}$ over flat terrain show a large maximum in the surface layer and a secondary maximum at the top of the CBL. Profiles of $\overline{\theta'^2}$ for this experiment are shown in Fig. 6.27. After 1 hr. (Fig. 6.27a) there is a large maximum just above the surface which is partially an artifact of the vertical averaging, and secondary maxima at the top of the shallow CBL and at the top of the neutral layer aloft. Fig. 6.27b shows that after the deep CBL has formed, the only maxima are in the surface layer and at the top of the CBL.

Fig. 7.28 shows profiles of turbulence kinetic energy (TKE) at 1:30. TKE is normally defined as:

$$TKE = \tfrac{1}{2}(\overline{u}'^2 + \overline{v}'^2 + \overline{w}'^2),$$

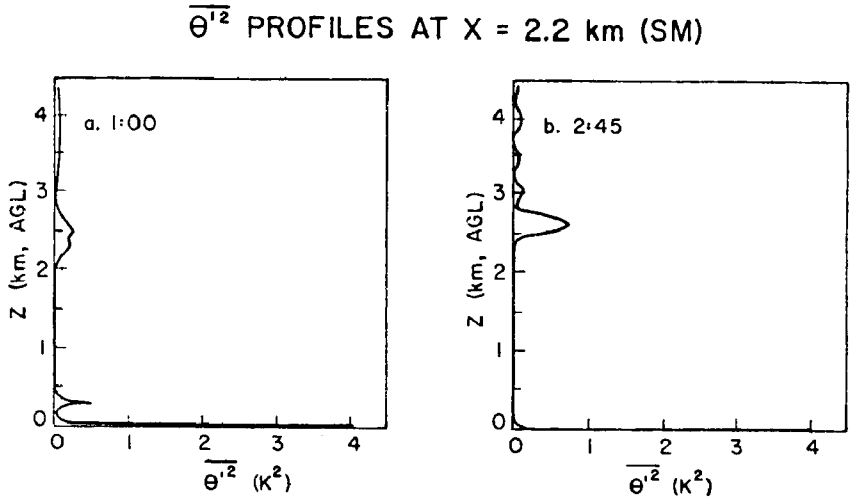

Figure 6.27: Model-generated vertical profiles of potential temperature variance ($\overline{\theta'^2}$) at the starred "Base Site" for (a) 1 hr. and (b) 2 hr., 45 min.

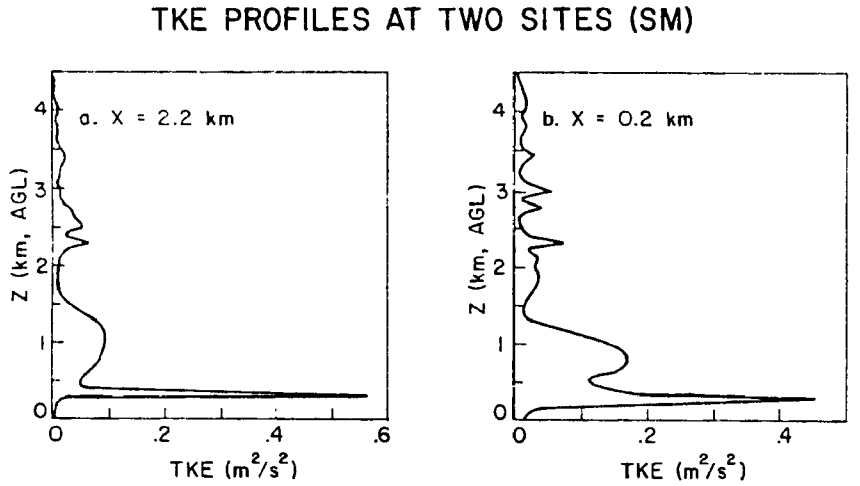

Figure 6.28: Model-generated, vertical profiles of turbulent kinetic energy (TKE) at 1½ hr. for two sites along the slope: (a) the starred "Base Site" and (b) a site 2 km. farther up the slope. Note the secondary maximum of TKE above the primary spike at ~ 300 m, which represents the top of the shallow CBL. The secondary maximum indicates the presence of turbulent energy in the neutral layer aloft.

out for present purposes, since $\overline{v}'^2$ is zero, the definition is revised to:

$$TKE = \tfrac{1}{2}(2\overline{u}'^2 + \overline{w}'^2).$$

Fig. 6.28a shows the TKE profile for the current "base" site and 6.28b,

for a site 2 km uphill from the base. Both exhibit a sharp maximum in the region of large shear between upslope and downslope flow. But also of interest is a broad secondary maximum in the central portion of the neutral layer aloft. This shows that, during the time before the cold pool erodes away, this dry-adiabatic layer over the mountains is not a quiescent, region, but rather it is an actively turbulent region. This turbulence was produced by buoyancy at the ridgetops and higher elevations and is advected into the neutral layer aloft by the ridgetop winds in much the same manner as suggested by Davidson and Rao (1958) and Ayer (1961). Thus, these modeling experiments support their contention that turbulence is present at the top of the nocturnal inversion layer, even though the model results do not support their hyopthesis that mixing at the top of this layer is an important mechanism for inversion breakup.

Turbulence quantities have also been determined as a function of the x coordinate at levels a given distance above the terrain. Fig. 6.29 presents TKE at a level approximately 745 m above the ground. Figs. 6.29a and 6.29b show a single maximum on the lee side of the ridge at 1 hr. and 2 hr. This maximum, with values of 0.24 and 0.29 m^2/s^2, is associated with the updraft region over the convergence zone. Fig. 6.29c shows TKE values at 2:45 after the vortex circulations are fully established. The peak value--again associated with the main updraft region--this time reaches nearly 1.0 m^2/s^2.

The vertical heat flux, $\overline{w'\theta'}$, given in Fig. 6.30a and 6.30b at 1 hr. and 2 hr., respectively, shows a double maximum during the second phase of the experiment. This is because the level passes through the middle of the circulation cell, so that one maximum represents the rising air, the minimum in between is where $w \sim 0$, and the second maximum represents

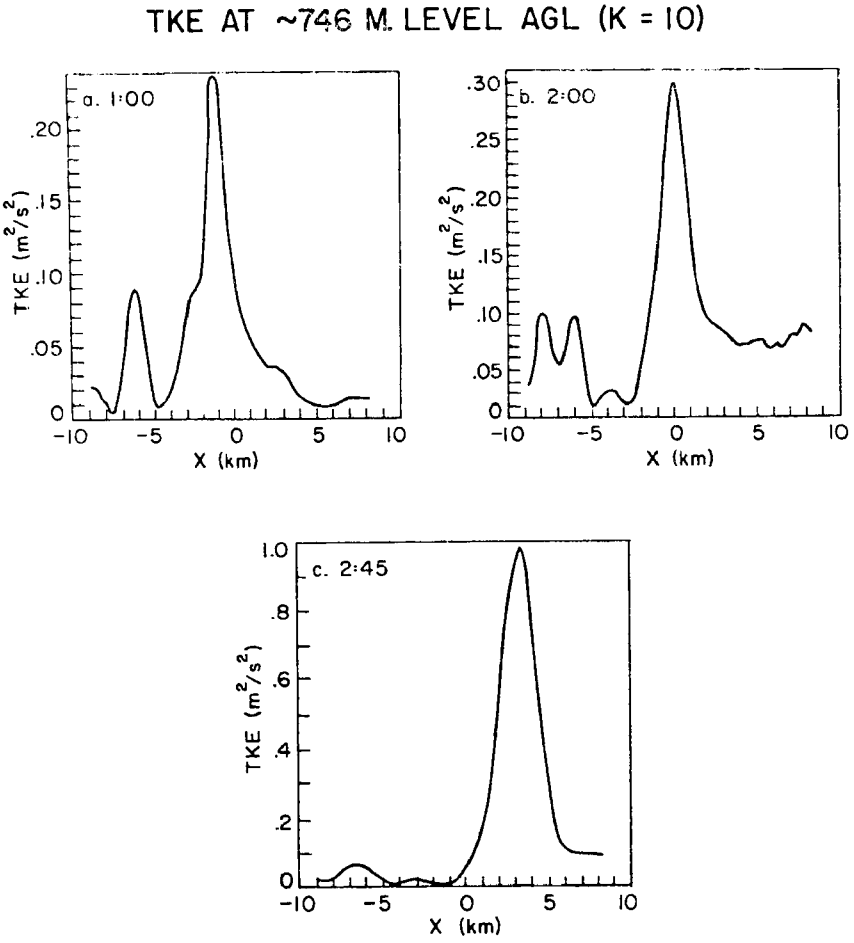

Figure 6.29: Horizontal plots, evaluated at the 746 m. level above the terrain, of TKE at (a) 1 hour, (b) 2 hours, and (c) 2 hours, 45 min. Note change in vertical scale.

the downdraft. Maximum values are modest, with peak magnitudes reaching .015 K m/s. In the third phase of the experiment, on the other hand, when large values of w' are produced, peak magnitudes associated with the vortex updrafts are ten times this big, as shown in Fig. 6.30c.

Similarly the turbulent momentum flux, $\overline{u'w'}$, shown in Fig. 6.31a and 6.31b for the second phase, is small with the only significant contribution from the updraft region above the convergence zone. Obviously, much of the momentum transport during this early phase is accomplished on scales larger than the averaging scale. As expected,

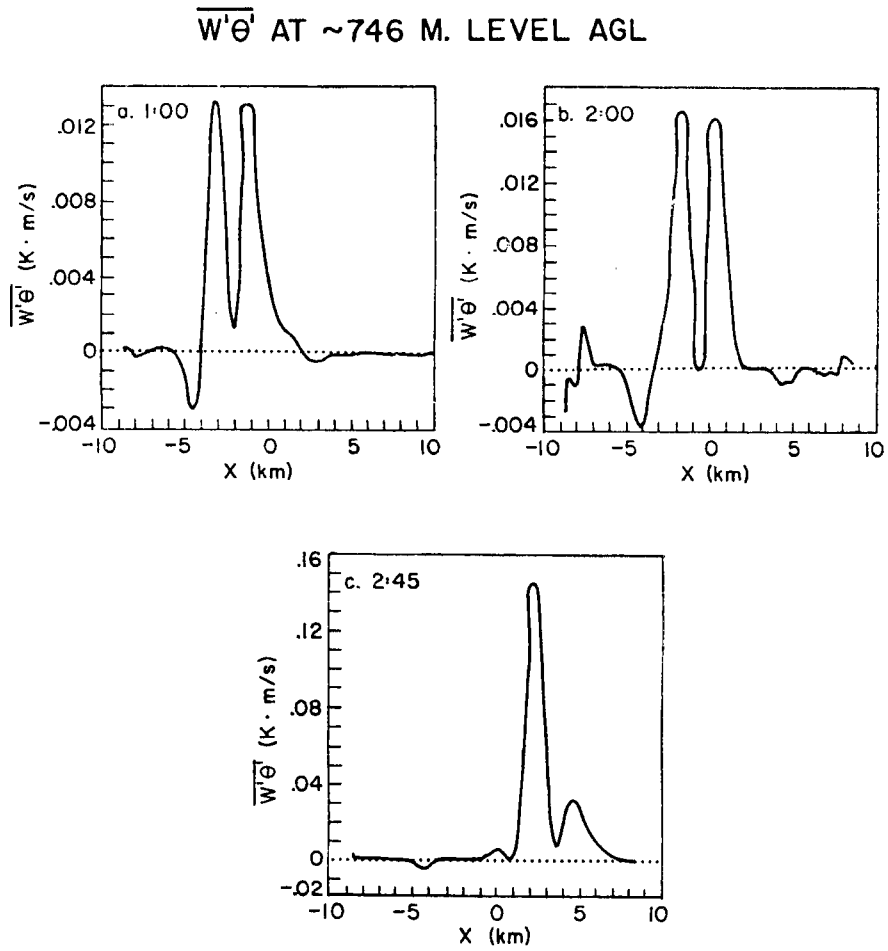

Figure 6.30: Horizontal plots, evaluated at the 746 m. level, of the kinematic heat flux ($\overline{w'\theta'}$) at (a) 1 hour, (b) 2 hours, and (c) 2 hours, 45 min. Note change in vertical scale.

however, the circulations during the third phase of the simulation produce large values of eddy momentum flux, as shown in Fig. 6.31c.

E. Final Remarks on the Modeling Experiments

The purposes of the modeling efforts described in this chapter were to discover what ingredients were necessary to obtain a successful simulation of a typical dry day in South Park, as determined from the data analyses in Chapter IV, and then to use the model to find out what else we could learn about slope flows. The first and most obvious conclusion to be drawn from the results presented in this chapter is that

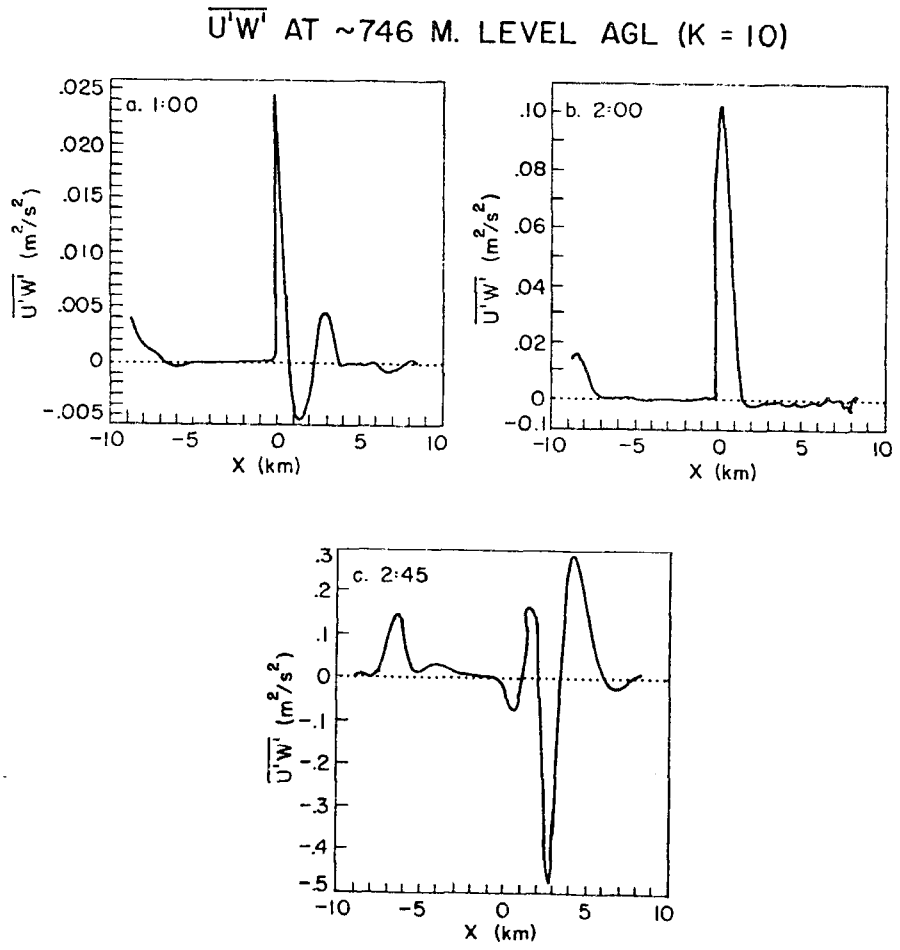

Figure 6.31: Horizontal plots, evaluated at the 746 m. level, of the momentum flux ($\overline{u'w'}$) at (a) 1 hour, (b) 2 hours, and (c) 2 hours, 45 min. Note change in vertical scale.

The model did a remarkably good job of simulating the features of the observational study. The development of the upslope flow, the growth of the shallow CBL, the development and movement of the leeside convergence zone, and the surfacing of the downslope winds after the development of the deep "afternoon" CBL are observed features which the model successfully simulated. The agreement between model and observation not only gives confidence in the modeling results, but also increases our confidence in the observational results, i.e. that the observations were reasonably representative, the analyses were performed properly, and our extrapolations and conclusions were reasonable.

The success of the modeling experiments in reproducing phenomena observed in South Park also supports the hypotheses used to formulate the experiments. Three such hypotheses used in these modeling studies were that (1) a proper initial potential temperature sounding and wind field and (2) a stability-dependent eddy mixing coefficient, K_m, were necessary to successfully simulate the South Park situation, and that (3) a successful simulation could be obtained by uniform heating of the surface everywhere, i.e. without local hot spots to produce a "heat island" along the slope. With regard to the last hypothesis, there is no doubt that the slope and aspect of terrain in the mountains has a very significant effect on the exact manner in which the flow evolves on a given day. What these numerical experiments show is that the presence of such localized heat sources is not necessary to the production of realistic upslope flows. It remains for future experiments to determine how the presence of these sources can modify the flow produced by the type of elevated heat source with uniformly-warmed surfaces that was modeled in these experiments.

A fourth hypothesis, and a potential source of criticism of these results, is that a two-dimensional model could represent the obviously three-dimensional flow in South Park. The first point is that these experiments are intended to model the flow along the western edge of South Park, where the ridge does seem to be rather two dimensional, and the modeling results support this contention of two-dimensionality. A valid objection is that the formation and/or intensification of the horizontal vortex in the second experiment could be a strictly two-dimensional phenomenon, and that in three dimensions this feature may not form at all or may form and fail to intensify. Determination of

whether this point is valid or not must await either 3-D simulations of this situation or field observations of this phenomenon, which would confirm the present results.

Further objection to the use of a two-dimensional model can be made on the basis of the resolved-scale turbulence generated by the model. Mechanical or shear production of turbulence is an inherently three-dimensional process which cannot be modeled at all in two dimensions. Thus in situations where shear-produced turbulence is important, two dimensional modeling studies will be totally inadequate. In the present study, however, the turbulence is largely generated by buoyant processes, which are not of necessity three dimensional. Thus, the aspects of the flow which have been reported here are probably valid even though the model is 2-D. Deardorff (1973) has discussed the problem of "...two-dimensional 'turbulence' and three-dimensional turbulence:"

> They are so different, in fact, that the use of a two-dimensional model to simulate three-dimensional flow is scarcely justifiable unless the problem is one in which continuous and strong forcing in two dimensions occurs (e.g. the sea-breeze problem).

The present slope-flow problem is another situation where there is "continuous and strong forcing in two dimensions."

One disappointing aspect of the turbulence generated by the resolved scales of this model is that there was little tendency for the flow to produce thermals, which were observed in the field (Chapter VI), either in the shallow CBL or in the deep CBL. The reason for this may be that the value for K_m which was needed to suppress numerical instabilities (like the one described in the last section) was relatively large. The resulting values for K_H may have been so large that the

subgrid diffusion of heat was very efficient, and this obviated the need for resolved-scale vertical transport of heat. Additionally, for the shallow CBL, which was only a few hundred meters deep, the horizontal grid interval of 200 m. may have been very close to the preferred wavelength of the thermal forcing. Suppression of $2\Delta x$ numerical noise would thus require the vertical transport to be accomplished by subresolution scale processes. Further experimentation, and possible 3-D modeling, will be required to determine why thermals were not produced.

In the present chapter, results were presented for two different experiments. One obvious conclusion which can be drawn by comparing the two is that the bigger hill of the second experiment disturbs the flow more. The smaller hill produced gentle transitions between the various flow regimes like those which we anticipated from the observations. The larger hill, too, produced intuitively "reasonable" flow patterns for the first two phases of the simulation. But in the third phase, suddenly a rapidly-intensifying eddy formed. Is there any evidence that such an eddy could actually exist?

In reality this question poses a dilemma. On the one hand it is hard to believe that such an intense vortex actually exists. On the other hand, the maximum vertical velocities generated during the first experiment or during the first two phases of the second were on the order of or less than 1 m/s. Fig. 4.23b shows that much larger vertical wind speeds than this do occur. Peak vertical velocities generated by the horizontal eddy in the model, however, exceed 5 m/s, a value more in line with those found by Hahn (1980) using aircraft data. Other evidence for intense updrafts exists. On several dry days in South Park chaff was released near the ground and tracked by radar. It was

observed to ascend rapidly to heights of 3-4 km on these occasions, indicating updraft speeds of 8-10 m/s or more (Danielson and Cotton, 1977). If we are to account for the intense updrafts which are known to occur over the mountains, eddies or vortices like the one generated in the latter stages of the second experiment are a likely mechanism for their generation.

As stated above, the agreement between the model and observations gives some confidence in the modeling results. This provides encouragement to further investigate the modeling results to try to learn about features and mechanisms that were not observed in the field. Moreover, another investigation which the model allowed us to make was the study of the balance of forces in the u equation of motion. It showed that the upslope pressure-gradient force, generated by heating at the surface, is important in producing upslope winds in the model as it was in other, simpler conceptual models like that of Wagner and Defant. However, in the present model this force was only important during the earlier stages of boundary-layer growth. As the shallow CBL eroded away, the downward eddy diffusion of the winds aloft, and then the horizontal advection of downslope momentum, were seen to overwhelm the thermally-induced pressure gradient. A further effect that this model could simulate was the production of dynamically-induced pressure systems, which often equalled or exceeded the thermally-induced ones in magnitude.

As a final remark on the applicability of these numerical experiments, one should note that, although the quantitative aspect of these simulations were selected to resemble South Park case studies, the qualitative results should be very general for flow in the vicinity of a 2-D ridge. The terrain shape itself, for example, was taken to be

a mathematical formula rather than the specific shape of the Mosqui o Range at the western edge of South Park, so the ridge could be any ridge with similar dimensions to those simulated. The presence of a cold pool is also a feature which is common to mountainous areas, so the development of upslope flow and a leeside convergence zone as simulated in these experiments is also not likely to be unique to South Park. Thus, the results presented in this chapter are likely to apply to heated flow over two-dimensional ridges in general.

VII. REVISED CROSS SECTIONS OF POTENTIAL TEMPERATURE

Using the observations presented in Chapter IV, cross sections of potential temperature were constructed to show the overall structure of the thermal field, and its qualitative relationship to the wind field. These cross sections, which were shown in Fig. 4.17, were described as preliminary. It is now possible to revise those figures using the aircraft cross sections from Chapter IV and the model results of Chapter VI. The revised cross sections are shown in Fig. 7.1.

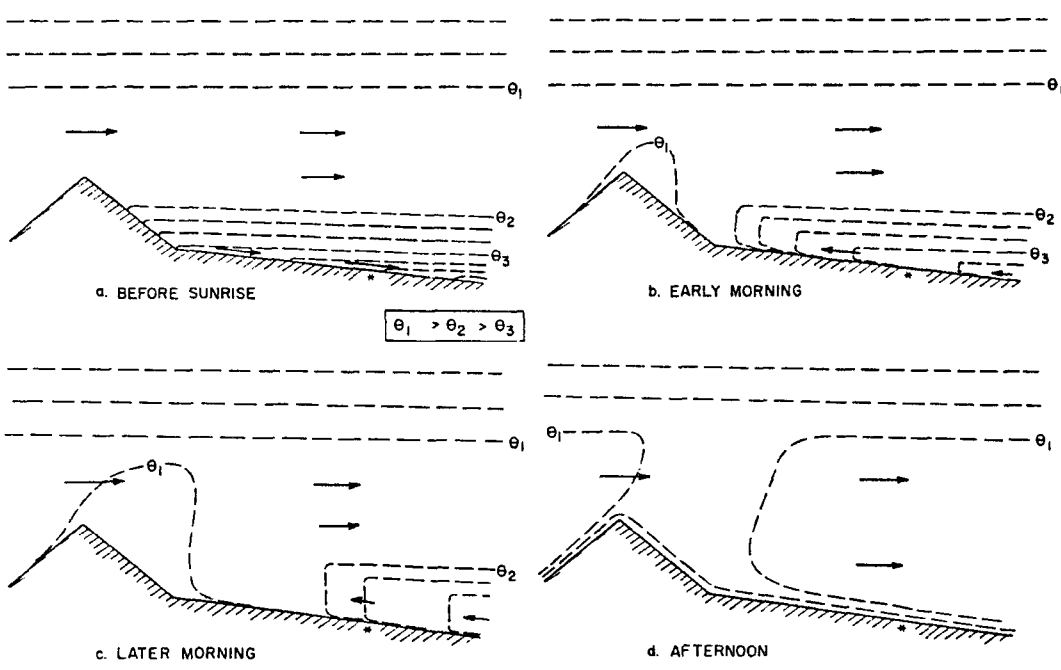

Figure 7.1: Revised potential-temperature cross sections. Dashed lines are isentropes at arbitrary intervals and shading represents the region where upslope-regime winds are present. The asterisk at the surface shows the relative location of the Base Site, where the soundings in Fig's. 4.15 or 4.16 would have been taken.

These new cross section have many features that are similar to he preliminary ones of Fig. 4.17. For example, Fig. 7.1a shows the pre-sunrise θ structure, with a stable θ configuration at lower levels representing the cold pool, and a region of constant θ between the top of the cold pool and the stable "free atmosphere" in the upper portion of the drawing. The isentropes in the cold pool slant downhill. Fig. 7.1b shows the early structure of the shallow CBL containing upslope winds beneath the cold pool. Fig. 7.1c depicts the later-morning situation, where the shallow CBL has warmed and deepened, and the stable layer atop the shallow CBL has thinned. Finally, Fig. 7.1d represents the deep afternoon CBL with superadiabatic surface layer. A further effect which the old cross sections and the new ones have in common is the downhill progression of the edge of the cold pool and upslope layer.

The major differences between the two figures are a de-emphasis on the horizontal temperature gradient induced by the warm (in the daytime) mountain, and the presence of a level capping inversion instead of a sloping one atop the neutral layer aloft. The model results showed the presence of a warm tongue of air extending upward from the ridge and being advected downwind. The tongue of air is only slightly warmer than the unheated air farther downstream. Thus the horizontal gradient of θ between the neutral layer aloft (or the deep CBL) over the ridge and that over the slope should be less dramatic than what was implied by the original cross sections. Also, the warmer region over the ridge should tilt downwind with height. These features have been incorporated into the newer cross sections.

The numerical modeling results showed that there was little tendency for the capping inversion at the top of the neutral layer aloft

(or deep CBL) to conform to the terrain. Rather, the inversion stayed nearly level except for a shallow region of entrainment above the warm tongue emanating from the mountain, and except for small-wavelength gravity waves which are not intended to be represented in these cross sections. This means that, even in this shallow region of the atmosphere below the capping inversion, a column of air reaching from the surface to the inversion undergoes vertical shrinking as it blows up the slope and vertical stretching as it blows down the slope.

At this point it is of interest to note that although the cross sections have been somewhat altered, the basic physical interpretation as presented at the beginning of Section C.3 of Chapter IV remains unchanged. Nocturnal drainage winds are still envisioned to form a lake or pool of cold air in the valley, upslope winds still form in a thin, shallow CBL along the underside of the cold-air pool, and as morning heating progresses, the cold air pool still shrinks and disappears as the deep afternoon CBL forms over the entire region. At one edge of the shrinking cold pool a zone of convergence was produced, which has been called the "leeside convergence zone" in this study.

Fig. 7.2 shows a potential temperature cross section through the leeside convergence zone illustrating how it is formed. Below (i.e. down the slope from) the convergence zone is the region of thermally-forced upslope winds at the surface. Above the zone the well-mixed winds at the surface are blowing down the slope by definition, since we are on the lee side of the ridge. As shown in the figure, these winds meet at the region marked C, at the upslope edge of the layer of upslope winds (shaded region).

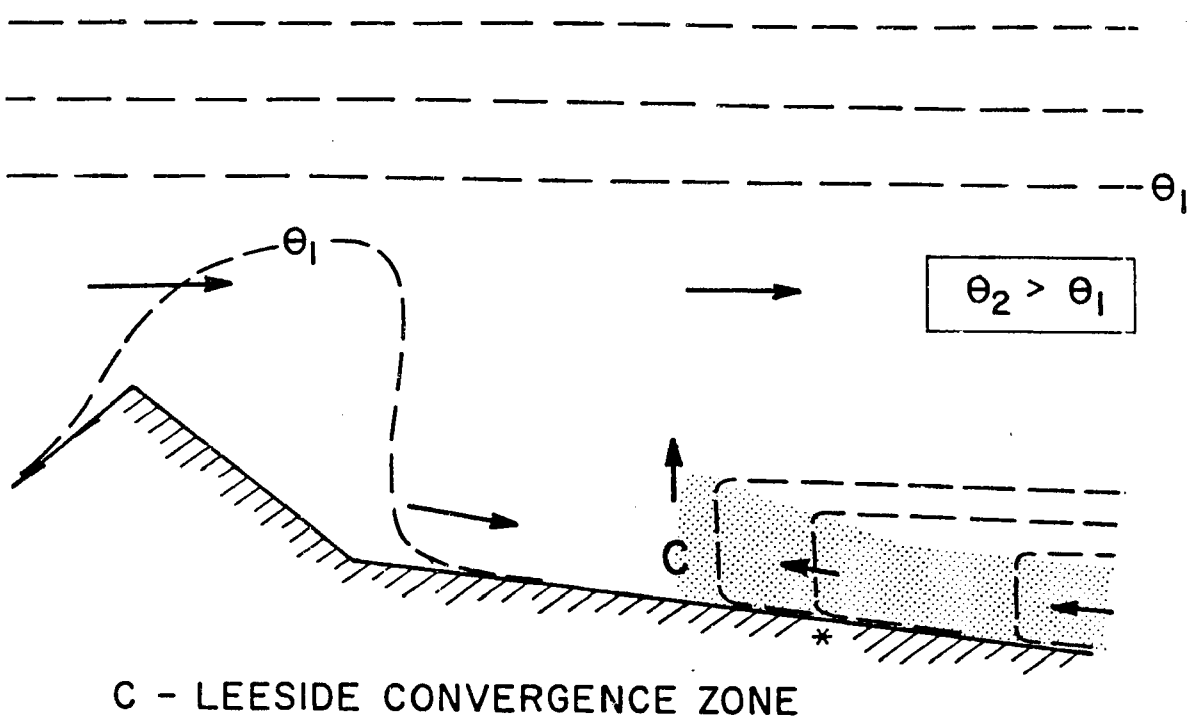

Figure 7.2: Potential temperature cross section through the leeside convergence zone, which is indicated by a C. Cross section corresponds to Fig. 7.1c.

One further topic of interest is the origin of the daytime ridgetop-level winds, which are the winds that ultimately mix down to the surface. As has already been discussed, these winds are not "gradient winds," since they are in communication with the earth's surface through turbulent mixing processes. The true gradient winds during daylight hours exist only above the capping inversion at the top of the neutral layer aloft. Ridgetop winds during daylight hours are thus similar to the winds in a horizontally-homogeneous CBL in that they are determined by three "forces": the large-scale pressure gradient, Coriolis, and surface friction. There is little thermally-forced diurnal variation of the ridgetop winds unless the synoptic pressure field is very weak.

VIII. CONCLUSIONS

Low-level atmospheric flow over the mountains was introduced in this study as the result of a complex set of interacting processes or effects, including the geometry of the topography, thermal forcing at the surface, and the presence of large-scale pressure gradients and ridgetop-level winds, to name just a few. Conceptual models of ridge-valley flows which have become accepted over the past several decades have largely ignored the presence of thermal structure in mountain valleys and the presence of ridgetop-level winds. These conceptual models concentrated on the effects of thermal forcing at the earth's surface on local wind systems in a valley. Tacit assumptions were that vertical thermal stratification within the valley and ridgetop-level winds have negligible effect on flow within the valley, and also that the thermally-induced pressure gradient is the only force important in producing the direction and approximate magnitude of the local winds (although some of those studies called this force "buoyancy").

The preceding study has provided several alternative models with varying degrees of complexity. The very simplest conceptual model presented in this study allowed for the interaction of two local-scale forces--the thermally-deiven pressure-gradient force of the previous simple models and the vertical eddy flux divergence (or "eddy diffusion") of momentum--in determining the local winds. With proper initial conditions at sunrise (viz. a nocturnal cold pool beneath a deep dry-

adiabatic layer), this basic "two-force" model, summarized pictorially in Fig. 7.1, could explain the formation of upslope at the underside of the cold pool, the surfacing of ridgetop-level winds in the afternoon, and the formation of a zone of convergence toward the leeward side of mountains or ridges. In addition to the broad South Park basin, there is evidence that this new simple model also applies in deep mountain valleys as well.

It is tempting to assert that the results of this study indicate that, during periods of strong solar heating after the cold pool has disappeared, mixing processes will always produce turbulent winds at the surface that are similar in direction and speed to the ridgetop winds. A properly broad interpretation of this conceptual model, however, should be that after the final dissolution of the cold pool, the surface winds result from the balance between the pressure force and the vertical mixing. Thus, there will undoubtedly be instances where the thermally-generated pressure force is strong enough to exceed the vertical eddy flux divergence and to produce upslope even after the nocturnal inversion layer has eroded away.

But other observational evidence and especially the results of the numerical model of flow over a simplified ridge indicate that this model is still too simple. Other terms in the horizontal equation of motion are important (as well as the interaction among this and the other equations). Other features might be required (i.e., the intensifying horizontal vortex) to reproduce the large values of w observed in the mountains. And to add to the complexity, pressure gradients produced by dynamic interactions often overwhelm the thermally-produced pressure gradients, so that often times the pressure force is not even acting the way it is "supposed to" according to the simple theories.

Thus at the extreme pessimistic end, one could say that a "typical dry day" in the mountains is completely fictitious, since of all the days studied in South Park, no two were alike. Each day in South Park--even each dry day--could be a separate case study in how boundary-layer processes interact with terrain and with mesoscale processes, and how all in turn interact with larger-scale processes, to produce the local wind systems on that particular day. But while all this is quite true, it is still of value to try to distill out those features which are persistent from one dry day to the next.

A purpose of this study, therefore, has been to find and describe the sequence of events which occurs on a typical dry day in the Park, and to investigate the balance of forces which leads to the establishment of the local wind systems on such a day. A second purpose, however, which has been achieved in part by presenting data from a variety of dry days, was to give some appreciation for the variability of conditions which can alter or even disrupt these "normal" processes. The day-to-day variability in the evolution of the local winds seems to be as important to their understanding as those aspects which do recur each dry day.

A. Scale Interaction and Updraft Generation

Two important issues which have surfaced in this study are that of the interactions of phenomena of various length or time scales and that of the generation of updrafts by dry processes in the mountains. The problem of interactions of many different scales of phenomena was shown to be important for the development of thunderstorms and lines of thunderstorms in South Park by Cotton et al (1982). They showed that features ranging in scale from individual cumuli and cumulus downdrafts

all the way up to the synoptic scale were important participants in such interactions. In the present study it has been demonstrated that interactions among a significant range of scales is important even in the development of the dry-convective circulations. Heating at the base of the cold pool occurs through penetrative convection, which is accomplished by thermal eddies that are similar in length to the depth of the convective layer (i.e., the CBL). Penetrative convection is an example of what we have been calling a "boundary-layer-scale" process. The heating produced by this convection produces a horizontal pressure gradient favorable to the formation of upslope flow, which is a small mesoscale flow, and to the formation of upvalley flow, which is a larger mesoscale phenomenon. At the edge of the cold pool--i.e., at the edge of the upslope/upvalley-moving air--is another mesoscale phenomenon, the leeside convergence zone. If this zone is important in the initiation of clouds or the organization of lines of moist convection, then this would be a link between the scales discussed in this paper and the scales discussed by Cotton et al. (1982).

The leeside convergence zone as described in this study in South Park is a relatively small-mesoscale phenomenon. Even smaller, and possibly more intense, convergence zones most likely occur at the heads of leeside valleys, both in isolated mountains and in mountain ranges. Additionally, a similar kind of convergence mechanism may be important on a larger scale--namely on the scale of entire mountain ranges--in providing a favorable region for initiation or enhancement of mesoscale moist convective systems to the lee of these ranges.

The leeside convergence zone is also an important part of the discussion of the generation of dry updrafts in the mountains. The

characteristics of such updrafts is a matter of crucial importance in the numerical modeling of orograpically-forced cumuli and thunderstorms, especially since Clark (1979) and Tripoli and Cotton (1982) have recently pointed out that storm simulations can be more a product of the initialization process than of other model properties (such as the base-state environment or wind field). Thus the question of how to initialize a cloud model is related to the question of what are the properties of updrafts produced by mountain circulations--for example, how big are the convergence/vertical velocity values in the updrafts and what are the thermal and moisture properties of them (i.e., where does the air in them originate).

Three mechanisms have produced vertical velocities in this study. The first is forced ascent over the mountain barrier; this is probably not often important in South Park because the ridgetops are below cloud base during the summer. The second is the leeside convergence zone, which according to the 2-D model results does not produce very large values for w. However, two points to be made are: (1) as discussed in Chapter IV, the third dimension of the convergence zone would act locally to focus the convergence, thus magnifying the peak w values, and (2) the convergence zone produces moist ascending air steadily for a long period of time, a situation which could be more favorable to moist convection than sudden intense updrafts. The third mechanism for updrafts was the intense horizontal vortex produced by the numerical model. This produced peak updrafts similar in magnitude to those observed in the mountains, but such an eddy has not been directly observed in Nature. Thus the problem of the characteristics of updrafts in the mountains remains unsolved.

B. Recommendations for Future Research

In a comprehensive study of the kind just presented many inadequacies in our state of knowledge become apparent. The problems just discussed, namely the generation of updrafts and the initiation of cumuli in the mountains, are two significant problems which should be addressed. Cumulus initiation could be studied in the near future by using data from some moist days in South Park and by adding moisture and condensation processes to the 2-d version of the numerical model presented here. Understanding in both areas would benefit greatly from (1) a comprehensive field project in a mountainous area, like SPACE, but designed to study boundary-layer updrafts and initial cumuli and (2) an extension of the current modeling effort to three-dimensions.

The problem of dry updrafts in the mountains also touches on another significant area for investigation, the problem of boundary-layer turbulence in the mountains. Evidence from this study suggests that there are some aspects of the mountain CBL that are similar to the CBL over flat terrain, e.g. the large-eddy structure probably consists of at lease some transient thermal plumes. Obviously, many aspects are not the same. A study of the nature of turbulence in the mountain boundary layer should be of paramount interest in transport and diffusion studies in this kind of terrain, since parameters related to eddy size and intensity determine the potential for diffusion on a local scale, while evolution of the local wind systems as well as the vertical thermal structure would have a significant effect on the intermediate to long range transport of contaminants originating in a mountain valley or basin.

BIBLIOGRAPHY

ASCOT, 1980: Atmospheric Studies in Complex Terrain (ASCOT) Information Survey, ed. M.H. Dickerson, May 1980. Lawrence Livermore National Laboratory, University of California, Livermore CA 94550.

Ayer, H.S., 1961: On the dissipation of drainage wind systems in valleys in morning hours. J. Meteor., 18, 560-563.

Bader, D.C., 1981: Simulation of the daytime boundary layer evolution in deep mountain valleys. M.S. thesis, Dept. Atmos. Sci., Colo. State Univ., Ft. Collins.

Ball, F.K., 1960: Control of inversion height by surface heating. Quart. J. Roy. Meteor. Soc. 86, 483-494.

Banta, R.M., 1981: The Development of the heated boundary layer and associated flow systems in South Park, Colorado. Preprints, Second Conf. on Mountain Meteorology, 9-12 November, Steamboat Springs, CO. Boston: Amer. Meteor. Soc., pp

_____ and W.R. Cotton, 1979: Horizontal and vertical structure of diurnal boundary-layer flow patterns over mountainous terrain. Preprints, Fourth Symposium on Turbulence, Diffusion, and Air Pollution, 15-18 January, Reno NV, Boston: Amer. Meteor. Soc, pp. 217-224.

_____ and _____, 1981: An analysis of the structure of local wind systems in a broad mountain basin. J. Appl. Meteor., 20, 1255-1266.

Benoit, R., 1977: On the integral of the surface layer profile-gradient functions. J. Appl. Meteor. 16: 859-860.

Beran, D.W., C.G. Little, and B.C. Willmarth, 1971: Acoustic Doppler measurements of vertical velocities in the atmosphere. Nature, 230, 160-162.

Betts, A.K., 1973: Non-precipitating cumulus convection and its parameterization. Quart. J. Roy. Meteor. Soc., 99, 178-196.

_____, 1974: Reply to comment on the paper "Non-precipitating cumulus convection and its parameterization." Quart. J. Roy Meteor. Soc., 100, 469-471.

Braham, R.R., and M. Draginis, 1960: Roots of orographic cumuli. J Meteor. 17, 214-226.

Brock, F.V., and P.K. Govind, 1977: Portable Automated Mesonet in operation. J. Appl. Meteor., 16, 299-310.

Brown, R.A., 1970: A secondary flow model for the planetary boundary layer. J. Atmos. Sci., 27, 742-757.

_____, 1972: On the inflection point instability of a stratified Ekman boundary layer. J. Atmos. Sci., 29, 850-859.

Brown, E.H. and F.F. Hall, Jr., 1978: Advances in atmospheric acoustics. Rev. Geophys. and Space Phys., 16, 47-110.

Busch, N.E., 1973: On the mechanics of atmospheric turbulence. Ch. in Workshop on Micrometeorology (D.A. Haugen, ed.). Boston: Amer. Meteor. Soc, pp. 1-65.

Businger, J.A., 1966: Transfer of heat and momentum in the atmospheric boundary layer. Proc. Arctic Heat Budget and Atmospheric Circulation. Santa Monica, Calif, RAND Corp., 305-332.

_____, 1973: Turbulent transfer in the atmospheric surface layer. Ch. 2 in Workshop on Micrometeorology (D.A. Haugen, ed. . Boston: Amer. Meteor. Soc., pp. 67-100.

_____, J. C. Wyngaard, Y. Izumi, and E.F. Bradley, 1971: Flux-profile relationships in the atmospheric surface layer. J. Atmos. Sci., 28, 181-189.

Clark, T.L., 1977: A small-scale dynamic model using a terrain-following coordinate transformation. J. Comp. Phys., 24, 186-215.

Cotton, W.R., 1975: On paramaterization of turbulent transport in cumulus clouds. J. Atmos. Sci., 32, 548-564.

Cotton, W.R., and R.L. George, 1978: A summer with PAM. Preprint volume, Fourth Symposium on Meteorological Observations and Instrumentation, Denver, AMS, Boston, 87-92.

_____, D.C. Hahn, and R.M. Banta, 1978: Air turbulence measurements in and below cumulus congestus over mountainous terrain. Preprints, Conf. on Cloud Physics and Atmospheric Electricity, 31 July - 4 August, Issaquah, WA, pp. 408-415. Boston: Amer. Meteor. Soc.

_____, R.L. George, and K.R. Knupp, 1982: An intense, quasi-steady thunderstorm over mountainous terrain. Part I: Evolution of the storm-initiating mesoscale circulation. J. Atmos. Sci., 39, 328-342.

Coulman, C.E., 1978: Boundary-layer evolution and nocturnal inversion dispersal - Part I. Bound.-Layer. Meteor., 14, 471-491.

_____, 1980: Diurnal evolution of properties of the sub-cloud layer over land. Bound.-Layer Meteor, 19, 31-50.

Cramer, O.P., 1972: Potential temperature analysis for mountainous terrain. J. Appl. Meteor., 11, 44-50.

_____ and R.E. Lynott, 1961: Cross-section analysis in the study of wind flow over mountainous terrain. Bull. Amer. Meteor. Soc., 42, 693-702.

_____ and _____, 1970: Mesoscale analysis of a heat wave in western Oregon. J. Appl. Meteor., 9, 740-759.

Cronenwett, W.T., G.B. Walker, and R.L. Inman, 1972: Acoustic sounding of meteorological phenomena in the planetary boundary layer. J. Appl. Meteor., 11, 1351-1358.

Danielson, K.S., and W.R. Cotton, ed., 1977: SPACE Log. Department of Atmospheric Science, Colorado State University, Ft. Collins.

_____ and V.E. Derr, 1978: Phase detection of convestive cloud hydrometeors using LIDAR. Preprint volume, Conference on Cloud Physics and Atmospheric [sic] Electricity, 31 July - 4 Aug., Issaquah, Wash., pp. 341-346. Boston: Amer. Meteor. Soc.

Davidson, B., 1963: Some turbulence and wind variability observations in the lee of mountain ridges. J. Appl. Meteor., 2, 463-472.

_____, and P.K. Rao, 1958: Preliminary report on valley wind studies in Vermont, 1957. New York University, College of Engineering, Dept. of Meteorology and Oceanography.

Deardorff, J.W., 1973: The use of subgrid transport equations in a three-dimensional model of atmospheric turbulence. J. Fluids Eng., 95, 429-438.

_____, 1974: Three-dimensional numerical study of the height and mean structure of a heated planetary boundary layer. Bound.-Layer Meteor., 7, 81-106.

_____, 1978: Observed characteristics of the outer layer. A chapter in the Short Course on the Planetary Boundary Layer, ed. by A.K. Blackadar. Boston: Amer. Meteor. Soc.

Defant, F., 1949: Zur Theoric der Hangwinde, vebst Bewerkungen zur Theorie der Berg- und Talwinde. Arch. Meteor. Geophys. Biokliwat., A1, 421-450.

_____, 1951: Local winds. Compendium of Meteorology, Boston: Amer. Meteor. Soc., 655-672.

Dyer, A.J., 1965: The flux-gradient relation for turbulent heat transfer in the lower atmosphere. Quart. J. Roy. Meteor. Soc., 91, 151-157.

_____, 1967: The turbulent transport of heat and water vapors in an unstable atmosphere. Quart. J. Roy. Meteor. Soc., 93, 501-508.

_____, and B.B. Hicks, 1970: Flux-gradient relationships in the constant flux layer. Quart. J. Roy. Meteor. Soc., 96, 715-721.

Ficker, H.V., 1913: Wirbelbildung bei Ballonfahrten in Gebirge. Meteorol. Z., 48, 243-245.

Fosberg, M.A., 1967: Numerical analysis of convective motions over a mountain ridge. J. Appl. Meteor., 6, 889-904.

_____, 1969: Airflow over a heated coastal mountain. J. Appl. Meteor., 8, 436-442.

_____, and M.J. Schroeder, 1966: Marine air penetration in central California. J. Appl. Meteor., 5, 573-589.

Frisch, A.S. and S.F. Clifford, 1974: A study of convection capped by a stable layer using Doppler radar and acoustic echo sounders. J. Atmos. Sci., 31, 1622-1628.

_____, R.B. Chadwick, W.R. Moniger, and J.M. Young, 1976: Observations of boundary-layer convection cells measured by dual-Doppler radar and echosonde and by microbarograph array. Bound.-Layer Meteor., 10, 55-68.

Gal Chen, T., and R.C.J. Somerville, 1975a: On the use of a coordinate transformation for the solution of the Navier-Stokes equations. J. Comp. Phys., 17, 209-228.

_____, and _____, 1975b: Numerical solution of the Navier-Stokes equations with topography. J. Comp. Phys., 17, 276-310.

Geiger, R., 1965: The Climate Near the Ground, Harvard University Press, Cambridge.

George, R.L., 1979: Evolution of mesoscale convective systems over mountainous terrain. Atmos. Sci. Paper No. 318, Colorado State University, Ft. Collins, 80523. 160 pp.

Gill, G.C., 1975: Development and use of the Gill UVW anemometer. Preprint volume, Third Symposium on Meteorological Observations and Instrumentation, Washington, D.C., AMS, Boston, 65-72.

Gilman, G.W., H.B. Coxhead, and F.H. Willis, 1946: Reflection of sound signals in the troposphere. J. Acoust. Soc. Amer., 18, 274-283.

Gleeson, T.A., 1951: On the theory of cross-valley winds arising from differential heating of the slopes. J. Meteor., 8, 398-405.

Hahn, D.C., 1980: Observed Characteristics of turbulence in the atmospheric boundary layer over mountainous terrain. Atmos. Sci. Paper No. 332, Dept. of Atmos. Sci., Colo. St. Univ., Ft. Collins 80523, 104 pp.

Hall, F.F., Jr., 1972: Temperature and wind structure studies by acoustic echo-sounding, Ch. 18 in Remote Sensing of the Troposphere. (V.E. Derr, ed.). Washington, D.C.: U.S. Government Printing Office.

_____, J.G. Edinger, and W.D. Neff, 1975: Convective plumes in the planetary boundary layer, investigated with an acoustic echo sounder. J. Appl. Meteor., 14, 513-523.

Hardy, K.R., and H. Ottersten, 1969: Radar investigations of convective patterns in the clear atmosphere. J. Atmos. Sci., 26, 666-672.

Hewson, E.W., and G.C. Bill, 1944: Meteorological investigations in the Columbia River valley near Trail, B.C. Bur. Mines Bull., U.S. Dept. of Interior, 453, 23-228.

Holzworth, G.C., 1964: Estimates of mean maximum mixing depths in the contiguous U.S. Mon. Wea. Rev., 92, 235-242.

_____, 1979: Rawinsonde indications of the vertical extent of instability. Preprint volume, Fourth Symposium on Turbulence, Diffusion, and Air Pollution, Reno, AMS, Boston, 491-494.

Horst, T.W., 1973: Corrections for response errors in a three-component propeller anemometer. J. Appl. Meteor., 12, 716-725.

Huggins, Arlen Wesley, 1975: The precipitation sequence in mountain cumuli. Unpublished M.S. thesis, Dept. of Atmos. Sci., Colorado State University, Ft. Collins, 80523. 158 pp.

Hughes, R.L., 1978: A numerical simulation of mesoscale flow over mountainous terrain. Atmos. Sci. Paper No. 303, Colorado State University, Ft. Collins 80523. 123 pp.

Kaimal, J.C., and J.A. Businger, 1970: Case studies of a convective plume and a dust devil. J. Appl. Meteor., 9, 612-620.

_____, J.C. Wyngaard, D.A. Haugen, O.R. Cote, Y. Izumi, S.J. Caughey, and C.J. Readings, 1976: Turbulence structure in the convective boundary layer. J. Atmos. Sci., 33, 2152-2169.

Kao, S.K., H.N. Lee, and K.I. Smidy, 1975: An analysis of the topographical effect on turbulence and diffusion in the atmosphere's boundary layer. Bound.-Layer Meteor., 8, 323-334.

Katen, P.C., 1977: Modeling atmospheric dispersion of lead particulates from a highway. Environmental Research Paper No. 11, Dept. of Atmos. Sci., Colo. St. Univ., Ft. Collins 80523, Ph.D. dissertation.

Klemp, J.B., and D.K. Lilly, 1975: The dynamics of wave-induced downslope winds. J. Atmos. Sci., 32, 320-339.

_____ and _____, 1978: Numerical simulation of hydrostatic mountain waves. J. Atmos. Sci., 35, 78-107.

Klemp, J.B., and R.B. Wilhelmson, 1978: The simulation of three-dimensional convective storm dunamics. J. Atmos. Sci., 35, 1070-1086.

Knupp, K., and W.R. Cotton, 1981a: An intense quasi-steady thunderstorm over mountainous terrain - Part II: Doppler radar observations of the storm morphological structure. J. Atmos. Sci., 39, 343-358.

Knupp, K., and W.R. Cotton, 1981b: An intense quasi-steady thunderstorm over mountainous terrain - Part III: Doppler radar observations of the turbulent structure. J. Atmos. Sci., 39, 359-368.

Le Mone, M.A., 1972: The structure and dynamics of the horizontal roll vortices in the planetary boundary layer. Ph.D. dissertation, University of Washington, 128 pp.

_____, 1973: The structure and dynamics of horizontal roll vortices in the planetary boundary layer. J. Atmos. Sci., 30, 1077-1091.

_____ and W.T. Pennell, 1976: The relationship of trade wind cumulus distribution to subcloud layer fluxes and structure. Mon. Wea. Rev., 104, 524-539.

Lenschow, D.H., 1970: Airplane measurements of planetary boundary layer structure. J. Appl. Meteor., 9, 874-884.

_____, 1974: Model of the height variation of the turbulent kinetic energy budget in the unstable planetary boundary layer. J. Atmos. Sci., 31, 465-474.

_____, C.A. Cullian, R.B. Friesen, and E.N. Brown, 1978: The status of air motion measurements on NCAR aircraft. Preprint volume, Fourth Symposium on Meteorological Observations and Instrumentation, Denver, AMS, Boston, 433-438.

_____, and W.T. Pennel, 1974: On the measurement of in-cloud and west-bulb temperatures from an aircraft. Mon. Wea. Rev., 102, 447-454.

_____, B.B. Stankov, and L. Mahrt, 1979: The rapid morning boundary-layer transition. J. Atmos. Sci., 36, 2108-2124.

_____ and P.L. Stephens, 1980: The role of thermals in the convective boundary layer. Bound.-Layer Meteor., 19, 509-532.

_____ and B.B. Stankov, 1981: A case study of inhomogeneous flow in the boundary layer. Extended Abstracts, Fifth Symposium on Turbulence, Diffusion, and Air Pollution, March 9-13, Atlanta. Boston: Amer. Meteor. Soc., pp. 90-91.

Lilly, D.K., 1962: On the numerical simulation of buoyant convection. Tellus, 14, 148-172.

Little, C.G., 1969: Acoustic methods for the remote probing of the lower atmosphere. Proc. IEEE, 57, 571-578.

Louis, J.-F., 1979: A parametric model of vertical eddy fluxes in the atmosphere. Bound.-Layer Meteor, 17, 187-202.

Lumley, J.L. and H. A. Panofsky, 1964: The Structure of Atmospheric Turbulence. New York: John Wiley & Sons, 239 pp.

Mc Allister, L.G., J.R. Pollard, A.R. Mahoney, and P.J.R. Shaw, 1969: Acoustic sounding - A new approach to the study of atmospheric structure. Proc. IEEE, 57, 579-587.

Mc Bean, G.A., 1972: Instrument requirements for eddy correlation measurements. J. Appl. Meteor., 11, 1078-1084.

MacHattie, L.B., 1968: Kananaskis Valley winds in summer. J. Appl. Meteor., 7, 348-352.

Mc Nider, R.T., and R.A. Pielke, 1979: Application of the University of Virginia Mesoscale Model to air pollutant transport. Preprints, Fourth Symposium on Turbulence, Diffusion, and Air Pollution, 15-18 January, Reno NV. Boston: Amer. Meteor. Sco., pp. 397-404.

_____, S.R. Hanna, and R.A. Pielke, 1981: Numerical simulation of the transport and dispersion of pollutants in slope and mountain-valley flows. Extended Abstracts, Fifth Symposium on Turbulence, Diffusion, and Air Pollution, 9-13 March, Atlanta. Boston: Amer. Meteor. Soc., pp. 220-221.

Mahrer, Y. and R.A. Pilke, 1976: Numerical simulation of the air flow over Barbados. Mon. Wea. Rev., 104, 1392-1402.

_____ and _____, 1977: A numerical study of the air flow over irregular terrain. Beitr. Atmos. Phys., 50, 98-113.

Moll, E., 1935: Aerologische Untersuchung periodischer Gebirgswinde in V-formigen Alpentalern. Beitr. Physik fr. Atmos., 22, 177-197.

Morris, A.L., D.B. Call, and R.B. Mc Beth, 1975: A small tethered balloon sounding system. Bull. Amer. Meteor. Soc., 56, 964-969.

Neff, W.D., 1975: Quantitative evaluation of acoustic echoes from the planetary boundary layer. Tech. Rep. ERL 322- WPL 38. Boulder: Natl. Oceanic and Atmos. Admin., 34 pp.

Nickerson, E.C., and V.E. Smiley, 1975: Surface layer and energy budget parameterizations for mesoscale models. J. Appl. Meteor., 14, 297-300.

Orville, H.D., 1964: On Mountain upslope winds. J. Atmos. Sci., 21, 622-633.

_____, 1965: A photogrammetric study of the initiation of cumulus clouds over mountainous terrain. J. Atmos. Sci., 22, 700-709.

_____, 1968: Ambient wind effects on the initiation and development of cumulus clouds over mountains. J. Atmos. Sci., 25, 385-403.

Panofsky, H.A., 1963: Determination of stress from wind and temperature measurements. Quart. J. Roy. Meteor. Soc., 89, 85-94.

_____, 1973: Tower micrometeorology. Ch. 4 in Workshop on Micrometeorology (D.A. Haugen, ed.) Boston, Amer. Meteor. Soc., pp. 151-176.

_____. H. Tenneker, D.H. Lenschow, and J.C. Wyngaard, 1977: The characteristics of turbulent velocity components in the surface layer under convective conditions. Bound.-Layer Meteor., 11, 355-361.

Paulson, C.A., 1970: The mathematical representation of wind speed and temperature profiles in the unstable atmospheric surface layer. J. Appl. Meteor., 9, 857-861.

Peltier, W.R. and T.L. Clark, 1979: The evolution and stability of finite-amplitude mountain waves. Part II Surface wave drag and severe downslope windstorms. J. Atmos. Sci., 36, 1498-1529.

Prandtl, L., 1942: Führer durch die Strömungslehre. Braunschweig: F. Vieweg & Sohn, 373-375.

Pilke, R.A., 1981: Mesoscale numerical modeling. Advances in Geophysics - Vol. 23 (Barry Saltzman, ed.). New York: Academic Press, pp. 185-344.

Priestly, C.H.B., 1959: Turbulent Transfer in the Lower Atmosphere. The University of Chicago Press.

Raymond, D., and M. Wilkening, 1980: Mountain-induced convection under fair weather conditions. J. Atmos. Sci., 37, 2693-2706.

Russell, P.B., E.E. Uthe, F.L. Ludwig, and N.A. Shaw, 1974: A Comparison of atmospheric structure as observed with monostatic acoustic sounder and lidar techniques. J. Geophys. Res., 79. 5555-5566.

Schroeder, M.J., 1961: Down-canyon afternoon winds. Bull. Amer. Meteor. Soc., 42, 527-542.

Sommeria, G., 1976: Three-dimensional simulation of turbulent processes in an undisturbed trade wind boundary layer. J. Atmos. Sci., 33, 216-241.

Start, G.E., C.R. Dickson, and L.L. Wendell, 1975: Diffusion in a canyon within rough mountainous terrain. J. Appl. Meteor., 14, 333-346.

Tang, W., 1976: Theoretical study of cross-valley circulation. Arch. Met. Geoph. Biokl., A25, 1-18.

Telford, J.W., 1966: The convective mechanism in clear air. J. Atmos. Sci., 23, 652-666.

Tennekes, H. 1970: Free convection in the turbulent Ekman layer of the atmosphere. J. Atmos. Sci., 27, 1027-1034.

Tennekes, H., 1973: A model for the dynamics of the inversion above a convective boundary layer. J. Atmos. Sci., 30, 558-567.

Tennekes, H., 1978: The Planetary Boundary Layer. A chapter in the Short Course on the Planetary Boundary Layer, ed. by A.K. Blackador. Boston: Amer. Meteor. Soc.

Tennekes, H. and A.G.M. Driedonks, 1981: Basic entrainment equations for the atmospheric boundary layer. Boundary Layer Meteor., 20, 515-531.

Tennekes, H. and J.O. Lumley, 1972: A First Course in Turbulence. Cambridge, Mass: MIT Press, 300 pp.

Thyer, H.H., 1966: A theoretical explanation of mountain and valley winds by a numerical method. Arch. Meteor. Geophys. Biokl., 15(A), 318-348.

Tripoli, G.J. and W.R. Cotton, 1982: The Colorado State University three-dimensional cloud mesoscale model 1981 Part I - General theoretical framework and sensitivity experiments. J. Rech. Atmos., in press.

Wagner, A., 1932: Hangwind-Ausgleichsströmung-Berg-und Talwind. Meteor. Z., 49, 209-217.

Wagner, A., 1938: Theorie und Beobachtung der periodischen Gebirgswinde. Gerlands Beitr. Geophys. (Leipzig), 52, 408-449. (Translation courtesy of C. David Whiteman).

Warner, J. and J.W. Telford, 1963: Some patterns of convection in the lower atmosphere. J. Atmos. Sci., 20, 313-318.

Warner, J. and J.W. Telford, 1967: Convection below cloud base. J. Atmos. Sci., 24, 374-382.

Wenger, R., 1923: Zur Theorie der Berg-und Talwind. Meteor. Z., 40, 193-204.

Whiteman, C.D., 1980: Breakup of temperature inversions in Colorado mountain valleys. Atmos. Sci. Paper No. 328, Dept. of Atmos. Sci., Colorado. St. Univ., Ft. Collins, 80523, Ph.D. dissertation. 250 pp.

Whiteman, C.D., and T.B. McKee, 1977: Observations of vertical atmospheric structure in a deep mountain valley. Arch. Meteor. Geophys., Biokl., 26(A), 39-50.

Whiteman, C.D., and T.B. McKee, 1978: Air pollution implications of inversion descent in mountain valleys. Atmos. Environ., 12, 2151-2158.

Wilczak, J.M. and J.E. Tillman, 1980: The three-dimensional structure of convection in the atmospheric surface layer. J. Atmos. Sci., 37, 2424-2443.

Wilkens, E.M., 1955: A discontinuity surface produced by topographic winds over the upper Snake River plain, Idaho. Bull. Amer. Meteor. Soc., 36, 397-408.

Wyngaard, J.C., 1973: On surface layer turbulence. Ch. 3 in Workshop on Micrometeorology (D.A. Haugen, ed.). Boston; American Meteor. Soc., pp. 101-149.

Wyngaard, J.C. and O.R. Cote, 1971: The budgets of turbulent kinetic energy and temperature variance in the atmospheric surface layer. J. Atmos. Sci., 28, 190-201.

Wyngaard, J.C., O.R. Cole, and Y. Izumi, 1971: Local free convection, similarity and the budgets of shear stress and heat flux. J. Atmos. Sci., 28, 1171-1182.

Wyngaard, J.C., W.T. Pennel, D.H. Lenschow, and M.A. LeMone, 1978: The temperature-humidity covariance budget in the convective boundary layer. J. Atmos. Sci., 35, 47-58.

Wyckoff, R.J., D.W. Beran, and F.F. Hall, Jr., 1973: A comparison of the low-level radiosonde and the acoustic echo sounder for monitoring atmospheric stability. J. Appl. Meteor., 12, 1196-1204.

Yoshino, M.M., 1975: Climate in a Small Area. University of Tokyo Press, Tokyo.

Yamada, T., 1978: A three-dimensional numerical study of complex atmospheric circulations produced by terrain. Proc. of the Conf. on Sierra Nevada Meteorology, AMS, Boston, 61-67.

APPENDIX A: THE CONVECTIVE BOUNDARY-LAYER OVER FLAT TERRAIN

1. Approaches to Studying the CBL and General Features

Approaches to the study of the convective boundary layer can be divided into several categories. The first approach is to study the detailed large eddy structure of the CBL. These large, organized eddies may take the form of thermals or plumes, or they may form roll vortices. The second approach is to consider vertical profiles of thermodynamic, dynamic, and flux quantities averaged over some horizontal distance. In this approach, the CBL is assumed to be horizontally-homogeneous. The third approach is to consider bulk, vertically-conservative properties of the entire CBL, which is usually assumed to be well-mixed. The CBL is treated essentially as a 1-D "control volume", described in terms of mean properties of the CBL as a whole, which are changed by fluxes through the lower boundary (surface) and entrainment through the upper boundary (inversion). The focus of this Appendix will be on a discussion of the first approach, and in particular on thermals, since thermal structure is an important part of the mountain boundary layer observations presented in this study.

The gross structure of the CBL is most easily described by referring to vertical profiles of mean quantities. Figure 2.1, which was presented at the beginning of Chapter II, shows typical profiles of $\overline{\theta}$, the potential temperature, $\overline{q}$, the specific humidity, and $\overline{u}$, the mean wind (Tennekes and Driedonks, 1981). The height of the convective inversion,

which marks the top of the CBL, is designated z_i. The lowest 10% of the CBL, up to about 0.1 z_i, is called the "surface" or "constant flux" layer. The portion of the CBL above the surface layer has been called the "Ekman layer", but this name calls to mind a turning of the wind with height. Since most of the turning of the wind in a barotropic CBL usually occurs at the top across the convective inversion, we shall call this region the "outer layer" of the CBL, as Deardorff (1978) and others have done. At the top of the CBL is the "entrainment" or "transition" layer, above which is the free atmosphere.

2. Details of the CBL: Large-Eddy Structure

The large eddies which occur most commonly in the CBL are plumes (or thermals) and roll vortices. Over land during sunlit hours, plume-type convection is by far the most common (Deardorff, 1978). Much of the daytime boundary-layer data taken in South Park during SPACE-77 showed evidence of plume activity, so that this type of convection is not just a feature of the CBL over flat terrain. Some of this evidence is presented in Chapter V.

Thermals have been identified on fluctuating temperature traces of tower or aircraft measurements. On these traces one sees thermally-quiescent periods of relatively uniform base-level temperature interspersed with disturbed periods, which consist of warm pulses (or "ramps") with a temperature elevation of around 1°C (seldom more than 2°C). The disturbed region represents the thermal, and it is also characterized by mean rising motion and a strong correlation between w and T fluctuations, i.e. strong upward heat flux. The thermally-quiescent region between thermals, on the other hand, is associated with descending air motion

and very little turbulent heat flux (since the temperature fluctuations are small). In contrast to the structure evident in the temperature trace, the velocity data show that the winds are always turbulent, outside the plume as well as inside, although the vertical velocity gusts may have a slightly larger amplitude inside the plumes. Since the turbulent heat flux is concentrated in the thermals, they are the atmosphere's mechanism for carrying heat upwards from near the earth's surface into the bulk of the convective boundary layer — provided the surface-layer winds are not too strong [Priestly (1959, pp 67ff), Warner and Telford (1963, 1967), Kaimal and Businger (1970), Wilczak and Tillman (1980)]. Besides using temperature (which goes from being an excess in thermals at low levels to being a deficit at upper levels), the humidity trace has also been shown to be an excellent indicator of thermals at all levels in the CBL (Lenschow and Stephens, 1980).

Three levels of organization of the plumes have been identified as they ascend. Nearest to the ground is a layer in which the temperature trace shows completely random fluctuations with no quiescent periods. The depth of this layer of random fluctuations has been found to vary from less than 1 m over a smooth surface to 25 m or more over rough terrain. It is also shallower with light winds than with strong winds (Warner and Telford, 1963).

Near the top of the random layer, the "scattered buoyant elements" seem to draw together "from near the surface into an organized vertical circulation" (Kaimal and Businger, 1970). The organized circulations are in the form of plumes, with the characteristic thermally-disturbed and quiescent regions and with diameters of 30-50 m or so. Additionally, these low-level plumes have the following characteristics:

1. They move more slowly than the mean wind at the level of observation and tilt downwind with height [Priestly (1959), Kaimal and Businger (1970), Wilczak and Tillman (1980)].

2. The maximum temperature in their thermally-disturbed regions often tends to occur just after an abrupt "microfront" at the upwind edge of the plume. This often gives the plume signature a distinct "ramp-like" appearance (Wilczak and Tillman, 1980). Kaimal and Businger (1970) found that this microfront may be less than 1 cm thick.

3. This maximum temperature remains relatively constant from one thermal to the next, as does the minimum temperature observed in the thermally-quiescent periods between thermals (Priestly, 1959).

4. Outside the plume, the vertical temperature gradient in the quiescent region is dry-adiabatic down to very low levels [Kaimal and Businger (1970), Wilczak and Tillman (1980)].

5. The vertical pressure gradient in the plume exceeds the hydrostatic value [Kaimal and Businger (1970), Lenschow and Stephens (1980)].

6. Since there is an intervening random layer between the surface and the level where the plumes have identifiable structure, the plumes do not necessarily originate at identifiable terrain irregularities (Warner and Telford, 1967).

Near the top of this still rather thin layer (probably less than $0.1z_i$), the smaller thermals coalesce into larger thermals [Kaimal, et al. (1976), Wilczak and Tillman (1980), Lenschow and Stephens, 1980)]. Observations from a 300 m tower (Wilczak and Tillman, 1980) and aircraft observations show that the bulk of the CBL consists of these larger thermals, hundreds of meters across. Warner and Telford (1967) found that the thermals were 200-300 m in diameter, that this diameter varied little with height above 100 m, and that thermals tended to be separated by quiescent regions somewhat larger than their own diameter. Lenschow (1970) reported that thermals over northeast Colorado were elongated in the direction of the mean wind. At 100 m above the ground, thermals had a diameter of 200 m for his cross wind runs and greater than 400 m for his along wind runs. At Z = 450 m, he found fewer than at Z = 100 m,

but the thermals were twice as big. Wilczak and Tillman (1980) found that the horizontal shape of thermals is a strong function of the instability, as measured by L, the Monin-Obukhov length. Other properties of these thermals which occupy the bulk of the CBL include:

1. They move with the mean CBL wind [Hall et al. (1975), Wilczak and Tillman (1980)].

2. The amplitude of the temperature pulses decreases with height, until the disturbed period and the quiescent period are indistinguishable, in the upper part of the CBL (Warner and Telford, 1963).

3. "An appreciable fraction, perhaps as much as half, of the total (convective) field is occupied by thermals" (Telford, 1966).

4. The stratification in the thermally-quiescent region between plumes is neutral to slightly stable, so there is very little mean vertical advection of heat by the descending branch of the thermal circulation (Warner and Telford, 1967).

5. The width and number-density of thermals obeys mixed-layer scaling laws (Lenschow and Stephens, 1980).

Kaimal et al. (1976) show time-height cross sections of the CBL, obtained from measurements by in-situ sensors attached to the mooring cable of a tethered balloon. The data extend to a height above z_i. They show that the strong positive heat flux in the thermals extends to the top of the CBL, even though the thermals are not distinguishable on the temperature trace. The observations also show some of the details of the entrainment process at the convective inversion. Apparently the air being entrained into the CBL from aloft descends as warm plumes which occur between the rising thermals.

The temperature structure of the CBL - with a rapidly-fluctuating temperature pattern inside the thermals and a uniform, quiet pattern outside - has made it an interesting object of study for the acoustic sounder. The monostatic acoustic sounder detects only that portion of

its signal which is scattered from small-scale temperature fluctuations (Little, 1969, p. 574; McAllister et al., 1969, p. 580; Beran et al., 1971, p. 160; Hall, 1972, p. 1810; Wyckoff et al., 1973, p. 1196; Brown and Hall, 1978, p. 72). Thus it receives strong returns from the thermally-active plume interiors (which show up as dark on the instruments' facsimile display) and weak echoes from the thermally-quiescent regions between plumes. The following are a few examples where the acoustic sounder has been used to study the CBL: Gilman et al. (1946), McAllister et al. (1969), Beran et al. (1971), Hall (1972), Cronenwett et al. (1972), Wyckoff et al. (1973), Frisch and Clifford (1974), Neff (1975), Hall et al. (1975), Frisch et al. (1976), and Brown and Hall (1978).

Further organization of the thermals in the CBL was suggested by Hardy and Ottersten (1969). Based on examinations of clear air returns from their sensitive microwave radars, they conclude that, when the surface winds are light, the thermals tend to organize into rings. These rings resemble Bénard convection cells, which have been studied in the laboratory.

The CBL tends to organize into thermals or plumes under light-wind conditions. When the surface-layer winds are greater than about 7 m/s, however, the unstable boundary-layer organizes into horizontal roll vortices, the axes of which align nearly parallel with the mean wind. Since this type of convection was not observed in South Park, roll vortices will not be discussed in detail in this paper. They have been described by Lemone (1972, 1973), Lemone and Pennel (1976), Brown (1970a,b) and Deardorff (1978).

3. Vertical Profiles of the Horizontally-Homogeneous CBL

While the CBL actually consists of a field of large convective eddies or thermals, one can regard these thermals as long-wavelength perturbations superimposed on a horizontally-homogeneous base state. One obtains properties of this base state by assuming that the thermal field itself is horizontally homogeneous and by averaging across many wavelengths of thermals. Horizontal-mean quantities can then be presented as a function of height, in the form of vertical profiles. The accuracy of these horizontal averages depends upon how well the thermal field is sampled. In his aircraft observations, for example, Lenschow (1970) found that the presence or absence of one thermal of 300 m diameter could affect the temperature statistics of a 15 km flight leg.

a. Some Definitions

In describing the CBL several definitions will be helpful. The lowest approximately 10% of the boundary layer is a region in which the winds increase logarithmically with height and the vertical fluxes are nearly constant with height (see e.g., Wyngaard, 1973, and Tennekes, 1978); this region has been called the "constant-flux layer" or the atmospheric "surface layer". The vertical flux of enthalpy or "heat" can be written:

$$H_s = \rho c_p \overline{w'T'} \quad , \qquad (4.1)$$

where H_s is the surface heat flux, ρ the air density, c_p the specific heat of air at constant pressure, w' a local deviation from the horizontal mean vertical velocity $\overline{w}$, T' a local deviation from the horizontally-averaged temperature $\overline{T}$, and the overbar represents a horizontal averaging operator over some region. The surface-layer turbulent momentum flux, or stress, is expressed as:

$$\tau_s = \rho \overline{u'w'} = \rho u_*^2 \quad , \tag{A.2}$$

where τ_s is the surface-layer stress, u' is a local deviation from the horizontally-averaged streamwise wind component $\bar{u}$, and u_* is called the "friction velocity". From (2.2)

$$u_* = (\overline{u'w'})^{\frac{1}{2}} = (\tau_s/\rho)^{\frac{1}{2}} \quad . \tag{A.3}$$

Thus friction velocity is a measure of mechanical or shear-produced turbulence in the surface layer.

In the absence of water vapor or other contaminants, the surface layer is "stable" when the heat flux is negative, or directed downwards (i.e. $\overline{w'T'} < 0$). It is unstable when the heat flux is positive, or directed upwards (i.e. $\overline{w'T'} > 0$). When water vapor is present, these criteria must be altered to account for the buoyancy effects of the water vapor; this is done by replacing the temperature, T, with the virtual temperature, T_v. Virtual temperature is defined as:

$$T_v = T \cdot (1 + .61q) \tag{A.4}$$

where q is the specific humidity of water vapor (cf. Busch, 1973). The stability criteria then become:

$\overline{w'T_v'} < 0$	stable	
$\overline{w'T_v'} = 0$	neutral	(A.5)
$\overline{w'T_v'} > 0$	unstable	

A measure of the stability is the Richardson number, which is the ratio of the buoyant production of turbulent kinetic energy (TKE) to the mechanical or shear production:

$$Ri = \frac{(g/\overline{T})\ \overline{w'T'}}{\overline{u'w'}\ \partial\overline{u}/\partial z} \quad . \tag{A.6}$$

This quantity has the disadvantage that it varies with height in the surface layer, and it "blows up" if the mean shear vanishes. It is convenient, therefore, to define another stability parameter:

$$\frac{z}{L} = -\frac{gz\ \overline{w'T_v'}}{\overline{T}\ u_*^3} \quad , \tag{A.7}$$

where L is known as the "Monin-Obukhov length" (Obukhov, 1946; Monin and Obukhov, 1954); thus the quantity

$$L = -\frac{\overline{T}}{g}\ \frac{u_*^3}{\overline{w'T_v'}} \tag{A.8}$$

is constant in the surface or "constant flux" layer. -L is an important vertical scaling length in the unstable surface layer. Businger (1973) shows that -L is proportional to (and an upper bound for) the height at which the buoyant production of TKE is equal to the shear production in the unstable surface layer - below this height, shear production predominates, while above it, buoyant production prevails. Tennekes (1970) interprets -L as a length scale related to the rate at which heat penetrates through the surface layer; he calls z/L "a handy representative of the vertical heat flux" (Tennekes, 1973). Wyngaard (1973) presents an interesting discussion of the asymptotic behavior of z/L for the strongly stable and the strongly unstable cases.

The CBL described in this paper is driven by solar heating at its lower boundary, the earth's surface. Thus, we shall consider cases where the surface layer is unstable, i.e., the heat flux is upwards and the surface-layer stability parameter z/L is negative.

In forming vertical profiles, one may be interested in mean values, such as the mean wind, $\bar{u}$, or the mean potential temperature, $\bar{\theta}$; one may be interested in mean-square-fluctuations or variances, such as the variance of the streamwise wind velocity $\overline{u'^2}$, or the turbulent kinetic energy (TKE), e, which is half the sum of the variances of the three wind components:

$$e = \tfrac{1}{2} (\overline{u'^2} + \overline{v'^2} + \overline{w'^2}); \qquad (A.9)$$

or one may be interested in correlations between fluctuations of different quantities (covariances) such as the vertical heat flux, $\overline{w'T'}$, or the vertical flux of u', $\overline{u'w'}$, which is proportional to the vertical turbulent momentum flux (or Reynolds' stress).

Many of the studies of the horizontally-homogeneous CBL have evaluated the terms in the TKE equation. This equation can be written:

$$\frac{\partial e}{\partial t} = - \overline{u'w'} \frac{\partial \bar{u}}{\partial z} + \frac{g}{T} \overline{w'T'} - \frac{\partial}{\partial z} \left(\overline{w'e} + \frac{\overline{p'w'}}{\bar{\rho}} \right) - \varepsilon \qquad (A.10)$$

[Lumley and Panofsky (1964, p. 120), Lenschow (1970), Busch (1973, p.19)]. The first term on the right-hand side of the equation is the mechanical or shear production term, the second is the buoyant production, the third is the vertical turbulent flux divergence and pressure-diffusion, and the last term is the dissipation, ε, of TKE into heat. In the surface layer this equation can be nondimensionalized by u_*^3/kz to yield:

$$\frac{kz}{u_*^3} \frac{\partial e}{\partial t} = \Phi_M - \frac{z}{L} - \frac{z}{L} \frac{\partial \Phi_D}{\partial (z/L)} - \frac{kz}{u_*^3} \varepsilon \quad , \qquad (A.11)$$

where Φ_M is the nondimensional wind shear and Φ_D is the nondimensional vertical flux (Busch, 1973). Note that in this equation the stability parameter z/L represents the nondimensional buoyant production of TKE.

b. The horizontally-homogeneous surface layer

The surface layer is a region next to the ground in which the vertical fluxes are nearly constant with height, as discussed above. Under unstable conditions, it is a region in which surface-based, shear generation of turbulence, which diminishes rapidly with height, is still of about the same magnitude as buoyant generation. The horizontally-averaged lapse rate is superadiabatic; this gradient actually represents a mean between the plume interiors, where the lapse rate is strongly superadiabatic; and the exterior thermally-quiescent regions, where the lapse rate is neutral down to low levels in the surface layer.

Above the viscous sublayer immediately adjacent to the earth (i.e., at heights large compared to the roughness parameter, z_o), the surface layer is the realm of validity for Monin-Obukhov similarity theory, as discussed by Wyngaard (1973) and Wyngaard et al. (1971). According to this theory, properties of the flow - appropriately nondimensionalized - are functions only of the nondimensional stability parameter, z/L, which was defined above.

Monin-Obukhov scaling for the nondimensional wind shear, Φ_M, and the nondimensional lapse rate, Φ_H, was verified by Businger et al. (1971) over flat terrain in Kansas. For the unstable case, they found that

$$\Phi_M = \frac{kz}{u_*}\frac{\partial \bar{u}}{\partial z} = (1 - 15\,\frac{z}{L})^{-1/4}$$

$$\Phi_H = \frac{kz u_*}{\overline{w'\theta'}}\frac{\partial \bar{\theta}}{\partial z} = 0.74\,(1 - 9\,\frac{z}{L})^{-1/2} \qquad \text{(A.12)}$$

fit the data quite well. In addition, Wyngaard and Coté (1971) and Wyngaard et al. (1971), using the same data, verified Monin-Obukhov scaling for other surface-layer quantities, including the terms of the TKE equation and other budget equations. Except under extremely unstable conditions, most surface-layer variables obey Monin-Obukhov theory, with the exception of the horizontal velocity variances, $\overline{u'^2}$ and $\overline{v'^2}$. The major contribution to these fluctuations is the long wavelength variations due to the thermals, since the CBL is assumed to be horizontally homogeneous. Thus, $\overline{u'^2}$ and $\overline{v'^2}$ scale with velocities more characteristic of the outer region of the CBL, where buoyancy drives the circulations, than the surface layer [Panofsky (1973), Wyngaard and Coté (1974), Panofsky et al. (1977)].

The functional forms of (2.11) were suggested by Businger (1966) and by careful data taken by Dyer (1965, 1967; Dyer and Hicks, 1970), so equations (2.11) are sometimes referred to as the "Businger-Dyer" equations. These equations relate the fluxes of momentum and heat to the velocity and temperature gradients. It is useful, however, to express the fluxes in terms of mean values of wind velocity and temperature in the surface layer. Paulson (1970) used integral expressions recommended by Panofsky (1963) to accomplish this. More accurate expresssions have since been derived by Nickerson and Smiley (1975) and Benoit (1977).

APPENDIX B: BASIC METEOROLOGICAL EOUATIONS USED IN THE DRY MODEL

The Colorado State University Cloud/Mesoscale model has been described in detail by Tripoli and Cotton (1982). The purpose of this Appendix is not to repeat information which can be found in that paper, but rather to present in somewhat simpler form the equations which must be solved in running the dry version of the model, which was used in this study.

In the basic model equations, pressure and density are computed as small perturbations from a hydrostatic reference state. The reference state thus obeys the following relationships:

$$p_o = \rho_o \, RT_o$$

$$\frac{\partial p_o}{\partial z} = - \rho_o \, g$$

The reference state is determined by specifying an initial profile of temperature as a function of height (z), and a surface value for pressure. This reference state then remains unchanged throughout the simulation.

The quasi-Boussinesq set of equations for the mean or resolved-scale variables include an equation of state and the time-dependent equations. A linearized equation of state appropriate for deep convection is assumed to apply:

$$\frac{1}{\gamma}\frac{\overline{p'}}{p_o} = \frac{\overline{p'}}{p_o} + \frac{\overline{\theta'}}{\theta_o}$$

As discussed in the text, the time-dependent equations are solved at two different time intervals. Terms in the equations which are active when sound waves are present are solved on a very short acoustic time step. After a certain number of acoustic time steps, the terms which are not significantly affected by sound waves are updated. Thus the nonacoustic terms are computed on a longer time step which is more representative of meteorological processes.

The terms and equations which are evaluated on the longer time steps are as follows:

$$Fu_i = \rho_o \text{ ADV } (\bar{u}_i) + \rho_o \text{ DIFF } (\bar{u}_i)$$

$$\frac{\partial \bar{\theta}}{\partial t} = \text{ADV } (\bar{\theta}) + \text{DIFF } (\bar{\theta})$$

where the elastic advection operator is defined as:

$$\text{ADV } (\bar{A}) = \frac{-1}{\rho_o}\left[\frac{\partial \rho_o \bar{u}_j \bar{A}}{\partial x_j} - \bar{A}\frac{\partial \rho_o \bar{u}_j}{\partial x_j}\right]$$

and the turbulent diffusion operators are:

$$\text{DIFF } (\bar{u}_i) = \frac{\partial}{\partial x_j} K_m \left(\frac{\partial \bar{u}_i}{\partial x_j} + \frac{\partial \bar{u}_j}{\partial x_i}\right)$$

$$\text{DIFF } (\bar{\theta}) = \frac{\partial}{\partial x_j} K_H \frac{\partial \bar{\theta}}{\partial x_j}$$

The parameterization for K_m has been described in Chapter VI of the text and will not be repeated here. The quantity Fu_i represents the

"larger-scale" tendency on the momentum component, $\bar{u}_i$; the pressure and buoyancy terms are absent from this momentum equation since they are evaluated at the shorter time step. The scalar $\bar{\theta}$ is updated completely on the longer time step. The spatial derivatives are all evaluated using second-order centered differencing. The time derivaties for the advective terms are evaluated using a leapfrog scheme, and the diffusion terms, using forward differencing. Computational modes arising from the use of the leapfrog scheme are suppressed using the Asselin/Robert time filter (Asselin, 1972).

Equations which are solved on the shorter time step include the linearized elastic continuity equation and the acoustically-active portion of the momentum equations:

$$\frac{\partial \overline{p'}}{\partial t} + \frac{\partial \rho_o \bar{u}_j}{\partial x_j} = 0$$

$$\frac{\partial \rho_o \bar{u}_i}{\partial t} + \frac{\partial \overline{p'}}{\partial x_j} + \overline{p'g}\ \delta_{i3} = \overline{Fu}_i$$

Solution of this equation set is accomplished by a two step, semi-implicit, "forward-backward" scheme: (i) $\bar{u}_i$'s are predicted from the current time level of $\bar{u}_i$, $\overline{p'}$ and (ii) predicted value for $\overline{p'}$ is obtained from the current value for $\overline{p'}$ and from the just-predicted values for the $\bar{u}_i$'s calculated in step (i). The perturbation pressure is obtained from the linearized equation of state.

For simplicity these equations have been presented without the coordinate transform terms. The reader who is interested in the complete set of equations is referred to the papers by Gal-Chen and Somerville (1975), Clark (1977), or Tripoli and Cotton (1982).

The spatial boundary conditions have been described in the text, and only the lower boundary condition will be described here. The original surface layer parameterization in this model for the fluxes of heat and momentum at the surface ($\overline{w'\theta'}_o$ and $\overline{u'w'}_o$, respectively) was patterned after the formulation of Louis (1979). These equations are based on the Businger-Dyer flux-profile relationships, but the calculation of the fluxes from mean quantities does not involve interation. For the unstable case, Louis' relationships are:

$$\overline{u'w'}_o = u_*^2 = a^2 \cdot \bar{u}(2)^2 \cdot F$$

$$\overline{w'\theta'}_o = \frac{a^2}{0.74} \cdot \bar{u}(2) \cdot \overline{\Delta\theta} \cdot F$$

where

$$F = 1 - b\ Ri_B/(1 + c|Ri_B|^{\frac{1}{2}})$$

$$Ri_B = g\ Z(2)\ \overline{\Delta\theta}/(\bar{\theta} \cdot \bar{u}(2)^2)$$

$$\overline{\Delta\theta} = \bar{\theta}(2) - \bar{\theta}(1).$$

$\bar{\theta}(2)$ and $\bar{u}(2)$ are the $\bar{\theta}$ and $\bar{u}$ values at the first grid point above the surface (i.e. at K = 2; refer to the staggered grid configuration in Fig. 6.1), and $\bar{\theta}(1)$ is the $\bar{\theta}$ value at the lowest grid point, i.e. at the surface, which must in general be specified. Instead of specifying $\bar{\theta}(1)$ in these model runs, however, it was decided to directly specify the quantity $\overline{\Delta\theta}$ in the early model runs, in order to make the calculated heat flux more uniform. The surface heat flux, $\overline{w'\theta'}_o$, thus became a linear function of u(2) at each grid point, in addition to its dependence

on F. In these early model runs, however, some runaway circulations were encountered. It was observed that the heat flux equation being used could contribute to a positive feedback loop, since the heat flux was driving the flow field, while at the same time larger values of $\overline{u}(2)$ produce larger values of the heat flux. To avoid this possible problem, the heat flux was not allowed to exceed a certain maximum value. When it later turned out that the runaway circulation was due to a problem with the lateral boundary conditions and not with the surface layer interactions, the maximum feature was still retained.

This is the version of the surface layer which was used in the model runs described in this paper. For the values of the constants used, the calculated heat flux values were at or near the maximum values. Thus essentially we were specifying the heat flux to be approximately the maximum value. The only exception to this was one or two points directly in the convergence zone at each time step, where the horizontal wind speed became very small. This situation yielded values of surface heat flux of about half the specified maximum value However, this was confined to a very small region, and the effect of the decrease in heat flux in the updraft region where it was localized would only serve to retard the circulations. Thus it is highly unlikely that these locally lower regions of heat flux have any effect on the qualitative aspects of the solution, or even any significant effect on the quantitative aspects. Therefore, as stated in the text in essence the heat flux which drives the upslope circulation is nearly the same at all points along the slope.

For most of the simulation, $\overline{\Delta\theta}$ is specified to be a constant, time-invariant value. For the first 15 min. of the model run, however,

$\overline{\Delta\theta}$ (and the heat flux) are zero, as the initial wind field and the terrain are allowed a period of adjustment. During the second 15 min. period, $\overline{\Delta\theta}$ is in transition from its initial value of zero to its final constant value. This transition is accomplished through a sinusoidally-varying function:

$$\overline{\Delta\theta} = \frac{a}{2}\left[\cos\left(2\pi\,\frac{t - t_1}{P}\right) - 1\right]$$

where a is the final constant value of $\Delta\theta$, t is the current time, t_1 is the time when heating is initiated (in this case 15 min.), and P is twice the time period over which the transition is to take place. Thus $\overline{\Delta\theta}$ actually reaches its final constant value only after 30 min. of model time.

In future model runs the surface flux parameterization will involve a specification of the heat flux through a surface energy budget. This will allow a more realistic specification of the fluxes and also allow the effects of terrain slope and aspect on surface heating to be investigated.